City, University of London Institutional Repository

Finite Element Study of the Second Order (χ^2) Non-linear Process of Second Harmonic Generation in Optical Waveguides.

by

Ferdinand Apietu Katsriku

A thesis submitted to the City University for the Degree of Doctor of Philosophy in Information Engineering

City University

Photonics Research Group, Department of Electrical, Electronic and Information Engineering, Northampton Square, London EC1V 0HB, UK.

July 2000

Table of Contents

If you aim, aim at the sun, should you fall, you will fall on the moon.

What happens if you aim at the moon?

To Ilemi

In this case if you fall, you will fall into the deep blue sea where the sharks and killer whales will be waiting!

Table of Contents

Chapter 1   Introduction to Optical Waveguide Theory

Chapter 2 Finite Element Method and Propagation Algorithms

Chapter 3 Theory of Second Harmonic Generation

Chapter 4 Finite Element Analysis of Anisotropic Waveguides

iv

Chapter 5   Numerical Modelling of SHG in Optical Waveguides Using the FEM

Chapter 6   Finite Element Analysis of SHG in GaAs/AlGaAs Waveguides

List of tables

List of Figures

Acknowledgements

To the many people who in diverse ways had contributed to the successful completion of this project I would like to say thank you. It is impossible to mention everyone by name without having to write another volume. However I would particularly like to thank Prof. Rahman and Prof. Grattan for their support, guidance and encouragement. Without them this whole project would have been still born. Their painstaking effort to proof read the whole of the thesis is very much appreciated. There is very little more one could have asked from a supervisor. Prof. Rahman freely gave of his time. Always there and patient, explaining things into minute detail. Prof. Grattan never ceased to remind me to dot my 'i's and to cross my 't's. To them I would like to say a big **THANK YOU**.

To my colleagues in the Photonics research group, Femi, Najm, Raj, Moo, Patrick, Chris, Niranthi and others I would also like to say thank you for the wonderful companionship. I am glad you were not 'worried but only wondering'. You were great guys to work with.

To my numerous friends and acquaintances I would also like to say thank you all. Here truly it is impossible to mention names otherwise this acknowledgement would become a litany of names. To the members of the Santrokofi Union-UK, my colleagues at NewVic, I say Thank you all.

Finally but not the least I would like to thank, my grandmother, Anastasia Oyintey of ever loving memory, my mother Philomena Apietu (Akua Martha), my uncle Mgr. Rudolph Apietu (Kwaku Apietu) and my sister Mary Theodora (Wiwi), for their loving care from infancy unto this day. These were the people who watched over my first faltering steps and have guided me through life. To these wonderful people I say 'Bilafe ku asaa orbla, bie bla fuee'. To all other members of my immediate family I would also like to say thank you.

Declaration

The University Librarian is hereby granted powers of discretion to allow this thesis to be copied in whole or in part without further reference to the author. This permission applies to only single copies made for the purposes of study and subject to the normal conditions of acknowledgement.

Abstract

At the heart of future communication systems will be integrated, all optical devices. The role of the second order nonlinear process in the realisation of such devices is well known and has been documented. Research activity in the field of second order nonlinear processes has focused primarily on the generation of new frequencies, which have an important role to play in multimedia systems. The second order process also has great potential for use in all-optical switches, all-optical transistor and intensity-dependent phase modulation. For the theoretical study of such devices, efficient mathematical models are required. The finite element method has established itself as an accurate, efficient and versatile method in the modal analysis of both linear and nonlinear systems but its application to the evolutionary analysis has been minimal.

The application of the finite element method to the theoretical study of such devices is the subject of this thesis. A formulation of the finite element method that takes into consideration material anisotropy and different diffusion profiles is developed, as is a finite element based beam propagation model. Such a model combines the strengths of the finite element method with the well-established beam propagation method for the evolutionary analysis of the fundamental wave and the generated second harmonic wave. The model is applied to the study of second harmonic generation in various material systems and waveguide structures.

The propagation model developed has been applied to the study of second harmonic generation in both LiNbO$_3$ and semiconductor waveguides. Second harmonic generation in waveguides with one-dimensional confinement is first studied and provides a basis for comparative analysis with previously published results. The method is then extended to more realistic guides with two-dimensional confinement. Second harmonic generation by the Cerenkov radiation scheme is illustrated. Quasi-phase matching schemes for enhancing the output power are also discussed. Semiconductor material systems provide the basis for the monolithic integration of optical waveguides and hence are of great technological importance. The method developed is thus applied to the study of SHG in GaAs and AlGaAs devices. Methods of QPM and fabrication tolerances on output power as well as waveguide loss are treated. Finally the phenomenon of cascaded second harmonic generation is considered.

As a first task, it was necessary to determine the modes or characteristic solutions of the waveguide structure through the solution of the stationary wave equation. The finite element vector **H** formulation was thus extended to the study of 3-D waveguides with material anisotropy and diffused index profiles, both the transverse directions. Some new and interesting observations were made. The solution obtained from the above is then used at the second stage, an input for the BPM. A step by step solution of the paraxial wave equation in the propagation direction then produces a second harmonic output. Various types of waveguides are analysed and the results fully discussed.

Symbols and Abbreviations

ATM	Asynchronous Mode Transfer
CW	Continuous Wave
EDFA	Erbium-doped Fiber Amplifiers
FTTH	Fiber to the Home
IO	Integrated Optics
ISDN	Integrated Services Digital Network
OIDA	Optoelectronics Industry Development Association
PIC	Photonics Integrated Circuits
WDM	Wavelength Division Multiplexing
TE	Transverse Electric
TM	Transverse Magnetic
FEM	Finite Element Method
FDM	Finite Difference Method
BPM	Beam Propagation Method
SHG	Second Harmonic Generation
MOCVD	Metal Organic Chemical Vapour Deposition
QPM	Quasi Phase Matching
l_c	Coherence length
α	Attenuation constant
β	Propagation constant
χ	Nonlinear susceptibility constant
Δz	Step size in the propagation direction
ε	Permittivity
π	$pi \cong 3.14159265$
Ω	Discretization domain
λ	Wavelength in μm
μ	Permeability
ω	Angular frequency

Chapter One

Introduction to Optical Waveguide Theory

1.1   Overview of research and development in lightwave technology

Optics is concerned with the propagation and interactions of electromagnetic waves with matter. The study of light has extended the range of human vision. It enabled man to be made aware of the existence of phenomena far beyond the range of normal human vision. The nature of the wave phenomenon itself and of the medium that was postulated to support them remained a mystery until Maxwell considered the properties of electromagnetic waves. The recognition that light is an electromagnetic wave was one of the great milestones of scientific thought. It unified the description of a great diversity of phenomena, and also enabled predictions to be made about previously unknown phenomena. As a natural occurrence, light has been used by man since time immemorial: however, as a means of communication, it was first used when man learnt how to make fire.

Tremendous advances have since been made, particularly after the establishment of the electromagnetic theory of light. Maxwell's electromagnetic theory of light helped to bring into one body some of the diverse aspects of light, and arguably could be said to be the greatest scientific achievement of the 19th century as it has formed the basis of

modern communications technology. Heinrich Hertz demonstrated long radio waves in 1888 and in 1895 Guglielmo Marconi demonstrated wireless communication. Since these pioneering research works, the move has been towards obtaining more powerful communication systems using higher carrier frequencies. The range of applications has also greatly diversified, from early voice communication systems, requiring a bandwidth of 15kHz to analogue television with a bandwidth of 6MHz, through to microwaves for radar applications with frequencies measured in Gigahertz. Optical frequencies are important for of present-day systems, involving optical communications, for example optical switches, optical storage systems and optical computing.

The invention of the laser has given a major boost to the field of optical systems. The first laser operating at a wavelength of 694nm represented an optical frequency of 5×10^{14} Hz. Since the demonstration of this, the ruby laser, the transmission and processing of optical signals has been of the greatest interest to scientists. The exploitation of the tremendous potential bandwidth offered by laser light has been potentially limited by a number of factors:

a)   It was discovered quite early that free space propagation of the laser beam was not a suitable means of establishing effective communications links. Laser light is strongly scattered by rain, fog, smog and snow. There was also the need for a line-of-sight link, and hence the work turned to establishing suitable transmission media. There are, however, a number of applications where it is possible, even desirable, to use free space transmission e.g. communication between satellites in orbit.

b)   Electronic components place a limitation on the bandwidth of any optical communication system, in that it is not yet possible to use the full potential of a $10^{14} - 10^{15}$ Hz system.

A solution to the first of these problems was to allow light to propagate through another medium, which protects it from atmospheric interruptions. The transmission of light by glass (and other transparent media) by multiple internal reflections had been known and used since ancient times. In 1880, Alexander Graham Bell developed a device, the

'Photophone', that varied the intensity of light incident upon it as a function of the amplitude of speech vibrations (Kapany, 1967). The development of this idea was however hampered by very high propagation losses. Early measurements of loss in glass of near infra red light was put at 1000dB per km, which was attributed to the impurities in glass (Kao and Hockham, 1966). This effect was confirmed by Kapron *et al.*, (1970) who succeeded in making pure glass with a loss of 20dB per km and opened up the way for effective fibre optics. Today's optical fibers have a loss of less than 0.2dB/km on certain spectral bands.

1.1.1   Research trends in optoelectronics

The development of low loss optical fibre has helped address the problem of suitable transmission media for modern optoelectronic systems. Present day optical fibres have transmission rates of over two billion bits per second over hundreds of kilometres with an error of about one per billion bits and performance figures are improving year by year. Along with the development of low loss optical fibre came the development of the compact single mode semiconductor laser since the early 1960s (Hall *et al.*, 1962; Nathan *et al.*, 1962; Quist *et al.*, 1962). By the early 1970s semiconductor lasers were providing continuous wave (cw) coherent sources of laser light (Alferov *et al.*, 1970; Hayashi *et al.*, 1970). Improvements from the 1980s made them reliable sources for use in optical communications systems.

Optical signals transmitted using optical fibres will ultimately have to be converted into electronic form for processing. The speed of operation of electronic components is a major determining factor in the bandwidth of a communications system. This limitation has led to major research into a field now known as optoelectronics, replacing electronic devices with optical devices, switches, modulators, filters, transmitters, connectors and receivers. The potential of this new field is enormous. Will the development of an optical switch eventually lead to an optical computer? That is the hope and aspiration of many workers in this field. Advances in recent times in optoelectronics have led to the development of a wide range of optical components and devices such as directional couplers, Y-branches, waveguide crossings, optical filters, modulators, optical amplifiers

and many others (Tamir, 1979). These advances in optical technology have resulted in the availability of consumer goods based on optical technology, such as laser copiers, laser printers, barcode readers, CD players and many others.

Research in the now established field of optoelectronics has developed along the following five main directions:

1. Optical communications systems
2. Optical storage technology
3. Waveguide devices and optoelectronic packaging technology
4. Photonic devices and materials
5. Optical sensor technology, including speciality fibers

1.1.1.1   Optical communications systems

Research in this area has been mainly in the area of telecommunications, local area networks and optical intercommunications. Many commercial organisations are building their research, development, and marketing programs around multimedia concepts like Visual, Intelligent, and Personal communications systems. The potential role of optoelectronics in the development of such systems cannot be overstated. These technologies, which enable such multimedia systems to be developed, include high-speed digital communications, switching, high-capacity information storage, image processing, high-definition and flat-panel displays, new kinds of consumer electronics and local networks.

High-speed digital transmission (10 Gbit/s and beyond), and switching for telecommunications have been major development thrusts for companies like Lucent, Alcatel, Fujitsu, Hitachi, and NEC for nearly two decades. Transmission equipment developed by these companies pioneered the use of single-mode fiber, high bit rates, and long wavelengths. Some of these companies were early to commit to the Asynchronous Transfer Mode (ATM) standard for multiplexing and switching.

Two important systems recently developed have been synchronous digital hierarchy (SDH) ~10 Gbit/s trunking systems using optical amplifiers (erbium-doped fiber amplifiers or EDFAs) for amplification at 1550nm, and fiber to the home (FTTH) systems capable of a two-way ISDN (integrated services digital network) at 1310nm, combined with one-way video at 1550nm. These systems will pave the way for interactive broadband services for homes and small businesses, generally accepted as a key requirement for the so-called "Information Age" revolution just now beginning. Equipment for fiber-optic broadband systems was forecast by the end of the 20th century to constitute two-thirds of all optical communications equipment sales, with a total value of \$12 billion; and by 2003, fiber-optic broadband equipment is forecast to constitute three-quarters of \$30 billion in total optical communications sales (OIDA 1994). (The corresponding worldwide markets for all optoelectronics, including displays and storage, are estimated at \$140 billion and \$230 billion, respectively, in those years.)

1.1.1.2   Optical storage technology

Optical data storage, which once appeared to be a failing technology in the marketplace, is quickly finding its way into homes and offices with the multimedia revolution. In the past, it was believed that optical storage, because of its long access times, would not be a significant threat to magnetic storage. However it has become one of the important enabling technologies fusing together the entertainment and computing industries. Developments in optical storage technology underlie developments in multimedia systems and it is envisaged that it will form one of the major optoelectronics technologies for this, the twenty-first century.

As in all data storage systems, optical disk systems are characterised by their storage capacity, data transfer rate, access time, and cost. The wavelength of the laser used for "read and write" operations imposes a fundamental limitation on the information storage density and the speed of data retrieval. The storage capacity of an optical storage system is a direct function of spot size (minimum dimensions of a stored bit) and the geometrical dimensions of the media. A good metric to employ to assess the efficiency

in using the storage area is the areal density (MB/sq. in.). Areal density is governed by the resolution of the media, the numerical aperture of the optics and the wavelength of the laser in the optical head used for recording and readout. The data transfer rate in an optical recording system operating at a fixed rotational speed is inversely proportional to the laser wavelength. Research and development in the field of optical storage is typically directed at:

- Reducing the spot size using lower-wavelength light sources

- Reducing the weight of optical pickup heads using holographic components

- Increasing rotation speeds using larger optical power lasers

- Improving the efficiency of error correction codes; and increasing the speed of the servo systems.

The introduction of the CD format in the late 1980s, opened up another direction for optical storage devices. Due to their low-cost replication capability, high capacity, robustness, and removability, optical CD-ROM systems have become competitive with magnetic floppy disks for applications such as software distribution and home multimedia applications. The success of CD-ROM technology in the consumer market has allowed the cost of optoelectronic components such as CD lasers to drop sharply over the last few years, paving the way for new applications and new optical storage systems. It is expected that CD systems will remain essential for the wide commercial acceptance of optical storage systems in the years to come.

Those features which uniquely make optical storage systems attractive are their higher capacity per disk, removability, mass replicability, and long memory persistence for archival applications. They are most commonly used for software distribution, backup memory for personal computers and workstations, external memory for some mainframes, and a large-capacity off-line memory. Key applications include text and graphics filing, statistical data and ledger storage, public and historical database storage,

and possibly as a replacement for paper. New applications and markets opening to optical storage systems as their prices are dropping include home multimedia, multimedia servers, high-definition television and digital videodisks (DVD), and massive storage systems.

1.1.1.2.1 The Data Storage Market

The growth of any data storage market is determined by various information processing and storage applications. For the optical storage market, it is a new application, multimedia entertainment systems, which is fuelling its growth. The volume of the data storage market approached $100 billion as early as 1994, of which the hard disk segment was $47 billion, the magnetic tape segment $42 billion, and the optical disk segment $6 billion.

In the past, the majority of desktop computing users did not need such a high capacity of data storage. However, during the 1993-95 period, the advent of image computing and processing of multimedia documents with still images has quickly raised the floor of the minimum useful desktop storage capacity to about 1 GB. This has made optical storage devices more attractive. As a consequence, demand for optical storage devices exceeded supply in 1994 for the first time. With increasing demand, most optical storage manufacturers have continued to drop prices to increase their market share. An optoelectronics Industry Development Association (OIDA) survey predicts an explosive growth in the optical storage market of $50 billion by the end of the next decade (2010). It is believed that video- and computing-related products will strongly support this growth.

1.1.1.2.2   Emerging optical storage technologies

For any storage technology to remain competitive over time, it is critical that its access time, system volume, and cost be kept constant (or preferably reduced) while its capacity and data rate are increased. This requires low-cost pickup sensors that can move quickly and accurately to access an increasing amount of data. Mechanical constraints dictate

that fast and accurate movements can only be achieved over short distances; this consideration leads to the conclusion that data must be kept as *local* as possible with respect to the pickup heads. Historically, this consideration has driven the increase in areal densities, allowing much larger amounts of data to be stored, accessed, and retrieved without an increase in access time and system cost.

However, as optical areal densities approach optical diffraction limits, researchers have started seeking new solutions. On the one hand, solutions may entail further increasing the areal density by combating the diffraction limits of optics using, for example, near-field optics. On the other hand, solutions may take advantage of additional available dimensions such as are proposed for various 3-D optical storage concepts. Indeed, data residing in a volume may be considered as being local to the pickup sensors if both the performance cost and actual cost of accessing it in 3-D is affordable. In this case, *volumetric density* (Mbit/in^3) becomes critical. The volumetric density is governed by the effective volume of the spot, which in turn is limited by the volumetric resolution of the medium, the numerical aperture of the optics, the wavelength, and the positional accuracy of the pickup head in the third dimension. The spot size is limited by the recording wavelengths through diffraction effects, as well as by the sensitivity and integration time of the readout detector. The approach promises low-cost, high-volumetric-density ROM disk media with a thousand or more layers for image storage, and also low-cost compact disk player drive units employing semiconductor blue and/or green lasers.

The potential impact of layered 3-D optical disks on the capacity of optical storage can be much greater than the impact of, for example, the use of blue lasers. This is because the growth factor in capacity is directly proportional to the number of layers. Assuming that the areal density is not affected, the 3-D layering provides the potential for realising optical disks with capacities exceeding 100 GB, beyond the turn of the millennium. If this factor is now coupled with a reduction in spot size, then the potential storage capacity of optical storage systems will be phenomenal.

A major increase in capacity is expected over the next 3 to 5 years using lasers with progressively shorter wavelengths. As mentioned earlier, areal density is governed by

spot size. This can be expressed in terms of the wavelength (λ) and the numerical aperture (NA), of the optical system as:

$$\text{spot size} = \frac{1.8\lambda}{NA}$$ 1.1

In order to reduce the spot size, the numerical aperture may be increased, or the wavelength may be reduced. However, since the numerical aperture also affects the depth of focus (and the depth of focus is directly proportional to NA), increasing the numerical aperture imposes restrictions on the media thickness and the servo controllers. Practically, it is expected that the numerical aperture will be increased only up to 0.62 from its present value of 0.55, allowing an increase in the storage capacity of about 12%.

It is anticipated that laser wavelengths used will change over the coming years from the present standard of 780 nm to 430 nm with the development of the low cost blue laser. This would lead to an increase in the information storage capacity by a factor of nearly four and also more than double the data transfer rate. Sony is actively pursuing this direction by developing zinc-selenide-based lasers. They have currently developed such a laser operating at room temperature, still with a relatively short lifetime. In contrast, researchers at Nichia are actively pursuing GaN-based lasers. They have demonstrated lasing using this material (Nakamura, 1994) and remain active in commercialising such devices. The major drawback at present of these lasers has been their extremely short operating lifetimes but work to improve this aspect is underway. Growing GaN on a lattice mismatch Al_2O_3 substrate is also accompanied by a large number of defects but work is continuing to overcome these difficulties.

An alternative method of obtaining shorter wavelengths is by use of frequency-doubled blue lasers, through the non-linear process of second harmonic generation. Several laser-based blue-green sources are now under development and systems are commercially available. These frequency conversion technologies rely on the availability of suitable laser diodes, which must meet stringent requirements of high output power, single spatial mode, spectral stability and operate within a specific range of wavelength. Efficient harmonic generation requires that the harmonic and the fundamental waves travel with a

fixed phase relationship. Where this is not feasible, then the direction of the spontaneous polarisation is reversed in the non-linear waveguide at regular intervals, which corresponds to the situation when the two waves are out of phase by 180°. Work in both directly generated and second harmonic devices is continuing at a rapid rate.

1.1.1.3   Guided wave devices

Another area of intensive research has been photonic devices and materials, with the emphasis on laser and optoelectronic integrated circuit technology, including both surface-emitting and edge-emitting lasers, as well as devices for use in telecommunications, sensors, and consumer products. Within the past decade, guided wave, or integrated optical (IO) components in various materials have become available from a variety of vendors, world-wide and are now being deployed in commercial systems. Integrated optical devices include modulators and passive circuits in LiNbO$_3$, glass, and semiconductors; these devices are applied to telecommunications, cable television (CATV), and instrumentation.

These components are key to advanced transmitters in many fiber-optic-based CATV and long haul telecommunications systems. The devices themselves are based on planar optical waveguides, in which light is confined to channels at the substrate surface and routed on the chip. These channels are typically less than a few microns across and are patterned using microlithography techniques. Using appropriate optical circuits based on channel guides, both passive functions (i.e., power splitting from one to several channels) and active functions (i.e., electrical-to-optical signal conversion, known as modulation) can be performed on the light. The primary materials used in the commercial market are glass (bulk or SiO$_2$/Si) for passive devices and LiNbO$_3$ for active devices. A closely related technology that is in the research stage is the development of photonic integrated circuits (PICs), in which a variety of semiconductor optoelectronic devices are monolithically integrated and interconnected with waveguides such as lasers and modulators.

Applications for integrated optics have historically been in niches of the analogue, digital, and sensor fiber-optic markets; at present, however, major new markets are emerging. Perhaps the largest new market is telecommunications, where IO devices will be used for multigigabit data transmission, signal splitting and loop distribution, and bi-directional communication modules. A second new market is CATV, where IO modules will be used for external modulation in fiber-optic-based signal distribution systems. In both telecommunications and CATV, IO devices enable signal transmission at higher data rates and over longer distances. In a third market, instrumentation, a major application is fiber-optic gyroscopes. An early market study of IO modulators predicted a 24% annual growth rate in North America over the 1993 - 2003 period (Tamir 1987). A significant portion of this growth was for aerospace and military applications (e.g., fiber gyros). The forecast annual sale by 2003 is nearly $200 million. The photonics market enabled by IO modulators (e.g., transmitters and gyros) is many times larger and is expected to exceed $1 billion.

Closely coupled to this work are efforts to pigtail multiple fibers, at once, to an IO circuit (IOC). Research and development (R&D) efforts at major centres in the world are focused on large planar lightwave circuits (PLCs), including planar erbium-doped amplifiers, components for wavelength division multiplexing (WDM), and structures for the silicon microbench. Much of the leading research has been performed at AT&T in the United States and NTT in Japan. In the semiconductor modulator area, the major focus is on developing devices suitable for 10 Gbit/s communications. For example, Hitachi is working on a discrete modulator and an integrated diode laser and an electroabsorption modulator is under development at AT&T in the United States and at NTT, NEC, and Fujitsu in Japan.

Commercial IOCs (based on annealed proton-exchange waveguides in $LiNbO_3$) are available and widely used. IOCs are being used in telecommunications for high-speed modulation, signal splitting and switching and bi-directional communication. $LiNbO_3$ modulators are being used in 2.5 Gbit/s (OC-48) systems to enable transmission over distances of greater than 100 km without repeaters. $LiNbO_3$ modulators make it possible to use CW (continuous-wave) 1.5 micron lasers that have closely spaced wavelengths for transmission over the standard fiber already installed, which is

optimised for 1.3 micron operation. Since installing new fiber is a major cost, the externally modulated multigigabit approach is a significant cost-saver for long-haul telecommunications operating companies. With such systems, 10 Gbit/s system operation is achieved, for example, by multiplexing four wavelength channels at 2.5 Gbit/s each.

Interest in $LiNbO_3$ modulators for radio frequency (RF) link applications is being actively pursued at many research centres. The development of hybrid integrated optical disk pickup heads and quasi-phase-matching structures for diode laser frequency doubling is a topic of major research interest. Work on guided wave devices in many places is focused on linearized modulators, high-speed and high-optical-power modulators, modulators with gain, and frequency-doubled structures all using $LiNbO_3$. In Japan, interest in quasi-phase-matching in $LiNbO_3$ for frequency conversion is being researched at Oki for 1.5 micron applications and at Sony for frequency doubling (blue light generation).

1.1.1.4   Photonic devices

Research in the area of photonic devices can be classified into the following major categories: semiconductor light-emitting diodes (LEDs), lasers, semiconductor optical amplifiers, switches, and integrated receivers.

LEDs are the light sources used for many semiconductor-based devices. The AlGaInP material system is widely used in generating highly efficient red light for the automobile industry and in traffic light systems and also finds application in optoisolators and low data rate (<50Mbit/s) optical links.

Lasers have been widely used in a number of areas: transmission lasers, pumping lasers for erbium (Er)-doped fiber amplifiers and local-loop or access lasers, are used mainly in the telecommunication industry. Included in the category of transmission lasers are photonic integrated circuits (PICs), wavelength-division multiplexed (WDM), and time-division multiplexed (TDM) laser sources, and 1.3 micron and 1.55 micron wavelength

devices based on InP. Analogue lasers are used mainly in the cable TV or other subcarrier multiplexing applications, although they are finding increasing application in satellite communications and phased-array radars. Visible, shorter-wavelength lasers are used for optical storage, sensing, or display applications.

The use of lasers in compact optical disk players has brought about a revolution in the diode laser industry. For the first time, there has been created an application that requires the production of more than a few thousand units per month. Thus the corresponding advantages of real mass production can be employed. Rohm, a resistor manufacturing company that expanded into lasers, perhaps best illustrates these advantages. Through the heavy use of automation (previously foreign to the laser diode business), Rohm was able to capture half of the CD market, and in 1994 produced about 60 million laser diodes. This kind of demand has now pushed the price down to less than $1 per laser, even with the conventional cleaved-facet technology.

Besides optical storage, major applications for lasers in the 600-800 nm range lie in optical pointers, bar-code scanners, printers, data links, and displays. The production of laser pointers relies upon visible light emission, and wavelengths in the 630-650 nm range are much better for visibility than those at approximately 670 nm, even though higher power tends to be available there. For the print heads and bar-code scanners an analogous argument holds, but here the shorter-wavelength lasers are preferable because of the sensitivity of the detecting medium. For display, again, the 670 nm is somewhat too long.

1.2   Nonlinear effects in optics

Much of the economic potential to be realised through the application of optics in telecommunications and information processing can be ascribed to the best use of the nonlinear effects in optics. In recent years, there has been a significant increase in the number of published papers on nonlinearity in optics, due mainly to their economic potential. The foundation of the subject was laid in the early 1960s with the pioneering

work of several groups, e.g. Franken *et al.* 1961, Franken and Ward, 1963, Boyd *et al.*, 1965, Armstrong *et al.*, 1962, Miller, 1964.

Most material media exhibit weak nonlinearities if exposed to electromagnetic radiation of high intensity. The discovery of many of these nonlinear effects and especially their development however has been made possible by the invention of the laser, when the practical applications of these effects were quickly realised. At very high intensities, the light waves may interact with each other or with the material medium. These nonlinearities arise from an anharmonic motion of electrons in response to the applied field. This can lead to the observation of several effects, the most important of which can be divided into two classes depending on their origin, be it quadratic or cubic.

If the material is regarded simplistically as a collection of charged particles, then with the application of an electric field, an oscillation is induced in the electron cloud. At relatively low intensities, the induced polarisation, the displacement of the electron cloud or dipole, *P* is directly proportional to the magnitude of the electric field of the lightwave

$$P = \chi E \qquad\qquad 1.2$$

where χ is the linear optical susceptibility, a function of the refractive index of the material. It is well known in physics, that the linear dependence of one physical quantity on another is almost always an approximation, and valid only over a limited range. The most familiar example is Hooke's law of elasticity. Laser light generates very intense fields, which give rise to nonlinear optical effects and the expression for the polarisation can then be written as (a detailed derivation is given in Chapter 3)

$$P = \chi^{(1)} E + \chi^{(2)} E^2 + \chi^{(3)} E^3 + ... \qquad\qquad 1.3$$

where $\chi^{(2)}$ and $\chi^{(3)}$ are constants, the second and third order susceptibilities.

1.2.1 Quadratic nonlinear effects

The second term of equation 1.3 gives the quadratic polarisation term which gives rise to effects, which are all of the mixing (interaction of light with nonlinear dielectric) type. This involves the generation of sum and difference frequencies, which may take a variety of forms. These are

Second harmonic generation: This is the coalescing of two identical photons. It represents a special case of a process more commonly known as sum frequency generation. In this process, light waves at two different frequencies are summed to form the output. When the applied optical field contains just one frequency, i.e. when the two waves are equal in frequency, power or amplitude, the quadratic polarisation will contain a static term and a term oscillating at twice the applied frequency. The polarisation oscillating at twice the applied frequency radiates into the medium, giving rise to SHG. The overall effect of this process can be described as follows: part of the energy of an optical wave of frequency ω propagating through a crystal is partly converted to that of a wave at 2ω.

Parametric amplification: This is used to build a signal from a zero value. If power is provided at the frequency ω_3 and the power at the frequency ω_2 is initially assumed to be zero then the growth in the signal power at $\omega_2 = \omega_3 - \omega_1$. It is assumed here that $\omega_3 \gg \omega_1$. It must also be noted that the power at ω_1 is amplified. Thus this device generates an 'idler' signal at ω_2 and at the same time amplifying the signal at ω_1. In effect, power from a 'pump' wave at ω_3 is transferred to waves at frequencies ω_1 and ω_2, where $\omega_3 = \omega_1 + \omega_2$. Fundamentally it is similar to second harmonic generation but the difference is in the direction of the flow of power. In this process $\chi^{(1)}$ is changed by an amount proportional to the pump intensity.

Frequency Up-Conversion: This is used to convert a signal from a low frequency ω_1 to a high frequency ω_3 by mixing it with a strong laser beam at ω_2, such that

$\omega_1 + \omega_2 = \omega_3$. It is also another special case of sum frequency generation. From a quantum mechanical point of view, this can be thought of as the annihilation of photons at frequencies ω_1 and ω_2, and the generation of a photon at ω_3. This can be used in the detection of infrared radiation by converting the frequency into the visible or near visible part of the spectrum.

The linear electro-optic (Pockels) effect: This is the linear variation in the refractive index of a dielectric medium caused by the application of a static electric field. This is the simplest of the mixing processes. In this, one of the frequencies is zero i.e. an optical wave is sent through the medium in the presence of a dc electric field. The quadratic polarisation will then contain a term proportional to the product of the optical and dc fields, in effect being equivalent to changing $\chi^{(1)}$ by an amount proportional to the dc field. This causes the medium to become electrically anisotropic, thus making the phase velocity of the propagating wave dependent on the direction of the electric field vector of the wave. This phenomenon is useful in the design of phase modulators. If the change in phase velocity is dependent on an applied field, it then follows that phase or frequency modulation can be achieved in the medium.

1.2.2 Cubic nonlinear polarisation effects

Cubic nonlinear effects arise from the cubic polarisation term $\varepsilon_o \chi^{(3)} E^3$. This gives rise to third harmonic generation, quadratic electro-optic effects, two-photon absorption and other related mixing phenomena, i.e.

The quadratic Electro-optic effect: It is the simplest case of effects arising from cubic polarisation. This is the variation arising in the refractive index due to a quadratic term. An optical wave propagating through a medium in the presence of direct current (dc) field causes a change in the refractive index of the material proportional to the square of the direct current field. This effect is also known as the Kerr effect and may be used in fast acting optical shutters.

Third harmonic generation: This can occur when an incident field at frequency ω induces a polarisation at the frequency 3ω. This process is governed by the third order nonlinear susceptibility tensor $\chi^{(3)}$. An optical field propagating through a nonlinear medium induces a cubic polarisation, which is proportional to the third power of the field. The refractive index is thus modulated by an amount proportional to the optical intensity. The induced nonlinear polarisation may then generate a travelling wave at the third harmonic frequency.

Two-photon absorption: If two intense electromagnetic waves at frequencies ω_1 and ω_2 propagate through a medium, then there is the probability that some energy will be absorbed from both of these waves as result of the transition at the sum frequency ω_t where $\omega_t = \omega_1 + \omega_2$. In semiconductor materials the transition is usually between the valence and conduction bands. This phenomenon can be used for the observation of extremely short light pulses.

Raman effect: Given light of a particular frequency, travelling in a dielectric medium, it is then possible to observe weak side bands of radiation close to the frequency of the incident light. The vibrational resonant frequency of the material determines the difference from the incident frequency of the side bands. This phenomenon is similar to a parametric processes: however there are two main differences. The 'idler' wave will now be replaced by an internal oscillation of the molecule, in other words a mechanical crystal vibration instead of the electromagnetic idler wave. This phenomenon is therefore possible only in materials whose molecules are capable of vibrational oscillation. No phase matching is also required. The spontaneous Raman effect is used in the spectroscopic investigation of the structure of molecules whereas the stimulated Raman effect is used in the design and fabrication of optical amplifiers and oscillators.

1.3   Fundamental Theory underlying optical waveguide analysis

The field of integrated optics can broadly be classified into areas involving optical fiber waveguides and the optical integrated circuits (Hunsperger, 1984). The optical integrated

circuit (OIC) can be regarded as the optical equivalent of the conventional electronic circuit, where the fundamental material that interconnects the various devices of an OIC is the optical waveguide. Unlike electrical circuits where the signal is carried by a current, the signal in an optical waveguide travels in distinct optical modes. A mode can simply be regarded as the spatial distribution of optical energy in one or more dimensions. In this section, Maxwell's equations for the propagation of waves in optical waveguides are presented, and different types of waveguides are then reviewed.

1.3.1 Maxwell's Equations

The work presented in this thesis is based on a numerical solution of Maxwell's equations, which govern the propagation of light through an optical medium and its interaction with the medium. These equations are valid for the entire frequency spectrum and in differential form can be stated as follows:

$$\nabla \times E + \frac{\partial B}{\partial t} = 0 \qquad \text{(Faraday's law)} \qquad 1.4$$

$$\nabla \times H - \frac{\partial D}{\partial t} = 0 \qquad \text{(Maxwell-Ampere law)} \qquad 1.5$$

$$\nabla \cdot D = \rho \qquad \text{(Gauss's law)} \qquad 1.6$$

$$\nabla \cdot B = 0 \qquad \text{(Gauss's law magnetic)} \qquad 1.7$$

For a lossless dielectric isotropic material, the electric **E** and magnetic **H** field vectors are related through the constitutive equations

$$D = \varepsilon E + P \qquad 1.8$$

$$B = \mu H \qquad 1.9$$

In the above **D** is the electric flux density (coulombs/m^2), **B** is the magnetic flux density (webers/m^2), ρ is the charge density, $\mu_o = 4\pi \times 10^{-7}$ F/m is a constant equal to the magnetic permeability of a vacuum and ε_o is the vacuum dielectric permitivity.

Assuming complex time dependence through the factor $\exp(j\omega t)$, where j is an imaginary unit, ω the angular frequency and t is time, and substituting for **B** and **D**, the time derivatives in the above equations may be rewritten as

$$\nabla \times \mathbf{E} + j\omega\mu\mathbf{H} = 0 \qquad\qquad 1.10$$

$$\nabla \times \mathbf{H} - j\omega\varepsilon\mathbf{E} = 0 \qquad\qquad 1.11$$

Taking the curl of these equations and making the necessary substitution from equations (1.4) and (1.5), equations (1.10) and (1.11) could be written as follows

$$\nabla \times \nabla \times \mathbf{E} - \omega^2\mu\varepsilon\mathbf{E} = 0 \qquad\qquad 1.12$$

$$\nabla \times \nabla \times \mathbf{H} + \omega^2\mu\varepsilon\mathbf{H} = 0 \qquad\qquad 1.13$$

Using the following vector identity

$$\nabla \times \nabla \times \mathbf{A} = \nabla(\nabla \cdot \mathbf{A}) - \nabla^2\mathbf{A} \qquad\qquad 1.14$$

the first terms of equations (1.12) and (1.13) may be written as

$$\nabla(\nabla \cdot \mathbf{E}) - \nabla^2\mathbf{E} - \omega^2\mu\varepsilon\mathbf{E} = 0 \qquad\qquad 1.15$$

$$\nabla(\nabla \cdot \mathbf{H}) + \nabla^2\mathbf{H} + \omega^2\mu\varepsilon\mathbf{H} = 0 \qquad\qquad 1.16$$

For a perfect insulator with no stored charges, the above two equations simplify to

$$\nabla^2 E + \omega^2 \mu \varepsilon E = 0 \qquad\qquad 1.17a$$

$$\nabla^2 H + \omega^2 \mu \varepsilon H = 0 \qquad\qquad 1.17b$$

These two equations can be written as:

$$\nabla^2 E + k^2 E = 0 \qquad\qquad 1.18a$$

$$\nabla^2 H + k^2 H = 0 \qquad\qquad 1.18b$$

where the wavenumber, $k = \omega \sqrt{\varepsilon \mu_o}$.

The equations (1.17) or (1.18) provide the general solution to Maxwell's equations in terms of material properties and the angular frequency of the electromagnetic signal. It is these two equations, which need to be solved for a particular waveguide structure, with appropriate boundary conditions, in order to obtain the optical mode, in other words the field and its characteristics.

1.3.2 Planar waveguides

Various types of optical waveguides exist, the simplest of which is the 2 dimensional (2-D) or planar waveguide. The 2 dimensional waveguide enables the confinement of light in one direction (y) whilst allowing it to spread in the other direction (x).

Fig.1.1 Example of a planar waveguide

For the waveguide that is shown in Fig 1.1, n_g is the refractive index of the guide core, n_c is the refractive index of the upper cladding and n_s is the refractive index of the substrate region. For a three layer asymmetric planar waveguide, the refractive indices are related as follows: $n_c < n_s < n_g$ and hence the light can be trapped inside the guide core. When the substrate index and the index of the upper cladding are equal $n_c = n_s$ then a symmetric guide is obtained. In the above, the refractive index is assumed to be a constant value within specified sections of the guide. Many waveguides have a graded index where the refractive index changes gradually as a result of the fabrication technique employed. Such waveguides will be considered in detail in a later section of the thesis.

1.3.2.1   Basic Equation

Expanding the curl operator in equation (1.17) in the rectangular co-ordinate system, where z is the propagation direction, the following is obtained

$$\frac{\partial^2 E}{\partial x^2} + \frac{\partial^2 E}{\partial y^2} + \frac{\partial^2 E}{\partial z^2} = -\omega^2 \mu \varepsilon E \qquad\qquad 1.19$$

The field vector **E** can be separated into the individual component parts, such that there is an equivalent differential equation for each of the vector components.

$$\frac{\partial^2 E_x}{\partial x^2} + \frac{\partial^2 E_x}{\partial y^2} + \frac{\partial^2 E_x}{\partial z^2} = -\omega^2 \mu\varepsilon E_x \qquad\qquad 1.20a$$

$$\frac{\partial^2 E_y}{\partial x^2} + \frac{\partial^2 E_y}{\partial y^2} + \frac{\partial^2 E_y}{\partial z^2} = -\omega^2 \mu\varepsilon E_y \qquad\qquad 1.20b$$

$$\frac{\partial^2 E_z}{\partial x^2} + \frac{\partial^2 E_z}{\partial y^2} + \frac{\partial^2 E_z}{\partial z^2} = -\omega^2 \mu\varepsilon E_z \qquad\qquad 1.20c$$

1.3.2.2   Analytic solution

In a planar waveguide structure, the field quantities are assumed to vary in only one transverse direction. Considering the three-layer waveguide structure shown in Fig. 1.1, and assuming the light confinement to be in the y-direction, then the partial derivative along the x-direction can be written as $\frac{\partial}{\partial x} = 0$. If the parameter ϕ is now defined such that

$$\phi = \begin{cases} E_x & \text{For TE mode} \\ H_x & \text{For TM mode} \end{cases} \qquad\qquad 1.21$$

then equations (1.18a and b) can be written as

$$\frac{\partial^2 \phi}{\partial y^2} + \left(k_o^2 n^2 - \beta^2\right)\phi = 0 \qquad\qquad 1.22$$

where $n = \sqrt{\varepsilon_r}$ and β is the phase constant.

For 2-D waveguides, the TE mode has no longitudinal component of the electric field, $E_z = 0$. The non-vanishing field components are thus defined as:

$$H_y = \frac{\beta}{\omega\mu} E_x \qquad\qquad 1.23$$

$$H_z = \frac{1}{j\omega\mu} \frac{\partial E_x}{\partial y} \qquad\qquad 1.24$$

$$E_x = \frac{\beta}{\omega\varepsilon} H_y + \frac{1}{j\omega\varepsilon} \frac{\partial H_z}{\partial y} \qquad\qquad 1.25$$

For TM modes, there is no magnetic field component along the direction of propagation, $H_z = 0$. The only non-vanishing field components are thus

$$E_y = -\frac{\beta}{\omega\varepsilon} H_x \qquad\qquad 1.26$$

$$E_z = -\frac{1}{j\omega\varepsilon} \frac{\partial H_x}{\partial y} \qquad\qquad 1.27$$

$$H_x = -\frac{\beta}{\omega\mu} E_y - \frac{1}{j\omega\mu} \frac{\partial E_z}{\partial y} \qquad\qquad 1.28$$

The solutions to (1.22) are either exponential or sinusoidal functions of y in each of the regions of the waveguide. The particular function is dependent on the factor $\left(k_o^2 n^2 - \beta^2\right)$. For the three-layered asymmetric planar waveguide, for a guided wave the phase constant β will satisfy the following condition $k n_s \leq \beta \leq k n_f$. Equation (1.22) will therefore have the solution (Koshiba, 1992)

$$\phi = \begin{cases} A_c \; exp(-\alpha_c \, y) & 0 \le y \\ A_f \; cos \, k_f \, y + B_f \; sin \, k_f \, y & -t \le y \le 0 \\ A_s \; exp[\alpha_s (y+t)] & y \le -t \end{cases} \qquad 1.29$$

In the above A_f , B_f , A_c and A_s are arbitrary constants determined by the boundary conditions, which must be satisfied at the interface of two media [Appendix 1]. The values $\alpha_c , \alpha_s ,$ and k_f are defined as

$$\alpha_c = \sqrt{\beta^2 - k^2 n_c^2} \qquad\qquad 1.30$$

$$\alpha_s = \sqrt{\beta^2 - k^2 n_s^2} \qquad\qquad 1.31$$

$$k_f = \sqrt{k^2 n_f^2 - \beta^2} \qquad\qquad 1.32$$

These are well-confined modes normally referred to as TE$_0$/TM$_0$ and TE$_1$/TM$_1$ modes. For $\beta > kn_f$, the function ϕ must be exponential in all three regions, which would imply infinite energy in the upper and lower cladding of the waveguide (Hunsperger, 1984). Such a mode will, of course, not exist. A substrate radiation mode is obtained for a value of $kn_s > \beta > kn_c$ and this mode is confined at the interface of the upper cladding but varies sinusoidally in the substrate. Such a mode can only be supported over short distances as it losses energy from the guiding region to the substrate region and hence is not very useful in signal transmission. It may, however, prove useful in tapered coupler applications. The number of modes that can be supported by a waveguide depends on the thickness of the waveguiding layer and on the material properties of the waveguide, as well as on the frequency. This implies that for a given waveguide thickness and given refractive indices, there is a cut-off frequency, ω_c below which waveguiding cannot occur. In optical waveguide applications, the wavelength is of fixed value, and the problem is therefore to determine the refractive index values for which a particular mode can be supported. It can be shown that for the asymmetric waveguide, the refractive

indices are related through $\Delta n = n_f - n_s \geq \dfrac{(2m+1)^2 \lambda_o^2}{32 n_f t^2}$, (Hunsperger, 1984), where $m =$

0,1,2... is the mode number, λ_o is the vacuum wavelength and t is the thickness of the waveguiding layer.

1.4   Methods of solution of optical waveguide problems

The properties of planar waveguides, useful in many applications can be studied by means of using analytic methods. Exact analytical solutions can also be obtained for planar guides with stepped refractive index values but for a continuously graded index guide, it is rather difficult to obtain exact analytical solutions. Planar waveguides, useful in many applications have a limited range of use due to their one-dimensional optical confinement. In many applications, two-dimensional confinement is required, and this can be provided by channel or three-dimensional waveguides. It is not possible to obtain exact analytical solutions to such waveguides, except in very special cases, and many practical waveguides have complex structures with arbitrary index distribution. The propagation mode is often a hybrid mode, E_{mn}^x (the main components of the electromagnetic field being E_x and H_y) or E_{mn}^y (the main components of the electromagnetic field being E_y and H_x) modes, where the subscripts m and n refer to the mode order such that m, $n = 1,2,3...$, corresponding to the total number of extrema appearing in distribution of the electric fields in both the x and y directions. In reality, one of the modes is dominant, TE^y in the case of E_{mn}^x mode and the TM^y in the case of E_{mn}^y where the existence of such modes compounds the complexity of obtaining an analytical solution. Amongst the many other reasons why it is difficult to obtain an exact analytical solution to Maxwell's equations are the following major factors:

    a.   the electromagnetic field may extend beyond the guide core

    b.   anisotropic materials and non-linear optical materials may be used to extend the range of applications of the waveguide and

c.   materials with complex refractive index such as in semiconductors may be used.

d.   Waveguide cross-section may be of irregular geometry

1.4.1 Approximate analytical methods

In view of the difficulties outlined above, various methods have been developed over the years for the analysis of waveguide problems. These methods can broadly be classified into two main categories, approximate analytical methods and numerical methods. The first group includes such approaches as circular harmonic point matching (Goell, 1969), the effective index method (Hocker and Burns, 1977), the spectral index method (Burke, 1990) and the Marcatili method (Marcatili, 1969). Some of the approximate methods provide very good results for the analysis of waveguides far from cutoff but many of these methods are not very suitable for the analysis of a wide range of important practical waveguides. Some of these methods are considered below.

1.4.1.1   Marcatili method

A channel waveguide is an example of a practical waveguide device. Such a structure will consist of a guide region surrounded on all sides by a confining medium of a lesser refractive index. Such a waveguide is difficult to analyse exactly. Marcatili (1969) derived an approximate solution to the rectangular waveguide problem by considering the structure shown in Fig. 1.2. A knowledge of fields in the two slab waveguides, obtained by extending to infinity the width and height of the guide core, is used to approximate the field in the rectangular core. The key assumption in this analysis is that the modes are well guided i.e. far from the cut off region. Within the guide core, the field is assumed to vary sinusoidally and to decay exponentially within the substrate region. With these assumptions and by matching the boundary conditions along the walls of the core region only, the transcendental equations are derived for each transverse direction (Tamir, 1990). The propagation constant is obtained from the simultaneous solution of

the transcendental equations with the assumption that most of the power is within the guide region.

Fig. 1.2. Cross-sectional representation of channel waveguide.

This approach, even though valid for well-confined modes, gives poor results near to cut-off (Chiang, 1994). An exact scalar formulation has been reported by Kumar *et al.* (1983) for a similar rectangular structure used by Marcatili. By using perturbation techniques, more accurate propagation characteristics of practical integrated optical waveguides were obtained.

1.4.1.2   The effective index method

Knox and Toulios (1970) first introduced the Effective Index Method. This is an improvement on the Marcatili method and has been extensively used by many research workers in view of its simplicity. In this approach two equivalent slabs are used to replace the core of the rectangular structure where each of these 2-D structures can then be considered homogeneous in either the *x* or the *y* directions, as shown in Fig. 1.3 (Koshiba, 1992).

Fig. 1.3 A model for the effective index method

The transcendental equation is obtained by applying the appropriate boundary conditions for one of the transverse directions. The effective index thus obtained by solving the transcendental equation is further used as the refractive index in the solution of the transcendental equation in the other transverse direction. The effective index obtained from the solution of the second equation can then be regarded as the overall effective index of the guide. A theoretical study of the method by Peng and Oliner (1981) revealed that the method was in fact the lowest order version of the mode matching method, in the case of some composite structures.

This method, in spite of its popularity, is inaccurate in the region near to cut-off. In view of this, several techniques have been proposed to improve on its accuracy such as a dual effective index method proposed by Chiang (1986) which required the linear combination of two effective indices, obtained by applying the effective index method in two different ways. Chiang (1996) proposed a new effective index method with perturbation to correct the error in the propagation constant of the rectangular guide.

1.4.2   Numerical Methods

In the last two decades, numerical methods have been widely used in the study of optical guided wave devices due to the availability of faster and cheaper computer power. These methods are concerned with finding numerical solutions to the Helmholtz's wave equation derived from Maxwell's equations. In many instances, a choice has to be made between a numerical method and an approximate method, where the choice is dependent on the level of accuracy required. For planar structures, or for structures with one dimensional (1-D) index variation, the approximate methods do give satisfactory results. However, for the accurate characterisation of three dimensional 3-D structures, a fully numerical method such as the finite difference or the finite element method is required. Pichot (1982) has used a numerical method based on a vector integral equation for the analysis of diffused channel waveguides. Sharma and Bindal (1992) have employed a variational approach based on the Hermite-Gaussian trial functions to analyse diffused planar and channel waveguides. Schweig and Bridges (1984) and Lagu and Ramaswamy (1986) have advanced the variational approach in the finite difference method (FDM) for the analysis of diffused channel waveguides.

The proliferation of numerical methods means that thought has to be given to the choice of the best method for the solution of a waveguide problem. Factors which need to be taken into consideration when choosing a numerical method, (Davies, 1972, Ng, 1974) include the following:

a)   the shape of the region, Ω, under consideration in particular whether it is curved or polygonal, concave or convex

b)   whether the method can be implemented as a computerised program for all types of geometries or if it has to be implemented specifically for each region of the guide structure

c)   whether the field distribution required is well away from cut-off region or near to the cut-off region and in particular its accuracy near to the cut-off region

d)   the type of modes required, the dominant mode or higher order mode, as well as being able to distinguish between optical modes which are quite close together and

e)   the efficiency in terms of computational time and storage requirements.

1.4.2.1   The variational method

The differential equation, which describes the propagation of electromagnetic waves in an optical medium, can be written as:

$$Lv(x) = f(x) \qquad\qquad\qquad 1.33$$

where L is a linear differential operator defined as:

$$L = \nabla \times (p\nabla \times) - \omega^2 q \qquad\qquad\qquad 1.34$$

$v(x)$ is the function sought and $f(x)$ is the source function. For typical eigenvalue problems, there are no sources of radiation and $f(x) = 0$. The function $v(x)$ and its derivatives must also satisfy some continuity conditions, that is the function is continuous and differentiable up to the highest order present in the integral form of the governing equation. For the function $v(x)$ to have a unique solution, certain boundary conditions need to be imposed on the function and its derivatives at the guide boundaries. These boundary conditions comprise of a set of linear operator equations satisfied on the boundary [Appendix 1].

1.4.2.1.1   **Weak formulation**

Equation (1.33), together with the boundary conditions, form the definition of the problem discussed, also known as the strong formulation. It is possible to find an approximate solution to the above problem using equation (1.33) as the starting point. It is however instructive to attempt to find a weak formulation, that is to reformulate the problem as a search for a function that satisfies some specified conditions also satisfied by the solution to the problem of (1.33). This weak formulation is also known as the variational formulation, the solution of which is also the solution of the original problem, provided those specified conditions are satisfied.

In order to find the variational form, an inner or scalar product of two functions $u(x)$ and $v(x)$ is defined as the integral

$$\int_\Gamma u(x)v(x)dx \qquad\qquad 1.35$$

where Γ is the domain in which the functions are defined. The inner product of $u(x)$ and $v(x)$, denoted by $\langle u,v \rangle$, is thus

$$\langle u,v \rangle = \int_\Gamma u(x)v(x)dx \qquad\qquad 1.36$$

1.4.2.1.2 **Properties of the inner product**

Given an inner product as defined by (1.36), then the following properties hold true (Retorys, 1980)

1. $\langle u,v \rangle = \langle v,u \rangle$

2. $\langle au_1 + bu_2,v \rangle = a\langle u_1,v \rangle + b\langle u_2,v \rangle$

3. $\langle u,u \rangle \geq 0$

4. $\langle u,u \rangle = 0$ if and only if $u(x) = 0$

1.4.2.1.3   Functional Formulation of the Curl equation

It can be shown [Appendix 2] that the function which minimises the following equation

$$\nabla \times (p\nabla \times v) - \omega^2 qv = f \, ,$$ 1.37

is given as

$$F = \langle \nabla \times (p\nabla \times v), v \rangle - \omega^2 \langle qv, v \rangle - \langle f, v \rangle - \langle v, f \rangle.$$ 1.38

In electromagnetic field problems, the fields have time dependence, and the inner product can therefore be modified slightly as follows

$$\langle u,v \rangle = \int_{\Omega} \left(u^* \cdot v \right) d\Omega$$ 1.39

The asterisk denotes the complex conjugate. The functional of equation (1.38) can now be written as

$$F = \int_{\Omega} v^* \cdot \nabla \times (p\nabla \times v) d\Omega - \omega^2 \int_{\Omega} v^* qv \, d\Omega - \int_{\Omega} v^* \cdot f \, d\Omega - \int_{\Omega} f^* \cdot v \, d\Omega \quad 1.40$$

If the following vector identity is now considered

$$\nabla \cdot (a \times b) = (\nabla \times a) \cdot b - a \cdot \nabla \times b$$ 1.41

then taking the integral of both sides of the above equation (1.41), the following is obtained

$$\int_{\Omega} \nabla \cdot (a \times b) d\Omega = \int_{\Omega} [(\nabla \times a) \cdot b - a \cdot \nabla \times b] d\Omega \qquad 1.42$$

From the divergence theorem it is known that

$$\int_{\Omega} \nabla \cdot (a \times b) d\Omega = \oint_{\Gamma} (a \times b) \cdot n \, d\Gamma. \qquad 1.43$$

It follows that

$$\oint_{\Gamma} (a \times b) \cdot n \, d\Gamma = \int_{\Omega} [(\nabla \times a) \cdot b - a \cdot \nabla \times b] d\Omega \qquad 1.44$$

rearranging the above, the following is now obtained

$$\int_{\Omega} a \cdot \nabla \times b \, d\Omega = \int_{\Omega} (\nabla \times a) \cdot b \, d\Omega - \oint_{\Gamma} (a \times b) \cdot n \, d\Gamma \qquad 1.45$$

Making the following substitutions $a = v^*$ and $b = p\nabla \times v$, then the following can be written

$$\int_{\Omega} v^* \cdot \nabla \times (p\nabla \times v) d\Omega = \int_{\Omega} (\nabla \times v^*) \cdot (p\nabla \times v) d\Omega - \oint_{\Gamma} (v^* \times (p\nabla \times v)) \cdot n d\Gamma \qquad 1.46$$

This can now be substituted into the functional of equation (1.38) to obtain

$$F = \int_{\Omega} (\nabla \times v^*) \cdot (p\nabla \times v) d\Omega - \omega^2 \int_{\Omega} v^* \cdot qv \, d\Omega - \int_{\Omega} (v^* \cdot f + f^* v) - \oint_{\Gamma} (v^* \times (p\nabla \times v)) \cdot n \, d\Gamma$$

$$1.47$$

which is the functional that needs to be minimised. Depending on the interpretation of *p*, *q*, *f* and *v*, any equation in the form of the curl equation can be solved using the above functional.

The variational form can now be used to construct approximate solutions, and by use of trial functions to represent field solutions, the integral equation is then reduced to a set of linear equations which can be solved by standard techniques. The accuracy of the solution depends on an appropriate choice of trial functions satisfying the specified boundary conditions. A systematic procedure for finding an appropriate function is provided by the Rayleigh-Ritz method where the function $v(x)$ is expanded as a series of trial functions (Adams, 1981) of the form

$$\phi = \sum_{i=0}^{N} a_i \phi_i \qquad\qquad 1.48$$

Several types of trial functions have been used in optical waveguide problems, such as Gaussian and Hermite Gaussian functions (Austin, 1984; Erteza and Goodman, 1995; Sharma and Bindal, 1992). Others include cosine-exponential functions, airy functions, (Goyal *et al.*, 1993) and the modified Hermite-Gauss exponential function.

1.4.2.2   The Equivalent Network Method

This method, also known as the mode matching method is used in the characterisation of open dielectric waveguides. The guide is assumed to be artificially bounded and hence the coupling between the TE-TM modes and the continuous spectrum distribution at the sides of the waveguide can be neglected (Koshiba *et al.*, 1982). The waveguide is considered in terms of discrete blocks or portions of uniform dielectric layered structures with a step discontinuity at the interfaces. An expansion of the fields in the various regions of the guide in terms of the transverse modes results in a microwave equivalent circuit representation of the guide. The uniform dielectric regions can then be represented as transmission lines with a characteristic impedance and admittance. The

step discontinuities are modelled as transformers. This method has been applied to rectangular waveguides using a vectorial wave analysis (Koshiba and Suzuki, 1985). Dagli and Fonstand (1987) have extended the method to study of GaAs rib waveguides and directional and three guide couplers.

1.4.2.3   The Spectral Index Method

This is a relatively fast and accurate semi-numerical method in which the electromagnetic wave equation is expressed in terms of Fourier transforms and Fourier series. The method has been applied in the solution of rib waveguide problems (Kendall *et al.*, 1989), (Stern *et al.*, 1990) and in the study of the strip loaded directional coupler (Burke, 1990). More recently the method has been extended to the study of multiple rib waveguides (Pola *et al.*, 1996). The accuracy and speed of the method relies on the use of Fourier transforms to generate a spectral index for the region below the rib.

In the method, the original structure is replaced by a 1-D structure with the refractive indices below the rib being represented by their corresponding spectral indices. Application of the method requires:

1.   A Fourier transform in the transverse horizontal direction

2.   A Fourier series in terms of trigonometrical functions inside the rib and

3.   A transfer relation linking the two equations into a transcendental equation.

The propagation constant is determined through the solution of the transcendental equation. To solve the problem of strong dielectric discontinuity in the rib region, the concept of an effective width is used and the evanescent regions are represented through imaginary spectral indices. Numerical algorithms for this method converge more slowly in the presence of dielectric corners, (Sudbo, 1992).

1.4.2.4   The Beam Propagation Method

The methods considered thus far have been used to obtain the modal properties of an optical waveguide through the solution of a two-dimensional wave equation. Such modal properties of a waveguide can also be obtained through the solution of a three-dimensional wave propagation equation. This method was first proposed for the solution of non-uniform waveguide problems in anisotropic media by Feit and Fleck (1980) and independently by Yeh *et al.* (1979).

The beam propagation method is based on the assumption of plane polarised waves. In essence, the method consists of calculating the paraxial approximation to the field as it propagates down the waveguide, and performing the Fourier transform of a correlation function relating the evolved field and the incident field to yield the mode spectrum Chiang (1994). For the analysis of non-uniform waveguides, the beam propagation method is now widely accepted as the most powerful method available. However, for the analysis of uniform structures, this method is not as efficient as those designed specifically for two-dimensional wave equations, because it is necessary to discretise the structure in both the transverse and the longitudinal planes. To overcome these difficulties, a two-dimensional method such as the finite difference method is best employed.

1.4.2.5   The Finite difference Method

The finite difference method is the oldest and probably the best known numerical method for the solution of boundary value problems. The importance of the finite difference method lies with the ease with which many logically complicated operations and functions may be discretised. In this method, the optical waveguide is enclosed in a rectangular box whose cross-section is divided into sub-regions. Operations are then performed not on continuous functions, but rather on values at discrete point sets on the grid. The major advantage of this method is that operations such as differentiation and

integration are reduced to simple arithmetic operations, which lend themselves easily to algorithmic solutions. The walls of the rectangular box may either be electric or magnetic. The field at the boundaries of the walls is assumed to be negligible, allowing infinite elements with an associated decay factor to be introduced. A grid with all the dielectric boundaries on it is then used to represent the cross-section. The nodal field of an arbitrary node can be expressed in terms of the neighbouring nodes in the two transverse directions using a five-point formula, (Davies, 1989) of finite differences. The differentiation of the wave equation at the nodes is thus replaced with differences of the fields evaluated at the nodes. This approach leads to a large non-symmetric matrix, which puts constraints on the storage requirements. An iterative procedure using lower order modes is employed to avoid the storage of large matrices by solving the matrix eigenvalue equation (Chiang, 1994) directly.

The finite difference method can also be formulated using the variational principle. The variational expression obtained is arranged into a set of coupled wave equations for each of the transverse directions, H_x and H_y. An eigenvalue matrix equation of the form $Ax - \lambda x = 0$ can be formed which can be solve using sparse matrix techniques.

The accuracy of this method is determined by the size of the computational window. If the computational window is too large, convergence will be slow. A small computational window would, on the other hand, invalidate the assumption of zero field at the boundaries. As the distance between points is made sufficiently small, the method becomes increasingly accurate.

1.4.2.6   The Finite Element Method

The finite element method (FEM) is a relatively new and powerful numerical technique in the analysis of optical waveguide problems. Following this approach, any optical waveguide cross-section can be divided into triangular elements and the field components within the elements approximated by polynomial expressions. The versatility of the method ensures that each element can be of a different dielectric material, anisotropic, non-linear or lossy. The finite element formulation is usually

established using a variational technique (Davies, 1989), or through the Galerkin method (Berk, 1956).

Vector variational formulations of Maxwell's equations provide a means of solving wave propagation problems where all six electromagnetic field components are required and scalar formulations are inadequate (English and Young, 1971). Such a formulation also provides a better convergence where the natural boundary condition is that of Dirichlet. Using a standard procedure discussed below, a variational formulation can be obtained. The steps involved are to

1. Find the variational integral whose first variation is zero for the given boundary conditions

2. Choose an appropriate trial function and expand the field components as a sum of the trial functions

3. Substitute the trial fields in the variational integral and find the first variation and equate it to zero and

4. The resulting simultaneous equations from the weak formulation of the boundary value problem are equivalent to a standard eigenvalue matrix equation of the form $Ax - \lambda x = 0$. This equation can then be solved by one of several standard matrix algorithms.

Different variational formulations have been proposed for use with the finite element method. The simplest of these is the scalar approximation, which is useful where the field can be said to be predominantly TE or TM. It has been applied to the analysis of different types of waveguide problems; e.g. in the work of Silvester (1969), Hayata *et al.*, (1986), Chiang (1985) and Mabaya *et al.*, (1981).

For practical waveguides, the scalar formulation is not accurate since the modes are hybrid. To overcome this shortcoming of the scalar approximation, a vector formulation

with at least two field components is used. Both the **E** and **H** field vector variational formulations (Berk, 1956) or combinations of the two have been used.

The finite element method in terms of the E_z-H_z variational formulation has been used in the analysis of both microwave devices, Csendes and Silvester (1970), Tzuang *et al.* (1986)) and optical waveguide devices (Yeh *et al.*, (1975), Ikeuchi *et al.* (1981)). This formulation is however not suitable for generally anisotropic waveguides. It is also difficult to implement the natural boundary condition using this method for guides with arbitrary index distribution. Most importantly, however, the two axial components on which the formulation is based are the least essential of the six vector field components. Coupled with the above, the method suffers from spurious modes which can be reduced at the expense of increased computational cost (Mabaya *et al.*, 1981).

A vector **E** has been used in the study of cylindrical waveguides (English and Young (1971)), magnetically anisotropic waveguides (Koshiba and Suzuki, 1985) and optical fibers (Katz and Werner 1982). The natural boundary condition for the **E** field is that of a magnetic wall. This implies a conducting electric boundary wall, **n** x **E** = 0, such a condition is however difficult to implement on arbitrarily shaped guide walls. The **E** field formulation also requires special care in preserving the continuity of the transverse components of the fields.

The vector **H** field formulation has been extensively used due to its ability to solve generally anisotropic waveguide problems (Rahman and Davies, (1984a, 1985), Koshiba *et al.* (1986), and Kobelansky and Webb. (1986)). Since the natural boundary condition is that of an electric wall there is no need to explicitly enforce this condition. This formulation can be written as (Rahman and Davies, 1984a)

$$\omega^2 = \frac{\int (\nabla \times \mathbf{H})^* \cdot \varepsilon^{-1} \cdot (\nabla \times \mathbf{H}) d\Omega}{\int \mathbf{H}^* \cdot \mu^{-1} \cdot \mathbf{H} d\Omega}$$

where ε and μ are the permittivity and permeability of a loss free medium, and they may both be of arbitrary anisotropy. Application of the Raleigh-Ritz procedure to the

above equation will yield a similar matrix equation as in the vector **E** formulation. A serious shortcoming of the above formulation is the appearance of spurious solutions, which can be attributed to the fact that the divergence condition $\nabla \cdot \mathbf{H} = 0$ is not satisfied. Enforcing this divergence condition through the imposition of 'penalty' function (Rahman and Davies, 1984c) could eliminate these spurious modes. Another method of eliminating the spurious modes has been achieved through the use of edge elements (Bossavit and Mayergoyz, 1989).

Variational formulations in terms of the transverse electric and magnetic field components have been used of late; e.g. in the work of Hayata *et al.* (1986, 1988) and Fernandez and Lu (1990). In such a formulation, the divergence condition is implicitly satisfied and minimum number of variables are required hence spurious modes can be avoided. This formulation can also provide the complex propagation constant for waveguides with loss and gain, however it can lead to a more complex matrix eigenvalue problem, (Hayata *et al.*, 1986) with larger memory and cpu time requirement.

1.5   Aims and Objectives of the thesis

Following from the discussion in the introduction, the important role optoelectronics has to play in present day communications systems is clear. A number of important areas have been identified in which ongoing research will contribute immensely towards communications systems of the future. The background information provided thus far has been important in defining the aims and objectives of this thesis, a small contribution to the efforts of many people to herald in a new communications age. The primary aim of this work can be summarised as follows:

1. To investigate the different approaches to the solution of the optical waveguide problems and to provide a justification for the use of the finite element method.

2.   To develop a rigorous, accurate, efficient and versatile method for the analysis of diffused and anisotropic optical waveguide problems based on the vector H finite element method.

3.   To develop an efficient and robust beam propagation method which combines the finite element discretization in the transverse domain with the stable z-stepping Crank-Nicholson scheme in the longitudinal direction for the study of nonlinear propagation.

4.   To apply the methods developed in 2 and 3 above to the study of second harmonic generation in $LiNbO_3$ waveguides and to investigate various methods of obtaining more efficient harmonic power in both planar and anisotropic channel waveguides.

5.   To apply the methods thus developed in 2 and 3 to the study of second harmonic generation in semiconductor waveguides, involving GaAs and AlGaAs and to show the effects of fabrication error on the technique of quasi-phase matching.

6.   To investigate the cascaded effect in the second order nonlinear process of second harmonic generation.

The methods thus developed, it is hoped, will aid in the better understanding of device design and analysis and hence provide a useful tool to the systems developer for the design of novel optical systems.

1.6   Structure of the thesis

The work presented in this thesis is based on the research carried out by the author in the use of the finite element based modal analysis method in the study of various types of waveguides and in the study of the nonlinear phenomenon of second harmonic generation. In particular, diffused anisotropic waveguides are considered. GaAlAs-based

semiconductor waveguides are also considered. The discussion, which follows, gives an outline of the structure of this thesis beginning with an introduction, which is presented in this first chapter. This first chapter gives a brief review of the historical development of optical waveguide development and its economic and technological impact on present day society. A number of linear and nonlinear effects are considered. This is then followed by a review of the theory underpinning optical waveguide analysis. Several methods of analysis are considered including semi-analytical and numerical methods.

The formulation of the theory of the finite element method as a powerful method in the solution of complex problems is presented in Chapter 2. A detailed study of the finite element method along with the use of both linear and second order elements and shape functions is undertaken with a view to developing an algorithm for the modal analysis of anisotropic diffused and nonlinear waveguides. The fundamental mathematical relations are derived from Maxwell's equations. Also considered in the chapter are several variational formulations with a detailed consideration of the vector H-field finite element variational formulation. The chapter concludes with a look at beam propagation algorithms based on finite element discretization in the transverse cross-section and finite difference discretization in the z-domain. The split-step finite element schemes are considered.

Chapter 3 is devoted to the theory of second harmonic generation. The origin of nonlinearity in optical materials is examined. Following Zernike and Midwinter (1973), an attempt is made at a detailed derivation of the nonlinear interaction equation, which is at the heart of nonlinear phenomena. The classification of SHG is then considered. A finite element variational formulation of the nonlinear equation is then obtained from first principles. The chapter concludes with a look at methods used to increase the second harmonic output.

In Chapter 4 the application of the finite element method to the analysis of optical waveguides is considered. The chapter begins with a discussion of channel waveguides and their fabrication techniques. Methods developed in Chapter 2 are applied to obtain results for planar waveguides in the first instance. A comparison of the results obtained by methods developed in this thesis show very good agreement with previously

published results. The method developed in Chapter 2 is then extended to diffused planar and anisotropic waveguides as well as to channel waveguides. Various diffusion profiles are considered. The particular profile assumed by a waveguide will depend to a large extent on the fabrication technique adopted. It is shown that better results are obtained near to cut off if the waveguide dimensions are assumed to be greater than the diffusion parameters. Finally the finite element method is then applied to directional couplers which form an important component in many optical devices. More recently they have been used in the enhancement of the second harmonic power output (Hempelmann, 1999).

The application of the finite element method to the simulation of the nonlinear optical phenomenon of second harmonic generation in the ferroelectric crystal material of LiNbO$_3$ is considered in Chapter 5. The chapter begins with a review of the theory of SHG and then considers various phase matching techniques. Using the method proposed in Chapter 2, a model is developed for propagation in a linear medium. Nonlinearity is then introduced into the model and used to obtain results for planar waveguides using the Cerenkov radiation scheme. The results obtained here show excellent agreement with those previously published. The method is then extended to channel waveguides again using the Cerenkov radiation scheme. It is shown that such a scheme does not require any special techniques in order to increase output power. It is however observed that since the power is radiated into the substrate, special techniques may have to be applied in order to obtain useful output. The chapter also presents results for the non-radiated output and how quasi phase matching may be employed to increase the output power.

Chapter 6 is devoted to second harmonic generation in semiconductor materials. Firstly the importance of semiconductors in the monolithic integration of optical devices is considered. A comparative study of second harmonic generation in both GaAs and GaAlAs is undertaken. An attempt is made at device optimisation using the modal based finite element method. In the first instance results are obtained for lossless devices when the quasi phase matching techniques of domain inversion and domain depletion are employed. The effect of loss is then taken into consideration. It is then concluded that GaAlAs based devices could provide better output power than GaAs devices even though they have a lower nonlinear susceptibility tensor. Results are also presented for

errors due to fabrication that might cause the phase matching distance to differ from the coherence length of the device. It is shown that such inaccuracies could lead to substantial departure from the theoretically predicted possible output power.

In most research work on second harmonic generation it is often assumed that there is no depletion of the fundamental power. This assumption is however not strictly accurate in the presence of a strong laser beam. In Chapter 7 we investigate second harmonic generation under the assumption that the fundamental beam is depleted. The wave equation for the propagation of the fundamental is written with the second harmonic wave as a source term. It is shown that under certain conditions the generated second harmonic wave and the fundamental wave can co-propagate in the medium without affecting each other.

The final chapter provides a summary of the work that has been carried out. A brief discussion is given on each chapter. This chapter also discusses some ideas and suggestions as to how the work carried out here may be extended in the future.

Appendices are provided at the end together with a list of publications by the author relevant to this work as well as a list of references cited throughout the thesis.

Chapter Two

The Finite Element Method and Propagation

Algorithms

2.1   Introduction

Many natural phenomena can be described using algebraic differential or integral equations. The derivation of these equations may in themselves not present undue difficulty: however, their solution by exact analytical methods is a formidable task (Reddy, 1993). As a result approximate solutions are sought through the use of numerical methods. A numerical method is, in simple terms, a technique, which converts the infinite degrees of freedom of an unknown analytical solution to a finite set of unknowns, which can then be solved computationally. The finite element method (FEM) is one such numerical technique for solving, to a high degree of accuracy, complicated boundary value problems.

The basic idea of the finite element method is to divide the region of interest into a large number of finite elements or sub-regions. These elements may be one, two or three-dimensional. The idea of representing a given domain as a collection of discrete elements is not new: it is recorded that ancient mathematicians estimated the value of π by representing the circle as a polygon with a large number of sides.

In the past, the FEM has been used to solve complex engineering problems including structural analysis in the aircraft industry, heat transfer, fluid flow, and mass transport. In recent years it has found application in electromagnetic field problems. Most waveguide problems can be described through the use of integral or differential equations. These equations can then be solved using numerical techniques. The finite element method has established itself as one of the most powerful and accurate methods for solving problems associated with the sophisticated integrated optical waveguides and microwave devices been developed today. The versatility of the method allows elements of various shapes to be used to represent an arbitrary cross-section. Each element could also be of a different material type, enabling a wide range of practical waveguides to be analysed. The type of waveguide problems considered in this thesis belongs to the class of eigenvalue problems and the emphasis will be on the vector **H** field formulation and the scalar fomulation.

2.2   Basic Concepts in the finite element method

In the finite element method, the key ideas are the

- discretization of the region of interest into elements

and

- using interpolating polynomials to describe the variation of the field within each of the elements.

Hence, instead of differential equations for the system under investigation, variational expressions are derived and the piecewise continuous function is approximated by a piecewise continuous polynomial within each element. From the equivalent discretized model and the contribution from each element, an overall system is assembled. This can be regarded as a sub-class of the Ritz-Galerkin method in which the trial functions are replaced with polynomial functions. In the classical

analytical procedure where the region is not subdivided into regions, only the simplest structures with basic material properties can be considered. The finite difference method is the simplest of all the discretization procedures and in the traditional version uses a rectangular grid with nodes at the intersections of the orthogonal straight lines (Fig 2.1}.

Fig 2.1 Example of domain division using a regular grid

Such an approach is not particularly suited to irregular geometries with curved boundaries and interfaces since the intersections with the gridlines could be at points other than at the nodes. It is also not well suited to the analysis of problems in which there are steep variations of the field. The finite element method, on the other hand, allows the domain to be subdivided into elements or sub-regions. These elements can be of various shapes such as triangles and rectangles thus enabling the use of irregular grid for a complex waveguide structure (see Fig 2.2).

The method can therefore be easily used to analyse problems with steep variations of the field and can be adapted quite readily to anisotropic and inhomogeneous problems. The accuracy of the method could be systematically increased by increasing the number of elements. The method does not rely on the variational method for its establishment: it could be established by the used of the Galerkin method, which is a weighted-residual method. The importance of this last point is

that the method could be applied in cases where no variational formulation exists or cannot be found.

Fig 2.2 Example of an arbitrary shape optical guide with several regions of different material types.

The steps involved in the finite element analysis can be summarised as follows:

- discretize the domain under investigation into sub-domains or elements. The accuracy of the method depends on the level of discretization. It is recommended to use more elements in areas where the field is thought to have steep variations. It is also not advisable to use elements across physical boundaries or interfaces. For symmetrical domains, the mesh should follow the same type of symmetry.

- the functionals for which the variational principle should be applied for the elements are then derived. In deciding on the interpolation function, certain continuity conditions must be satisfied by the interpolation function across inter-element boundaries. These requirements are normally obvious from the physical consideration of the problem. It is however also necessary that the function be an admissible member of the Ritz and Galerkin methods. It

follows that the polynomial function has to remain unchanged under a linear transformation from one co-ordinate system to the other.

- assemble all the element contributions to form a global matrix.

- solve the system of equations that was obtained, in this case a matrix equation.

Fig 2.3 shows how the discretization procedure can be applied to a waveguide with different regions, e.g. a cladding, film and substrate. The elements used in this case are triangular since it is much easier to represent an arbitrary cross-section with triangles rather than with rectangles. In 2-D waveguide analysis the triangles can be of any order but the most commonly used triangle orders are the first and second.

Fig 2.3 Discretization of an optical waveguide

2.3   Implementation of the Method

2.3.1 Finite Element Implementation of the Electromagnetic Wave Equation

Given the following Helmholtz equation

$$\nabla^2 \phi + k^2 \phi = 0 \qquad\qquad 2.1$$

as the governing equation in a waveguide problem, defined within the domain Ω, where ϕ is the electric or magnetic field component and ∇^2 is a Laplacian operator defined as

$$\nabla^2 = \frac{\partial^2}{\partial x^2} + \frac{\partial^2}{\partial y^2} + \frac{\partial^2}{\partial z^2} \qquad\qquad 2.2$$

then k^2 is a constant related to frequency, also that Γ_f and Γ_n are boundaries within the said domain, the following boundary conditions may be defined

$$\phi = \hat{\phi} \text{ on the boundary } \Gamma_f \text{ (Dirichlet boundary condition)} \qquad 2.3$$

$$\frac{\partial \phi}{\partial n} = n \cdot \nabla \phi = \hat{\psi} \text{ on the boundary } \Gamma_n \text{ (Neumann boundary condition)} \qquad 2.4$$

where n is the outward normal unit vector. The gradient operator, is defined by the following matrix differential operator

$$\nabla = \begin{bmatrix} \partial/\partial x \\ \partial/\partial y \\ \partial/\partial z \end{bmatrix} \qquad\qquad 2.5$$

in the Cartesian system of co-ordinates. Taking into consideration the stated boundary conditions, the functional for equation (2.1) could be written as (Koshiba, 1990)

$$F = \frac{1}{2} \iiint_\Omega \left[(\nabla\phi)^2 - k^2\phi^2 \right] d\Omega - \iint_{\Gamma_n} \phi\hat\psi \, d\Gamma \qquad\qquad 2.6$$

The stationary requirement of the above functional, $\delta F = 0$, coincides with the governing equation of the problem. The Neumann boundary condition is automatically satisfied in the variational procedure and as such it is referred to as the natural boundary condition. The Dirichlet boundary condition however needs to be imposed and is therefore called the forced boundary condition. The functional for each of the elements of the region could then be written as

$$F_e = \frac{1}{2} \iiint_e \left[(\nabla\phi)^2 - k^2\phi^2 \right] d\Omega - \iint_{\Gamma_e} \phi\hat\psi \, d\Gamma \qquad\qquad 2.6$$

The functional for the whole of the domain can then be regarded as a summation of the element functions

$$F = \sum_e F_e \qquad\qquad 2.7$$

For the n nodes within each element, the field, ϕ, can be approximated as follows

$$\phi = \sum_{i=1}^{n} N_i \, \phi_i \qquad\qquad 2.8$$

where ϕ_i is the ith nodal parameter of the element e and N_i is the interpolation or shape function. The above equation could be written in matrix form, as follows

$$\phi = \{N\}^T \{\phi\}_e \qquad\qquad 2.9$$

where the component of the vector $\{\phi\}_e$ is ϕ_i and that of the vector $\{N\}^T$ is the interpolation function N_i. The superscript T denotes a transpose, $\{\}$ and $\{\}^T$ denotes a column and row vector respectively.

For convergence of the solution, the shape function N_i must satisfy certain conditions when the functional contains first order derivatives

- the variable ϕ and its derivatives must include constant terms and

- the variable ϕ must be continuous at the interface of two adjacent elements.

The first of the two conditions is also known as the completeness condition and is simple to satisfy, provided complete polynomial expressions are used in each element. The second of the two conditions is called the compatibility condition. First order elements are the most fundamental and first order polynomials are used with them but higher order elements are used with higher order polynomials. Since the number of nodes within each element coincides with the number of terms in a complete polynomial expansion, the nodes are simply arranged to satisfy the compatibility condition.

2.3.2 Derivation of the Element Equations

In order to obtain the element equations, it is necessary to perform a co-ordinate transformation. This is required because the interpolation function is defined using the local co-ordinates and hence it is necessary to find a means of linking the global derivatives in terms of the local derivatives. Secondly the element volume over which the integration has to be carried out needs to be expressed in terms of local co-ordinates with change of limits as may be appropriate.

Assuming the local co-ordinates ξ_1, ξ_2 and ξ_3 have as a corresponding set the following global co-ordinates x, y and z as follows:

$$x = x(\xi_1, \xi_2, \xi_3) \qquad\qquad 2.10$$

$$y = y(\xi_1, \xi_2, \xi_3) \qquad\qquad 2.11$$

$$z = z(\xi_1, \xi_2, \xi_3) \qquad\qquad 2.12$$

Using the rules of partial differentiation, the transformation relation for differentiation can be written as

$$
\begin{bmatrix}
\dfrac{\partial}{\partial \xi_1} \\[2mm]
\dfrac{\partial}{\partial \xi_2} \\[2mm]
\dfrac{\partial}{\partial \xi_3}
\end{bmatrix}
= [J]
\begin{bmatrix}
\dfrac{\partial}{\partial x} \\[2mm]
\dfrac{\partial}{\partial y} \\[2mm]
\dfrac{\partial}{\partial z}
\end{bmatrix}
\qquad\qquad 2.13
$$

where the matrix $[J]$ is a Jacobian matrix defined as

$$
[J] =
\begin{bmatrix}
\dfrac{\partial x}{\partial \xi_1} & \dfrac{\partial y}{\partial \xi_1} & \dfrac{\partial z}{\partial \xi_1} \\[3mm]
\dfrac{\partial x}{\partial \xi_2} & \dfrac{\partial y}{\partial \xi_2} & \dfrac{\partial z}{\partial \xi_2} \\[3mm]
\dfrac{\partial x}{\partial \xi_3} & \dfrac{\partial y}{\partial \xi_3} & \dfrac{\partial z}{\partial \xi_3}
\end{bmatrix}
\qquad\qquad 2.14
$$

The global matrix of the derivatives can then be obtained through an inversion of the Jacobian matrix to give

$$
\begin{bmatrix} \dfrac{\partial}{\partial x} \\[2mm] \dfrac{\partial}{\partial y} \\[2mm] \dfrac{\partial}{\partial z} \end{bmatrix} = [J]^{-1} \begin{bmatrix} \dfrac{\partial}{\partial \xi_1} \\[2mm] \dfrac{\partial}{\partial \xi_2} \\[2mm] \dfrac{\partial}{\partial \xi_3} \end{bmatrix}
\qquad 2.15
$$

The following transformation relation for the integration is obtained

$$
\iiint f(x,y,z)\,dx\,dy\,dz = \iiint f(\xi_1,\xi_2,\xi_3)\,|J(\xi_1,\xi_2,\xi_3)|\,d\xi_1 d\xi_2 d\xi_3 \qquad 2.16
$$

2.3.2.1   Line Elements

As noted, line elements (one-dimensional) are the most fundamental of all the elements used. These elements can be of

a) first order
b) second order or
c) higher order

Fig 2.4 Examples of line elements a) Linear element b) Quadratic element.

Examples of some line elements are shown in Fig 2.4. These are normally used when solving one-dimensional problems and it is necessary to introduce the line co-ordinates L1 and L2.

The relation between the line co-ordinates and the Cartesian co-ordinates is given by

$$\begin{bmatrix} L_1 \\ L_2 \end{bmatrix} = \frac{1}{l_e} \begin{bmatrix} x_2 & -1 \\ -x_1 & 1 \end{bmatrix} \begin{bmatrix} 1 \\ x \end{bmatrix} \qquad\qquad 2.17$$

where x_1 and x_2 are the Cartesian co-ordinates of the edge of the line and the length of the element is l_e is given by

$$l_e = x_2 - x_1. \qquad\qquad 2.18$$

If the local co-ordinate is now defined as ξ_1 then

$$L_1 = \xi_1 \qquad\qquad 2.19a$$

$$L_2 = 1 - L_1 = 1 - \xi_1 \qquad\qquad 2.19b$$

The transformation relation for differentiation is then given as

$$\frac{d}{dx} = -\frac{1}{l_e} \frac{d}{d\xi_1} \qquad\qquad 2.20$$

For integration, the transformation relation is given by the following

$$\int_e f(x)dx = l_e \int_0^1 f(\xi_1)d\xi_1 \qquad\qquad 2.21$$

Using equations (2.20) and (2.21), both the differentiation and integration formulae could be written as

$$\frac{df}{dx} = \frac{1}{l_e}\left(-\frac{\partial f}{\partial L_1} + \frac{\partial f}{\partial L_2}\right) \qquad\qquad 2.22$$

$$\int_e L_1^k L_2^l dx = l_e \int_0^1 \xi_1^k (1-\xi_1)^l d\xi_1$$

$$= l_e \frac{k! l!}{(k+l+1)!} \qquad\qquad 2.23$$

The shape function vector for the linear element and its derivative are given as

$$\{N\} = \begin{bmatrix} L_1 \\ L_2 \end{bmatrix} \qquad\qquad 2.24$$

and

$$\{N_x\} = \frac{d\{N\}}{dx} = \frac{1}{l_e}\begin{bmatrix} -1 \\ 1 \end{bmatrix} \qquad\qquad 2.25$$

respectively. The nodal co-ordinates (L_1, L_2) of the linear element are given as follows:

node 1: (1,0)   node 2: (0,1).

For the quadratic element, the shape function and its derivatives are defined as

$$\{N\} = \begin{bmatrix} L_1(2L_1 - 1) \\ L_2(2L_2 - 1) \\ 4L_1 L_2 \end{bmatrix}$$

2.26

and

$$\{N_x\} = \frac{1}{l_e} \begin{bmatrix} 1 - 4L_1 \\ 4L_2 - 1 \\ 4(L_1 - L_2) \end{bmatrix}$$

2.27

respectively. The nodal co-ordinates for nodes 1, 2 and 3 are given as $(1,0)$, $(0,1)$ and $(1/2, 1/2)$ respectively.

2.3.2.2   Triangular Elements

Most practical electromagnetic problems are of the two dimensional type which makes the use of triangular elements a common practice. These elements can be of either

a)   First order
b)   Second order or
c)   Higher order

Examples of triangular elements of the first and second order are shown in Fig 2.5

In applying the first order elements, it can be seen that nodes occur at the vertices of the triangles while nodes are also defined at the middle of the edges for second order elements. In this work only first order triangular elements are used since the second order elements are costly in terms of the computational time. Since adjacent elements will have common nodes, it is important to adopt a numbering system that will assign to these common nodes the same numbers.

Fig 2.5 Triangular elements a) First order   b) second order.

Triangular elements shown in Fig 2.5 are used in two-dimensional problems. For such an element, the area co-ordinates L_1, L_2 and L_3 are introduced. The equation relating the Cartesian co-ordinates to the area co-ordinates is defined as

$$\begin{bmatrix} 1 \\ x \\ y \end{bmatrix} = \begin{bmatrix} 1 & 1 & 1 \\ x_1 & x_2 & x_3 \\ y_1 & y_2 & y_3 \end{bmatrix} \begin{bmatrix} L_1 \\ L_2 \\ L_3 \end{bmatrix} \qquad\qquad 2.28$$

or

$$\begin{bmatrix} L_1 \\ L_2 \\ L_3 \end{bmatrix} = \begin{bmatrix} 1 & 1 & 1 \\ x_1 & x_2 & x_3 \\ y_1 & y_2 & y_3 \end{bmatrix}^{-1} \begin{bmatrix} 1 \\ x \\ y \end{bmatrix}$$

$$= \frac{1}{2A_e} \begin{bmatrix} a_1 & b_1 & c_1 \\ a_2 & b_2 & c_2 \\ a_3 & b_3 & c_3 \end{bmatrix} \begin{bmatrix} 1 \\ x \\ y \end{bmatrix} \qquad\qquad 2.29$$

where (x_1,y_1), (x_2,y_2) and (x_3,y_3) are the Cartesian co-ordinates of the vertex k (k= 1,2 and 3) of the triangle. The coefficients a_k, b_k and c_k are defined as

$$a_k = x_l y_m - x_m y_l \qquad\qquad\qquad\qquad\qquad 2.30a$$

$$b_k = y_l - y_m \qquad\qquad\qquad\qquad\qquad\qquad 2.30b$$

$$c_k = x_m - x_l \qquad\qquad\qquad\qquad\qquad\qquad 2.30c$$

The subscripts k, l, m are cyclical around the three vertices of the triangle. The area A_e of the element is given as

$$2A_e = \begin{bmatrix} 1 & 1 & 1 \\ x_1 & x_2 & x_3 \\ y_1 & y_2 & y_3 \end{bmatrix} \qquad\qquad\qquad\qquad 2.31$$

If the local co-ordinates ξ, η are defined as

$$L_1 = \xi \qquad\qquad\qquad\qquad\qquad\qquad\qquad 2.32a$$

$$L_2 = \eta \qquad\qquad\qquad\qquad\qquad\qquad\qquad 2.32b$$

$$L_3 = 1 - L_1 - L_2 = 1 - \xi - \eta \qquad\qquad\qquad 2.32c$$

then the transformation relation for differentiation will be given by the following

$$\begin{bmatrix} \dfrac{\partial}{\partial \xi} \\[2mm] \dfrac{\partial}{\partial \eta} \end{bmatrix} = [J] \begin{bmatrix} \dfrac{\partial}{\partial x} \\[2mm] \dfrac{\partial}{\partial y} \end{bmatrix} \qquad\qquad\qquad\qquad 2.33$$

where

$$[J] = \begin{bmatrix} x_1 - x_3 & y_1 - y_3 \\ x_2 - x_3 & y_2 - y_3 \end{bmatrix}$$ 2.34

or

$$\begin{bmatrix} \dfrac{\partial}{\partial x} \\ \dfrac{\partial}{\partial y} \end{bmatrix} = [J]^{-1} \begin{bmatrix} \dfrac{\partial}{\partial \xi} \\ \dfrac{\partial}{\partial \eta} \end{bmatrix}$$ 2.35

with

$$[J]^{-1} = \frac{1}{2A_e} \begin{bmatrix} b_1 & b_2 \\ c_1 & c_2 \end{bmatrix}$$ 2.36

The relation for integration is given as

$$\iint f(x, y)\, dxdy = 2A_e \int_0^1 \int_0^{1-\xi} f(\xi, \eta)\, d\xi d\eta$$ 2.37

Using equations (2.32) through to (2.37), the formulae for both differentiation and integration can be written as

$$\frac{\partial f}{\partial x} = \frac{1}{2A_e}\left(b_1 \frac{\partial f}{\partial L_1} + b_2 \frac{\partial f}{\partial L_2} + b_3 \frac{\partial f}{\partial L_3} \right)$$ 2.38

$$\frac{\partial f}{\partial y} = \frac{1}{2A_e}\left(c_1 \frac{\partial f}{\partial L_1} + c_2 \frac{\partial f}{\partial L_2} + c_3 \frac{\partial f}{\partial L_3} \right)$$ 2.39

$$\iint_e L_1^k L_2^l L_3^m\, dxdy = 2A_e \int_0^1 \xi^k \left[\int_0^{1-\xi} \eta^l (1 - \xi - \eta)^m\, d\eta \right] d\xi$$

$$= 2A_e \frac{k!l!m!}{(k+l+m+2)!}$$
2.40.

2.3.2.3   Other Elements

Other type of elements in use include

a)   rectangular elements – two dimensional elements

b)   tetrahedral elements – three dimensional elements

c)   ring elements – axisymmetric two dimensional elements

d)   triangular ring elements – axisymmetric three dimensional elements

e)   special elements – edge, isoparametric or boundary elements

All of the above could either be of linear, second or higher order.

2.4   Finite Element Application

2.4.1 Application of the Finite element Method to Waveguide problems

For the purpose of numerical analysis and characterisation, optical waveguide problems can be classified as either one-dimensional (planar) or two-dimensional. The particular method of analysis used will depend on the waveguide property being sought. The finite element method is based on either the variational or the Raleigh-Ritz approach and several variational formulations have been proposed. Most of the formulations yield a standard eigenvalue problem (Rahman and Davies 1984a). Of the various methods, the following can be identified:

Scalar field formulation: This method is suitable for one dimensional problems for situations where the electric or magnetic field can be expressed approximately in terms of the predominant field component. It has been applied to the analysis of wave propagation in homogeneous isotropic media (Daly, 1984), open boundary problems (Wu and Chen, 1986) and for the analysis of anisotropic waveguides (Koshiba *et al.*, 1984).

For quasi-TE modes in the domain Ω, where the dominant field component is E_x, the formulation can be expressed as (Mabaya *et al.*, 1981):

$$L = \iint_{\Omega} \left[\left(\frac{\partial E_x}{\partial x} \right)^2 + \left(\frac{\partial E_x}{\partial y} \right)^2 - k_o n^2 E_x^2 + \beta^2 E_x^2 \right] d\Omega \qquad 2.41$$

where β is the propagation constant and n is the refractive index. For quasi-TM modes, with H_x being the dominant field component, the formulation may be given as follows:

$$L = \iint_{\Omega} \left[\frac{1}{n^2} \left(\frac{\partial H_x}{\partial x} \right)^2 + \frac{1}{n^2} \left(\frac{\partial H_x}{\partial y} \right)^2 - k_o H_x^2 + \frac{1}{n^2} \beta^2 H_x^2 \right] d\Omega \qquad 2.42$$

This formulation is not particularly suitable for media and where the guided modes are inherently hybrid.

Vector field formulation: For the accurate characterisation of general waveguides, a vector formulation with at least two field components is required. There are two main types of the full vector formulations namely, the **E**-field and **H**-field. The vector **E**-field approach was first applied by English and Young (1971). This formulation is suitable for generally anisotropic and loss-less problems. The natural boundary condition corresponds to a magnetic wall and as such it is essential to enforce the electric wall as the boundary condition (**nxE**=0). Such a condition is quite difficult to impose for an irregular structure. It also requires an additional

integral to ensure the continuity of the fields at the dielectric interfaces. The **H**-field formulation, on the other hand, has as its natural boundary condition the electric wall and the magnetic field is continuous everywhere. As such it is suitable for dielectric waveguide problems, as no boundary conditions need to be imposed. This formulation is given as

$$\omega^2 = \frac{\int (\nabla \times H)^* \cdot \hat{\varepsilon}^{-1} \cdot (\nabla \times H) d\Omega}{\int H^* \cdot \mu \cdot H d\Omega} \qquad 2.43$$

The above formulation leads to non-physical or spurious solutions since the divergence condition $\nabla \cdot H = 0$ is not satisfied. Various methods exist for detecting these spurious modes. A simple way is to examine the field profiles, since these modes are characterised by inconsistency and a random variation of the field they are easy to identify. The mathematical idea underpinning the physical solution is that the condition $\nabla \cdot H = 0$ is obeyed by the eigenvector. By calculating $\nabla \cdot H$ for each eigenvector, it is possible to identify the true solutions from the spurious ones. The objective, however, is not simply to detect these modes, but to eliminate them or at least suppress them. The penalty-function method (Rahman and Davies, 1984c) is one of the best established methods for eliminating these spurious solutions. The method includes an additional term α, and the penalty term, a dimensionless number in the variational formulation, which now is written as:

$$\omega^2 = \frac{\int (\nabla \times H)^* \cdot \hat{\varepsilon}^{-1} \cdot (\nabla \times H) d\Omega + \left(\frac{\alpha}{\varepsilon}\right) \int (\nabla \cdot H)^* (\nabla \cdot H) d\Omega}{\int H^* \cdot \mu \cdot H d\Omega} \qquad 2.44$$

2.4.2 The Matrix Equation

It has been stated that the vector formulation leads to a standard eigenvalue problem of the form

$$Ax - \lambda Bx = 0 \qquad\qquad 2.45$$

In the above x represents the eigenvector, which holds the nodal field values. If in equation (2.43) the following substitution is made for the numerator

$$x^T \cdot Ax = \int (\nabla \times \mathbf{H})^* \cdot \varepsilon^{-1} \cdot (\nabla \times \mathbf{H}) d\Omega \qquad\qquad 2.46$$

and the denominator is written as

$$x^T \cdot Bx = \int \mathbf{H}^* \cdot \mu \cdot \mathbf{H} d\Omega \qquad\qquad 2.47$$

then the functional

$$J = \int (\nabla \times \mathrm{H})^* \cdot \varepsilon^{-1} \cdot (\nabla \times \mathrm{H}) d\Omega - k_o^2 \int \mathrm{H}^* \cdot \mu \cdot \mathrm{H} d\Omega \qquad\qquad 2.48$$

can be written as

$$J = x^T \cdot A \cdot x - \lambda \cdot x^T \cdot B \cdot x \qquad\qquad 2.49$$

To find a stationary solution, it is required that

$$\frac{\partial J}{\partial x} = 0 \qquad\qquad 2.50$$

Applying this minimisation procedure to equation (2.49), the following eigenvalue equation (2.45) is obtained

$$Ax - \lambda Bx = 0$$

which can be solved using any standard matrix routine to obtain the field values at the nodes.

2.4.3 Shape Functions

The shape functions are a set of interpolation functions, defined in terms of complete polynomials and which are normalised over each element. If a typical element, as shown in Fig 2.6 is considered, then the shape function is chosen so that it uniquely defines the field within the element under consideration.

$$\phi_3(x_3, y_3)$$

$$P(x, y)$$

$$\phi_1(x_1, y_1) \qquad\qquad \phi_2(x_2, y_2)$$

Fig 2.6 Diagram of a typical element

The nodal points, the shape functions takes on values equal to the nodal values ϕ_1, ϕ_2 and ϕ_3 of the field. It is important therefore that the functions are expressed in

terms of their nodal values. Within the triangle, the field value can be adequately modelled by the expression

$$\phi = a + bx + cy \qquad \qquad 2.51$$

where a, b and c are constants. These constants can be represented in terms of the co-ordinates of the nodes. The nodal values of ϕ can then be expressed as

$$\phi_1 = a + bx_1 + cy_1 \qquad \qquad 2.52a$$

$$\phi_2 = a + bx_2 + cy_2 \qquad \qquad 2.52b$$

$$\phi_3 = a + bx_3 + cy_3 \qquad \qquad 2.52c$$

The above system of equations can be solved to determine a, b and c as

$$a = \frac{\phi_1(x_2 y_3 - x_3 y_2) + \phi_2(x_3 y_1 - x_1 y_3) + \phi_3(x_1 y_2 - x_2 y_1)}{2A_e} \qquad \qquad 2.53a$$

$$b = \frac{\phi_1(y_2 - y_3) + \phi_2(y_3 - y_1) + \phi_3(y_1 - y_2)}{2A_e} \qquad \qquad 2.53b$$

$$c = \frac{\phi_1(x_3 - x_2) + \phi_2(x_1 - x_3) + \phi_3(x_2 - x_1)}{2A_e} \qquad \qquad 2.53c$$

where, in the above, A_e is the area of the triangle. A substitution of these values into equation (2.51) will yield

$$\phi(x, y) = N_1\phi_1 + N_2\phi_2 + N_3\phi_3 \qquad \qquad 2.54$$

or

$$\phi(x, y) = [N]\{\phi\} \tag{2.55}$$

where

$$N_1 = \frac{1}{2A}\left[(x_2 y_3 - x_3 y_2) + (y_2 - y_3)x + (x_3 - x_2)y\right] \tag{2.56a}$$

$$N_2 = \frac{1}{2A}\left[(x_3 y_1 - x_1 y_3) + (y_3 - y_1)x + (x_1 - x_3)y\right] \tag{2.56b}$$

$$N_3 = \frac{1}{2A}\left[(x_1 y_2 - x_2 y_1) + (y_1 - y_2)x + (x_2 - x_1)y\right] \tag{2.56c}$$

The above can be rewritten as

$$N_1 = a_1 + a_2 x + a_3 y \tag{2.57a}$$

$$N_2 = a_4 + a_5 x + a_6 y \tag{2.57b}$$

$$N_3 = a_7 + a_8 x + a_9 y \tag{2.57c}$$

An important property of shape function is that

$$N_1 + N_2 + N_3 = 1. \tag{2.58}$$

The **H**-field components H_x, H_y and H_z can be written as

$$H_x(x, y) = N_1 H_{x1} + N_2 H_{x2} + N_3 H_{x3} \tag{2.59a}$$

$$H_y(x, y) = N_1 H_{y1} + N_2 H_{y2} + N_3 H_{y3} \tag{2.59b}$$

$$H_z(x, y) = N_1 H_{z1} + N_2 H_{z2} + N_3 H_{z3}$$

2.59c

In matrix form, the above equations can be expressed as

$$H = \begin{bmatrix} H_x \\ H_y \\ H_z \end{bmatrix} = \begin{bmatrix} N_1 & 0 & 0 & N_2 & 0 & 0 & N_3 & 0 & 0 \\ 0 & N_1 & 0 & 0 & N_2 & 0 & 0 & N_3 & 0 \\ 0 & 0 & N_1 & 0 & 0 & N_2 & 0 & 0 & N_3 \end{bmatrix} \begin{bmatrix} H_{x1} \\ H_{y1} \\ H_{z1} \\ H_{x2} \\ H_{y2} \\ H_{z2} \\ H_{x3} \\ H_{y3} \\ H_{z3} \end{bmatrix}$$

2.60

In a simplified form, this is equivalent to $H = [N]\{H\}$, where $[N]$ is the 3x9 matrix shown above and $\{H\}$ is the 9x1 column vector, which represents the components of the field.

Similarly, the expression for $\nabla \times H$ could be written as

$$\nabla \times H = [Q] \cdot H$$

2.61

where

$$[Q] = \begin{bmatrix} 0 & -\dfrac{\partial N_1}{\partial z} & \dfrac{\partial N_1}{\partial y} & 0 & -\dfrac{\partial N_2}{\partial z} & -\dfrac{\partial N_2}{\partial y} & 0 & -\dfrac{\partial N_3}{\partial z} & -\dfrac{\partial N_3}{\partial y} \\ \dfrac{\partial N_1}{\partial z} & 0 & -\dfrac{\partial N_1}{\partial x} & \dfrac{\partial N_2}{\partial z} & 0 & -\dfrac{\partial N_2}{\partial x} & \dfrac{\partial N_3}{\partial z} & 0 & -\dfrac{\partial N_3}{\partial x} \\ -\dfrac{\partial N_1}{\partial y} & \dfrac{\partial N_1}{\partial x} & 0 & -\dfrac{\partial N_2}{\partial y} & \dfrac{\partial N_2}{\partial x} & 0 & -\dfrac{\partial N_3}{\partial y} & \dfrac{\partial N_3}{\partial x} & 0 \end{bmatrix}$$

2.62

The $\mathbf{Q}$ matrix, after evaluation i.e. finding the derivative of the shape, with $j\beta z$ being the z-variation, becomes

$$[Q] = \begin{bmatrix} 0 & j\beta N_1 & a_3 & 0 & j\beta N_2 & a_6 & 0 & j\beta N_3 & a_9 \\ -j\beta N_1 & 0 & -a_2 & -j\beta N_2 & 0 & -a_5 & j\beta N_3 & 0 & -a_8 \\ -a_3 & a_2 & 0 & -a_6 & a_5 & 0 & -a_9 & a_8 & 0 \end{bmatrix} \quad 2.63$$

The $\mathbf{B}$ matrix can also be calculated in a similar fashion from equation (2.46). Since μ is a scalar quantity, it can be taken outside the integral to give

$$x^T \cdot B \cdot x = \mu \int H^* \cdot H \, d\Omega \qquad\qquad 2.64$$

since $H=[N]\{H\}$

$$B_e = \int_\Delta [N]^* \cdot [N] d\Omega \qquad\qquad 2.65$$

The solution of the above expressions yields a 9x9 matrix. The integration is carried out using equation (2.40) and the resulting B_e matrix is as follows:

$$B_e = \begin{bmatrix}
\frac{A}{6} & 0 & 0 & \frac{A}{12} & 0 & 0 & \frac{A}{12} & 0 & 0 \\
0 & \frac{A}{6} & 0 & 0 & \frac{A}{12} & 0 & 0 & \frac{A}{12} & 0 \\
0 & 0 & \frac{A}{6} & 0 & 0 & \frac{A}{12} & 0 & 0 & \frac{A}{12} \\
\frac{A}{12} & 0 & 0 & \frac{A}{6} & 0 & 0 & \frac{A}{12} & 0 & 0 \\
0 & \frac{A}{12} & 0 & 0 & \frac{A}{6} & 0 & 0 & \frac{A}{12} & 0 \\
0 & 0 & \frac{A}{12} & 0 & 0 & \frac{A}{6} & 0 & 0 & \frac{A}{12} \\
\frac{A}{12} & 0 & 0 & \frac{A}{12} & 0 & 0 & \frac{A}{6} & 0 & 0 \\
0 & \frac{A}{12} & 0 & 0 & \frac{A}{12} & 0 & 0 & \frac{A}{6} & 0 \\
0 & 0 & \frac{A}{12} & 0 & 0 & \frac{A}{12} & 0 & 0 & \frac{A}{6}
\end{bmatrix} \qquad 2.67$$

In the above, A_e is the area of each element or triangle. The coefficients of the A_e matrix could also be calculated using equation (2.39). Making the following substitutions H=[N]{H} and $\nabla \times H = [Q] \cdot \{H\}$, the equation below is obtained

$$x^T \cdot A_e \cdot x = \int \{H\}^* \cdot [Q]^* \hat{\varepsilon}^{-1} \cdot [Q]\{H\} d\Omega \qquad 2.68$$

A simplification of the above will yield an A_e matrix of the form

$$A_e = \int [Q]^* \hat{\varepsilon}^{-1} \cdot [Q] d\Omega \qquad 2.69$$

For isotropic media, ε is a scalar quantity and hence can be factored out of the integral sign. For anisotopic media, ε is a tensor defined by a 3x3 matrix

$$\varepsilon = \begin{bmatrix} \varepsilon_{11} & \varepsilon_{12} & \varepsilon_{13} \\ \varepsilon_{21} & \varepsilon_{22} & \varepsilon_{23} \\ \varepsilon_{31} & \varepsilon_{32} & \varepsilon_{33} \end{bmatrix} \qquad 2.70$$

Finding the inverse of ε, [P] (Appendix 3), equation (2.69) can be written as

$$A_e = \int [Q]^* \cdot [P] \cdot [Q] d\Omega \qquad 2.71$$

Carrying out the necessary algebraic manipulations a 9x9 matrix is obtained. Using the integration formula of equation (2.40), the integrals can be evaluated as

$$\int N_1^2 d\Omega = \frac{A}{6} \qquad 2.72a$$

$$\int N_1 d\Omega = \frac{A}{3} \qquad 2.72b$$

$$\int d\Omega = A \qquad\qquad\qquad\qquad\qquad 2.72c$$

As an example, the A_{e11} matrix will be given as follows

$$A_{e11} = p_{22}\beta^2 \frac{A}{6} + p_{23}a_3 j\beta \frac{A}{3} + p_{32}a_3 j\beta \frac{A}{3} + p_{33}a_3^2 A \qquad\qquad 2.73$$

The other 80 elements of the A_e matrix can be found in a similar fashion.

2.4.4 Element assembly

The next stage in the finite element method is the assembly of the element matrices $[A_e]$ and $[B_e]$ into global matrices $[A]$ and $[B]$ respectively. An appropriate matrix solver is then used to obtain the eigenvalues and eigenvectors of the equation. The assembly of the global matrix is done with respect to the nodes of the domain. Where two or more nodes are common to more than one element, then it is advisable to add the contribution of each adjacent element to the global matrix when the calculation for the common node is carried.

Fig 2.7 Example of domain discretisation using triangular elements

Fig 2.7 shows a simple diagram of a domain, which has been discretised using 6 first order triangular elements. The node numbers 1-8 are the global node numbers for the domain and are used in the global matrices. The nodal points inside each triangular element are numbered 1-3. For the above structure, the global matrix, G, is formed by the addition of the element matrices A, B, C, D, E and F.

As previously noted, for every element in the discretised variational formulation, there is an expression of the form

$$\{H\}[N]\{H\}^T = \{H_1 \cdots H_9\}\begin{bmatrix} N_{11} & \cdot & \cdot & \cdot & N_{19} \\ \cdot & & & & \cdot \\ \cdot & & \cdot & & \cdot \\ \cdot & & & & \cdot \\ N_{91} & \cdot & \cdot & \cdot & N_{99} \end{bmatrix}\begin{bmatrix} H_1 \\ \cdot \\ \cdot \\ \cdot \\ H_9 \end{bmatrix} \qquad 2.74$$

Each term in the matrix N_{ij} relates to two nodal field values where the indices, i and j, correspond to the nodal field values of the vectors $\{H\}$ and $\{H\}^T$ according to the local numbering of an element. If a scalar formulation is considered, then only one field component need be taken into account, H_x for example, and the expression can be written as

$$\{H_{x1}\ H_{x2}\ H_{x3}\}\begin{bmatrix} N_{11} & N_{12} & N_{13} \\ N_{21} & N_{22} & N_{23} \\ N_{31} & N_{32} & N_{33} \end{bmatrix}\begin{bmatrix} H_1 \\ H_2 \\ H_3 \end{bmatrix} \qquad 2.75$$

For the structure shown in Fig 2.7, the global matrix G_{pq} may be defined as

$$G = \begin{bmatrix} G_{11} & \cdot & \cdot & \cdot & G_{18} \\ & & & & \cdot \\ & & & & \\ \cdot & & & & \\ \cdot & & & & \cdot \\ G_{81} & \cdot & \cdot & \cdot & G_{88} \end{bmatrix}$$

If P is the total number of nodal points of the structure, the order of the global matrix is PxP, which defines the size of the matrix when only one unknown field component is considered for each node. The terms of the global matrix, G_{pq}, are the field contributions of two nodes, p and q according to the global numbering system, where p and q correspond to the row and column of the matrix. Each term of the global matrix G_{pq} consists of a local contribution from only one element, unless the nodes lie on a shared boundary. The terms of the global matrix, G_{11}, for the first node with respect to itself will be defined as

$$G_{11} = N_{11}^A \qquad\qquad\qquad 2.76$$

where N_{11}^A is the term for the element matrix for the element A. The terms of the global matrix for other nodes, which do not lie on a shared boundary, can be found in a similar manner: $G_{12} = N_{13}^A, G_{24} = N_{32}^B$ etc. When the nodes are on a shared boundary, then the contributions of each element are added to the node e.g.

$$G_{22} = N_{33}^A + N_{33}^B \qquad\qquad\qquad 2.77$$

2.4.5 Infinite Elements

In electromagnetic terms, the dielectric waveguide is an unbound structure. The electromagnetic field can therefore, in principle, extend over the whole of open space, the area of which is infinite. This may cause problems for waveguides in which the solution exits near the cut-off region. In the finite element method, the

discretization of the waveguide cross-section cannot extend to infinity. Several techniques have therefore been developed for modelling the infinite open space with a finite number of elements.

The most commonly adopted approach is to enclose the core of the waveguide in an artificial conducting boundary, chosen to be sufficiently distant from the core of the waveguide. The finite element method can then be applied to the core region. Although this approach is simple, it is an inefficient method of dealing with the problem as a large number of elements are required in order to give good results. It is still difficult to model accurately cut-off situations accurately with this method.

The use of boundary elements was proposed by Yeh *et al.* (1979) to model a wide range of optical waveguide structures. In the method, the field in the exterior region was assumed to decay with an exponential factor, an effect incorporated into the finite element matrix. The major disadvantage of the approach is that the decay factor has to be determined heuristically and hence iteratively. The two co-ordinate systems did not conform and hence the fields used were not continuous.

A method of 'infinite elements' has been proposed and was used by Rahman and Davies (1984a) to include explicit field representation in all of the necessary transverse directions by incorporating rectangular strips as shown in Fig 2.8. An infinite element is a finite element that does indeed extend to infinity, extending the domain of the explicit field representation to infinity without increasing the matrix order.

The shape function for such an element should be chosen realistically and must be square integrable over an infinite element area. For such an infinite element extending to infinity in the *x*-direction, an exponential decay *x* may be assumed and the shape function can be written as

$$N(x, y) = f(y)\exp(-x/L) \qquad\qquad 2.78$$

where L is the decay length and $f(y)$ is the conventional shape function in the y-direction. Exponential decay functions can be assumed in a similar manner for decay in both the x and y directions.

Fig 2.8 Showing the use of infinite elements at the guide boundary.

2.5   Beam Propagation Algorithms

The finite element method outlined in the previous section is suitable for the stationary analysis of waveguides or where it is assumed that the guide under consideration is invariant in the axial direction. In integrated optics, however, there are numerous occasions when it is required to study the propagation of electromagnetic waves in z-variant structures. Such will be the case for example in bends, tapers, junctions and many other devices. In second harmonic generation in particular, the output power is dependent on the crystal length and hence there is a need to propagate the electromagnetic field obtained through the use of the modal

analysis method. As the case might also be under quasi phase matching, where the sign of the non-linear tensor is altered after every coherence length, a modal analysis of structures, which are z-variant and materials with non-linear properties, is clearly less than satisfactory. The problem can thus be re-defined as follows: To find the electromagnetic field inside a device given that the input field is known and the boundary conditions defined. This problem statement can be described using the wave equation

$$\nabla \times \nabla \times \phi + \mu_o \varepsilon \frac{\partial^2 \phi}{\partial t^2} = 0 \qquad\qquad 2.79$$

For simplicity, only a scalar approximation will be considered where all the fields are totally determined by knowing one component. The formalism could be easily extended to the vectorial case where, in the above equation, an additional term involving the derivative with respect to z is included. This scalar approximation is quite often used since the field distributions are usually very similar to those of the TE or TM polarisation.

2.5.1 Paraxial Approximation

The problem described by equation (2.79) is quite general and difficult to solve directly. In cases where the direction of propagation is well defined, then a simple approximation is appropriate and equation (2.79) could be written as follows for a steady state or time harmonic case

$$\frac{\partial^2 \phi}{\partial x^2} + \frac{\partial^2 \phi}{\partial y^2} + \frac{\partial^2 \phi}{\partial z^2} + \omega^2 \mu_o \varepsilon \phi = 0 \qquad\qquad 2.80$$

where ϕ is for the electromagnetic field, in the case of TE polarisation this will be E_y mode. In the above

$$\omega^2 \mu_o \varepsilon \phi = k_o^2 n^2 (x, y, z)\phi \qquad\qquad 2.81$$

where $n^2(x, y, z)$ is the refractive index profile in the guide. The electromagnetic field can be written as follows

$$\phi(x, y, z) = \phi(x, y, z)e^{-j\beta z} \qquad\qquad 2.82$$

where β is the phase constant or the reference value of the wavenumber. If the following two assumptions are now made

1. That the field inside the guide structure can be represented by a field with narrow angular spectrum
2. That the waveguide structure has a definitely marked longitudinal direction (z) and the propagation occurs mainly in that direction,

then the paraxial or slowly varying amplitude approximation can be made. If the value of β is now chosen such that it forms a central estimate of the value in the spectrum, then the variation of the fields with z will be dictated primarily by the exponential factor in equation (2.82). The term $\varphi(x, y, z)$, will only vary slowly with the axial co-ordinate z. Substituting for the field in the governing differential equation (2.80) and omitting the exponent (as it is a common factor), the following is obtained

$$\frac{\partial^2 \phi}{\partial x^2} + \frac{\partial^2 \phi}{\partial y^2} + \frac{\partial^2 \phi}{\partial z^2} - j2\beta \frac{\partial \phi}{\partial z} - \beta^2 \phi + k_o^2 n^2 \phi = 0 \qquad\qquad 2.83$$

since $\phi(x, y, z)$ varies slowly in the axial direction, the second order z derivative can be ignored to give the following paraxial equation with $\beta^2 = k_o^2 n_o^2$

$$\frac{\partial^2 \phi}{\partial x^2} + \frac{\partial^2 \phi}{\partial y^2} - j2k_o n_o \frac{\partial \phi}{\partial z} + k_o^2 \left(n^2 - n_o^2\right)\phi = 0 \qquad\qquad 2.84$$

2.5.2 Methods of Solution

The equation obtained above can be solved numerically using one of a variety of methods. Most of the solution methods rely on z-stepping algorithms where the z-axis is divided into a succession of discrete steps beginning with $z = 0$ and so on. Instead of seeking a solution over the entire domain of z, approximate solutions are sought at the defined steps starting with an initially known solution at $z = 0$. The solution at the ith step is computed from a recurrence relation, that is an algebraic equation that relates the solutions at two or more successive steps. Some of the methods allow the use of different step lengths while others require uniform steps. All the algorithms, however, rely on the more traditional numerical methods described already as for example, all the derivatives can be approximated using the finite difference scheme. In this the finite difference method is used in both the transverse and longitudinal directions and could also be used in conjunction with the finite element method. In such a scheme, the finite element method is used in the transverse direction while the finite difference method is used in the axial direction. In this thesis, the combined finite difference and finite element method will be used in the solution of a range of problems.

2.5.2.1   Finite Difference/Finite Element Algorithm

In this section, methods are described that consist of establishing a finite difference approximation for the longitudinal direction. The first order derivatives are approximated using the finite differences and with the fields known at an initial level, a stepping algorithm is initiated to calculate the field at the next step.

2.5.2.1.1   Forward Difference Scheme

As an example, consider equation (2.84), where a z-stepping algorithm can be established if the equation is written in the form

$$j2k_o n_o \frac{\partial \phi}{\partial z} = \frac{\partial^2 \phi}{\partial x^2} + \frac{\partial^2 \phi}{\partial y^2} + k_o^2 \left(n^2 - n_o^2 \right) \phi \qquad\qquad 2.85$$

The first order z-derivative can now be approximated using the finite differences: for example using the forward difference the following is obtained

$$\frac{\partial \phi}{\partial z} = \frac{\phi^{k+1} - \phi^k}{\Delta z} \qquad\qquad 2.86$$

Making this substitution in equation (2.85) the following will now be obtained

$$\frac{j2k_o n_o}{\Delta z} \left(\phi^{k+1} - \phi^k \right) = \frac{\partial^2 \phi^k}{\partial x^2} + \frac{\partial^2 \phi^k}{\partial y^2} + k_o^2 \left(n^2 - n_o^2 \right) \phi^k \qquad\qquad 2.87$$

In the above ϕ^k is the value of the field as a function of x and y but evaluated at a k-step in the z-direction. The right hand side of the above equation can now be implemented using the finite element method. The resulting matrix will be of the form

$$\phi^{k+1} = A\phi^k \qquad\qquad 2.88$$

The solution to the forward difference scheme is usually unstable. A restrictive relation also exists between the discretisation in the transverse direction and that of the longitudinal direction, which needs to be satisfied for a convergence of the algorithm.

2.5.2.1.2   Backward Difference Scheme

In this method, the field is evaluated at the forward end of the z-step. If step $k+1$ is considered as the current step in the algorithm, a backward difference approximation will be given by

$$\frac{j2k_o n_o}{\Delta z}\left(\phi^{k+1} - \phi^k\right) = \frac{\partial^2 \phi^{k+1}}{\partial x^2} + \frac{\partial^2 \phi^{k+1}}{\partial y^2} + k_o^2\left(n^2 - n_o^2\right)\phi^{k+1}$$ 2.89

The right hand side is evaluated at the $k+1$ step and the resultant matrix will be of the form

$$A\phi^{k+1} = \phi^k$$ 2.90

This equation will result in a stable numerical solution. There are no limitations on the size of the steps in the z direction for convergence however the approximation in the z direction is only accurate to the first order.

2.5.2.1.3   The Crank-Nicolson Method

Better results than above could be obtained with a second order approximation for the z-derivative if instead of equation (2.86) the following substitution is rather made

$$\frac{\partial \phi}{\partial z} = \frac{\phi^{k+1} - \phi^{k-1}}{2\Delta z}$$ 2.91

This substitution would however necessitate calculating the field at two z steps simultaneously (k and $k+1$). The resulting algorithm from this approximation would be numerically unstable.

A better implementation of the same method can be achieved if the fields are evaluated at some intermediate point, that is say at $(k+0.5)$, where making the necessary substitutions will result in an equation of the form

$$\frac{j2k_o n_o}{\Delta z}\left(\phi^{k+1} - \phi^k\right) = \left(\frac{\partial^2 \phi^k}{\partial x^2} + \frac{\partial^2 \phi^k}{\partial y^2} + k_o^2\left(n^2 - n_o^2\right)\phi^k\right)\bigg|_{z=(k+0.5)\Delta z} \qquad 2.92$$

Without actually calculating the fields at the intermediate points, they could still be evaluated by considering them to be the average of the fields at the k and $k+1$ steps such that

$$\phi^{(k+0.5)} = \frac{\phi^{k+1} + \phi^k}{2} \qquad 2.93$$

2.5.2.1.4   The θ-Method

Equation (2.84) can be written in the form

$$\frac{\partial \phi}{\partial z} = A\phi + B \qquad 2.94$$

where $A = \dfrac{k_o^2}{j2k_o n_o}\left(n^2 - n_o^2\right)$ and $B = \dfrac{1}{j2k_o n_o}\left(n^2 - n_o^2\right)\nabla_t^2 \phi$

The θ method will then give the following approximation

$$\frac{1}{\Delta z}\left(\phi^{k+1} - \phi^k\right) = -A\left[\theta\phi^{k+1} + (1-\theta)\phi^k\right] + \theta\, B^{k+1} + (1-\theta)B^k \qquad 2.95$$

where $0 \le \theta \le 1$. A rearrangement of the terms in the above equation will result in

$$(1 + A\theta \, \Delta z)\phi^{k+1} + [A \, \Delta z(1-\theta) - 1]\phi^k - \Delta z \theta \, B^{k+1} - \Delta z(1-\theta) B^k = 0 \qquad 2.96$$

The three cases previously considered can be regarded as the specialised forms of the above generalisation. It can be verified that for $\theta = 0$ the forward difference scheme is obtained. For $\theta = 1$ the equation will correspond to the backward difference scheme and for $\theta = 0.5$ the Crank-Nicolson algorithm is obtained.

Summary

This chapter has considered the general formulation of the finite element method for optical waveguide problems. Various aspects of the implementation of the method have been considered, including domain discretisation, shape functions and field representation. The properties of the various formulations have been presented. The development of the vector **H**-field formulation has been considered in detail. The chapter also has reviewed means of eliminating spurious solutions, which affect the vector **H**-field formulation. The infinite element for open boundary type problems has also been considered.

In addition to the finite element method, this chapter also considered the various algorithms of the beam propagation method. The beam propagation method will be adopted in conjunction with the finite element method in the study of second harmonic generation. This chapter forms the basics of the work described in subsequent chapters of this thesis.

Chapter Three

Theory of Second harmonic Generation

3.1   Introduction

Since the first demonstration of the efficient conversion of the fundamental to the second harmonic wavelength, in quartz crystal, (Franken *et al.* 1961, 1963), there has been a growing interest in the practical uses of this phenomenon. Such a possibility could make available powerful sources of coherent radiation, which had hitherto been unattainable and would lead, to major improvements in fluorescence based bioanalytical instrumentation and high-end reprographic systems. As an alternative to air-cooled argon ion and He-Cd lasers, non-linear frequency upconversion of infra red laser diodes or diode pumped solid state lasers has emerged as a basic means of generating blue or green laser light. Although compact blue-green lasers were predicted nearly three decades ago, significant progress in their realisation was only made with the advent of high powered GaAlAs diode laser.

Traditionally, blue-green laser generation has been accomplished by either second harmonic generation or by sum frequency mixing. In both processes, the output is proportional to the length of the mixing crystal, the square of its non-linear optical

coefficient and a phase matching term. In the case of second harmonic generation, the power also varies as the square of the intensity of the input field. In the case of sum frequency generation, the output is proportional to the product of the intensities of the two input fields. Due to their relatively low output powers, continuous wave diodes and diode pumped solid state lasers cannot be used in single pass systems to produce efficient frequency conversion.

Two main techniques have been developed for increasing the conversion efficiency of diode based harmonic generators in order to increase output power (Dixon, 1993). In the first approach, the non-linear crystal is placed inside an optical resonator. This would result in an increase of the incident power at the fundamental wavelength. There are two main ways in which this could be realised. In the first the non-linear crystal is placed inside the resonator of the fundamental wavelength laser. Chinn, (Chinn, 1976), first proposed the intracavity method, of efficiently generating the second harmonic wavelength. Since the cavities of the diode pumped solid state lasers have low losses the intracavity power can be more that 100 times the maximum output power, (Dixon, 1993). Such high intensity would significantly increase the conversion efficiency. In a practical device, a high reflectivity mirror is used in place of a conventional output coupler and the non-linear process is used to couple power from the cavity. Such devices will operate at efficiencies exceeding 10%; their output power however fluctuates chaotically. These fluctuations were caused by the intracavity nonlinear process and by variations in power distribution between the different polarisation states and laser transition (Dixon, 1993). Attempts at controlling the fluctuations using electronic feedback techniques were unsuccessful.

In the second method, a single frequency input beam is spatially and spectrally mode matched to an external optical resonator containing the non-linear crystal (Ashkin *et al.*, 1966). Spatial mode matching is achieved by matching the phase-front curvature and diameter of the input beam to the fundamental mode of the cavity. Spectral mode matching occurs when the round trip phase shift experienced by the light injected into the resonator is equal to an integral multiple of 2π. With these conditions

satisfied, the intracavity power can exceed the input by the magnitude of the order of two.

The other technique for increasing efficiency involves the confinement of the input beam in a single mode waveguide, which prevents diffraction. This results in an increase in the input intensity and hence more efficiency. Several efficient second harmonic generation has been demonstrated using this technique in different materials such as lithium niobate, lithium tantalate and potassium titanyl phosphate (Fejer et al., 1992). In the typical waveguide for frequency doubling, the output from a single-stripe, index guided GaAlAs diode laser at 830 nm is focussed onto a lithium niobate channel waveguide to produce a harmonic at 415 nm. For efficient second harmonic generation, the harmonic and fundamental must travel through the waveguide with a fixed phase relationship.

3.2   On the Physical origin of the Non-linear Tensor

3.2.1 Linear Model

The physics underlying the theory of second harmonic generation is that of the non-linearity of the refractive index. The physical origin of the refractive index is thus considered in this section.

The Lorentz model of an atom consists of a single electron and a nucleus. If an alternating electric field is applied to this atom then a polarisation of the same frequency as the applied electric field is induced. The electron will now oscillate about its equilibrium position, thus forming a dipole, which in turn radiates an electromagnetic wave of the same frequency as the applied electric field but of a different phase. This electron can be described mathematically as a harmonic oscillator and its equation of motion given by

$$\frac{d^2 r}{dt^2} + 2\gamma \frac{dr}{dt} + \omega_o^2 r = -\frac{e}{m} E \qquad 3.1$$

In the above, r is the displacement of the electron from its equilibrium position, m is the mass of the electron of charge e, ω_o is the natural frequency and γ is the restoring force. The applied electric field E is given as

$$E = E(\omega)e^{-j\omega t} + E^*(\omega)e^{+j\omega t} \qquad 3.2$$

where $E^*(\omega) = E(-\omega)$ is the complex conjugate of the applied electric field. A substitution of the above in equation (3.1) will result in a linear equation (Zernike and Midwinter, 1973) the solution of which is given by

$$r = -\frac{e}{m} E(\omega) \frac{e^{-j\omega t}}{\omega_o^2 - 2j\gamma\omega - \omega^2} + \text{complex conjugate} \qquad 3.3$$

For a medium with an electron density N, radiating in the same direction, the polarisation is defined as

$$P = \frac{Ne^2}{m} \frac{E(\omega)e^{-j\omega t}}{\omega_o^2 - 2j\gamma\omega - \omega^2} + \text{complex conjugate} \qquad 3.4$$

Making the following substitution

$$\chi(\omega) = \frac{Ne^2}{m} \frac{1}{\omega_o^2 - 2j\gamma\omega - \omega^2} \qquad 3.5$$

in equation (3.4), the following is obtained

$$P = \chi(\omega)E(\omega)e^{-j\omega t} + \text{complex conjugate} \qquad 3.6$$

This indeed does show that the induced polarisation is proportional to the applied electric field and of the same frequency. This value is used as source term in Maxwell's equation.

In some crystalline materials, the interactions between the atoms are not in the same direction i.e. all the atoms do not radiate in the same direction. Such materials are said to display anisotropy. In such crystals, the dielectric constant is not a scalar quantity but a second rank tensor, since it relates the displacement in one direction with the fields in the three directions. Equation (1.5) can therefore be written as

$$D_i = \sum_j \varepsilon_{ij}(\omega)E_j, \qquad i = 1,2,3 \qquad\qquad 3.7$$

In matrix form this can be written as

$$\frac{1}{\varepsilon_o} \cdot \begin{pmatrix} D_x \\ D_y \\ D_z \end{pmatrix} = \begin{pmatrix} 1+\chi_{xx} & \chi_{xy} & \chi_{xz} \\ \chi_{yx} & 1+\chi_{yy} & \chi_{yz} \\ \chi_{zx} & \chi_{zy} & 1+\chi_{zz} \end{pmatrix} \cdot \begin{pmatrix} E_x \\ E_y \\ E_z \end{pmatrix} \qquad 3.8$$

Such materials are only able to transmit plane-polarised waves in one of two mutually orthogonal directions. These polarisations will 'see' different refractive indices. Incident light that is not plane-polarised is decomposed into two linearly polarised beams in the allowed directions. To find the two allowed directions of polarisation and the refractive indices in these directions, the index ellipsoid is used (Zernike and Midwinter, 1973)

$$\frac{x^2}{n_1^2} + \frac{y^2}{n_2^2} + \frac{z^2}{n_3^2} = 1 \qquad\qquad 3.9$$

Here, x, y and z are optical axes along which polarisation occurs. In some optically anisotropic materials, the three axes of the index ellipsoid are unequal, such crystals are called biaxial. In such crystals two optic axes can be defined. In uniaxial crystals,

two of the three axes are equal. In such a case the optic axis is perpendicular to the plane of the two equal axes. In such a case equation 3.8 reduces to

$$\begin{pmatrix} D_x \\ D_y \\ D_z \end{pmatrix} = \begin{pmatrix} 1+\chi_p & 0 & 0 \\ 0 & 1+\chi_s & 0 \\ 0 & 0 & 1+\chi_s \end{pmatrix} \cdot \begin{pmatrix} E_x \\ E_y \\ E_z \end{pmatrix} \qquad\qquad 3.10$$

3.2.2 Optical Non-linear Susceptibility

It has been seen in the previous section that the polarisation in a material is proportional to the inducing field. This polarisation was completely linear: an increase in the field, by a factor of m, will result in an increase of the polarisation, by the same factor. Some materials however do have non-linear properties, as such in addition to the linear response the field produces a polarisation proportional to the square of the field. Similar examples of non-linear dependence are known in other areas of physics. Perhaps the best known example is the break down of Hooke's law at large enough stresses. Polarisation is thus linear for certain limited values of the field strength. With the advent of the laser, much higher field strengths have become attainable and hence non-linear polarisation takes on new importance.

The non-linear response of the medium can lead to an exchange of energy between electromagnetic fields of different frequencies. The two most important applications of such a phenomenon are parametric frequency conversion and second harmonic generation. If the refractive index of such a crystal is modulated by a field of frequency ω_2, then a wave of frequency ω_1 passing through the crystal will be phase modulated giving rise to side bands at combination frequencies. Modulating the parameters of the crystal can thus create different frequencies. The modulating field ω_2 is itself affected by the modulated refractive index and can thus give rise to a harmonic overtone at $2\omega_2$.

The interactions between the different fields can be attributed to the non-linearity of polarisation. Non-linear terms can therefore be included in the polarisation such that equation (3.6) can be written as

$$P = \chi^{(1)} E + \chi^{(2)} E^2 + \chi^{(3)} E^3 + ...$$

3.11

where $\chi^{(2)}$ and $\chi^{(3)}$ are constants, the second and third order susceptibilities. Since in crystals with a centre of symmetry, the even numbered non-linearities are identically equal to zero, the polarisation P_1 due to the first non-linear term only can be written as follows

$$P_1 = 2dE^2$$

3.12

The non-linear polarisation can be described in terms of the anharmonic oscillator. It is known that optical polarisation is due to the outer bound electrons that are displaced by the optical field. The displaced electrons will be subject to a restoring force, if this is included in the equation of motion of the electron then the following is obtained (Yariv, 1971)

$$\frac{d^2 r}{dt^2} + 2\gamma \frac{dr}{dt} + \omega_o^2 r - \xi r^2 = -\frac{e}{m} E$$

3.13

If the following solution is assumed

$$r = r_1 + r_2 + r_3 + ...$$

3.14

where $r_l = a_l E^l$ and this is substituted into equation (3.13) and collecting terms of the same order, the following is obtained (Zernike and Midwinter, 1973)

$$\frac{d^2 r_1}{dt^2} + 2\gamma \frac{dr_1}{dt} + \omega_o^2 r_1 = -\frac{e}{m} E \qquad\qquad 3.15$$

$$\frac{d^2 r_2}{dt^2} + 2\gamma \frac{dr_2}{dt} + \omega_o^2 r_2 = \xi\, r_1^2 \qquad\qquad 3.16$$

If the interacting electric field is defined as

$$E = \sum_n E(\omega_n) e^{-j\omega_n t} = E(\omega_1) e^{-j\omega_1 t} + E^*(\omega_1) e^{j\omega_1 t} + E(\omega_2) e^{-j\omega_2 t} +$$

$$E^*(\omega_2) e^{j\omega_2 t} + \ldots + E(\omega_n) e^{-j\omega_n t} + E^*(\omega_n) e^{j\omega_n t} \qquad\qquad 3.17$$

A substitution of equation (3.17) in equation (3.15) will yield

$$-\frac{e}{m} \sum E(\omega_n) e^{-j\omega_n t} = -a_1 \sum \omega_n^2 E(\omega_n) e^{-j\omega_n t} - 2a_1 j\gamma \sum \omega_n E(\omega_n) e^{-j\omega_n t} +$$

$$a_1 \omega_o^2 \sum E(\omega_n) e^{-j\omega_n t} \qquad\qquad 3.18$$

Equating the sums of the individual terms at each frequency the following is obtained

$$r_1 = a_1 \sum E(\omega_n) e^{-j\omega_n t} = -\frac{e}{m} \sum \frac{E(\omega_n) e^{-j\omega_n t}}{\omega_o^2 - 2j\omega_n \gamma - \omega_n^2} \qquad\qquad 3.19$$

This result is similar to that found in the linear case only that it has been extended to more than one frequency. This result is the basis for finding non-linear terms of higher order. Substituting the above into equation (3.16) and using the relation

$$\left(\sum_n E(\omega_n) e^{-j\omega_n t} \right)^2 = \sum_n \sum_m E(\omega_n) E(\omega_m) e^{-j(\omega_n + \omega_m)t} \qquad\qquad 3.20$$

where m and n has the same range of values. It follows that

$$r_2 = -\frac{e^2 \xi}{m^2} \sum_n \sum_m \frac{E(\omega_n)E(\omega_m)e^{-j(\omega_n+\omega_m)t}}{F(\omega_o,\omega_n,\omega_m,\gamma)}$$ 3.21

where

$$F(\omega_o,\omega_n,\omega_m,\gamma) = (\omega_o^2 - 2j\omega_n\gamma - \omega_n^2)(\omega_o^2 - 2j\omega_m - \omega_m^2)$$
$$\times [\omega_o^2 - 2j(\omega_n + \omega_m)\gamma - (\omega_n + \omega)^2]$$ 3.22

A power series can then be used to represent the polarisation density. For the linear polarisation this is

$$P_{linear} = \sum \chi^{(1)}(\omega_n)E(\omega_n)e^{-j\omega_n t}$$ 3.23

where

$$\chi^1(\omega) = \frac{Ne^2}{m} \frac{1}{\omega_o^2 - 2j\gamma\omega_n - \omega_n^2}$$ 3.24

For the second order polarisation, the following is obtained

$$P_{sec} = \sum_n \sum_m \chi^{(2)}(\omega_n,\omega_m)E(\omega_n)E(\omega_m)e^{-j(\omega_n+\omega_m)t}$$ 3.25

In the above

$$\chi^{(2)}(\omega_n,\omega_m) = -\frac{m\xi}{N^2 e^3}[\chi^{(1)}(\omega_n)][\chi^{(1)}(\omega_m)][\chi^{(1)}(\omega_n + \omega_m)]$$ 3.26

The second order polarisation is thus due to the non-linear term $\xi\, r^2$ in the equation for the anharmonic oscillator. It will be observed from equation (3.25) that it contains

terms for all possible values of n and m, ± 1 and ± 2. Equation (3.26) also shows that the second order susceptibility $\chi^{(2)}$ depends on the product of the first order susceptibilities of the frequencies involved in the interaction.

Henceforth P will be used for the second order polarisation and χ^2 will be used for the second order non-linear susceptibility. Thus far, values have been represented as scalar quantities, which is accurate in the one-dimensional case. In reality however, they are vector quantities, as such χ is a tensor of the third rank and equation (3.25) can be rewritten taken this into account to give

$$P_{j(\omega_{n+m})} = \sum_{jk}\sum_{nm} \chi_{ijk}(\omega_{n+m},\omega_n,\omega_m)E_j(\omega_n)E_k(\omega_m)e^{-j(\omega_n+\omega_m)t} \qquad 3.27$$

In the above i, j, k correspond to the three principal axes in the crystal and $\omega_{n+m} = \omega_n + \omega_m$.

Equation (3.26) was generalised into three dimensions (Miller, (1964), Garrett and Robinson (1966)) to obtain the following rule, also known as Miller's rule

$$\chi^2_{ijk}(\omega_1,\omega_2,\omega_3) = \left|\chi^1_{ii}(\omega_1)\right|\left|\chi^1_{jj}(\omega_2)\right|\left|\chi^1_{kk}(\omega_3)\right|\Delta_{ijk} \qquad 3.28$$

The factor Δ_{ijk} was found to be remarkably constant over a wide range of materials. This has proved to be useful in the search for new materials. The observed constancy of the factor Δ_{ijk} might suggest that the large variations in the non-linear susceptibility might reflect their dependence on the linear susceptibility.

Equation (3.25) can be written in the form

$$P(2\omega_1) = \chi(2\omega_1,\omega_1,\omega_1)E^2 e^{-2j(\omega_1 t + k_{1z})} \qquad 3.29$$

which from equation (3.12) gives

$$d_{ijk} = \frac{1}{2}\chi(2\omega_1, \omega_1, \omega_1)$$ 3.30

The tensor d_{ijk} can be contracted to d_{ij} which forms a 3x6 matrix that operates on the field which is written in column vector form to yield

$$\begin{bmatrix} P_x \\ P_y \\ P_z \end{bmatrix} = \begin{bmatrix} d_{11} & d_{12} & d_{13} & d_{14} & d_{15} & d_{16} \\ d_{21} & d_{22} & d_{23} & d_{24} & d_{25} & d_{26} \\ d_{31} & d_{32} & d_{33} & d_{34} & d_{35} & d_{36} \end{bmatrix} \begin{bmatrix} E_x^2 \\ E_y^2 \\ E_z^2 \\ 2E_zE_y \\ 2E_zE_x \\ 2E_xE_y \end{bmatrix}$$ 3.31

As an example in films of suitably oriented GaAs or in hexagonal crystals such as CdS or ZnO with the c axis along the z direction, the nonlinear polarization term will only have a z component, such that,

$$P^{NL} = \chi_{32}E_f^2$$ 3.32

For a x-cut proton exchange LiNbO$_3$ waveguide, the optical axis c is parallel to the y-axis. In these guides only TE modes having components E$_y$, H$_x$ and H$_z$ can propagate. Assuming constant amplitude of the fundamental field, the non-linear polarisation can be written as

$$P_y(x,z) = \varepsilon_o d_{33} E_{fy}^2(x) e^{-j2\beta_{fz}}$$ 3.33

In a Z-cut waveguide, the optical axis c is parallel to the x-axis. In these guides only TM modes having components H$_y$, E$_x$ and E$_z$ can propagate. The nonlinear polarization is given by

$$P_x = \varepsilon_o d_{31} E_{fz}^2 + \varepsilon_o d_{33} E_{fx}^2 \qquad\qquad 3.34$$

$$P_z = \varepsilon_o d_{22} E_{fz}^2 + 2\varepsilon_o d_{31} E_{fx} E_{fz} \qquad\qquad 3.35$$

In both cases, the light propagates in the z-direction.

3.3   Formulation of the Non-linear Interaction Equation

In this section, consideration is given to how the wave equations describing the non-linear interactions in crystals are derived. Following the derivation by Zernike and Midwinter (1973) the non-linear polarisation is inserted as a source term in Maxwell's equations

$$\nabla \mathbf{x} \mathbf{H} = \frac{1}{c}\frac{\partial\, \mathbf{D}}{\partial\, t} \qquad\qquad 3.36$$

$$\nabla \mathbf{x} \mathbf{E} = -\frac{1}{c}\frac{\partial}{\partial\, t}(\mu \mathbf{H}) \qquad\qquad 3.37$$

$$\mathbf{D} = \varepsilon\mathbf{E} + 4\pi\mathbf{P} \qquad\qquad 3.38$$

The linear polarisation is included in ε and $\mathbf{P}$ is the non-linear polarisation. Assuming that the material is non-conducting and taking the curl of both sides of the curl of $\mathbf{E}$, we obtain

$$\nabla \mathbf{x} \nabla \mathbf{x} \mathbf{E} = -\frac{\mu}{c}\frac{\partial}{\partial\, t}(\nabla \mathbf{x} \mathbf{H}) \qquad\qquad 3.39$$

$$\nabla\nabla\cdot\mathbf{E} - \nabla^2\mathbf{E} = -\frac{\mu}{c}\frac{\partial}{\partial t}\left(\frac{1}{c}\frac{\partial}{\partial t}\left(\varepsilon\mathbf{E} + 4\pi\mathbf{P}\right)\right)$$ 3.40

For a nonconducting medium, $\nabla\cdot\mathbf{E} = 0$

$$-\nabla^2\mathbf{E} = -\frac{\mu}{c}\frac{\partial}{\partial t}\left(\frac{\varepsilon}{c}\frac{\partial\mathbf{E}}{\partial t} + \frac{4\pi\partial\mathbf{P}}{c\partial t}\right)$$ 3.41

$$\nabla^2\mathbf{E} = \frac{\mu\varepsilon}{c^2}\frac{\partial^2\mathbf{E}}{\partial t^2} - \frac{4\pi\mu}{c^2}\frac{\partial^2\mathbf{P}}{\partial t^2}$$ 3.42

$$\nabla^2\mathbf{E} = \frac{\partial^2}{\partial t^2}\left(\frac{\varepsilon}{c^2}\mathbf{E}\right) - \frac{4\pi}{c^2}\frac{\partial^2\mathbf{P}}{\partial t^2}.$$ 3.43

If the discussion is then limited to one dimension, by assuming that $\frac{\partial}{\partial x} = \frac{\partial}{\partial y} = 0$ and to the interaction of three travelling waves defined as;

$$E_1(z,t) = E_1(z)e^{-j(\omega_1 t - k_1 z)}$$
$$E_2(z,t) = E_2(z)e^{-j(\omega_2 t - k_2 z)}$$ 3.44
$$E_3(z,t) = E_3(z)e^{-j(\omega_3 t - k_3 z)}$$

where the subscripts 1,2,3 stand for the different frequencies present with the polarisation defined as

$$P_1(z,t) = 4dE_2^*(z)E_3(z)e^{-j[(\omega_3-\omega_2)t-(k_3-k_2)z]}$$
$$P_2(z,t) = 4dE_3(z)E_1^*(z)e^{-j[(\omega_3-\omega_1)t-(k_3-k_1)z]}$$ 3.45
$$P_3(z,t) = 4dE_1(z)E_2(z)e^{-j[(\omega_3+\omega_2)t-(k_1+k_2)z]}$$

then,

$$\frac{\partial^2 P_1}{\partial t^2} = -(\omega_3 - \omega_2)^2 4dE_2^*(z)E_3(z)e^{-j[(\omega_3-\omega_2)t-(k_3-k_2)z]}$$ 3.46a

$$\frac{\partial^2 P_2}{\partial t^2} = -(\omega_3 - \omega_1)^2 4dE_3(z)E_1^*(z)e^{-j[(\omega_3-\omega_1)t-(k_3-k_1)z]}$$ 3.46b

$$\frac{\partial^2 P_3}{\partial t^2} = -(\omega_1 + \omega_2)^2 4dE_1(z)E_2(z)e^{-j[(\omega_1+\omega_2)t-(k_1+k_2)z]}$$ 3.46c

Assuming the variation of the field amplitude is small such that $k\dfrac{dE}{dz} \gg \dfrac{d^2E}{dz^2}$ and

making the following substitution

$$E_1(z,t) = E_1(z)e^{-j(\omega_1 t - k_1 z)}$$ 3.47

we obtain the following

$$\nabla^2 \mathrm{E} = \frac{\partial^2 E_1(z,t)}{\partial z^2} = \frac{\partial}{\partial z}\left(jk_1 E_1(z)e^{-j(\omega_1 t - k_1 z)} + e^{-j(\omega_1 t - k_1 z)}\frac{dE_1}{dz} \right)$$

$$= -k_1^2 E_1(z)e^{-j(\omega_1 t - k_1 z)} + jk_1 e^{-j(\omega_1 t - k_1 z)}\frac{dE_1}{dz} + jk_1 e^{-j(\omega_1 t - k_1 z)}\frac{dE_1}{dz} + jk_1 e^{-j(\omega_1 t - k_1 z)}\frac{d^2 E_1}{dz^2}$$

$$= \left(2jk_1 \frac{dE_1}{dz} - k_1^2 E_1(z) \right)e^{-j(\omega_1 t - k_1 z)}$$ 3.48

$$\frac{\partial^2 E_1(z,t)}{\partial z^2} = -\left[k_1^2 E_1(z) - 2jk_1 \frac{dE_1(z)}{dz} \right]e^{-j(\omega_1 t - k_1 z)}$$ 3.49

$$\frac{\varepsilon}{c^2}\frac{\partial^2}{\partial t^2}E_1(z) = \frac{\varepsilon}{c^2}\frac{\partial}{\partial t}\left(-j\omega e^{-j(\omega_1 t - k_1 z)}E_1(z) \right)$$

$$= \frac{\varepsilon}{c^2}\left(-\omega^2 e^{-j(\omega_1 t - k_1 z)}E_1(z) \right)$$ 3.50

Making this substituting for the differentials the following is obtained

$$-\left(k_1^2 E_1(z) - 2jk_1 \frac{dE_1}{dz}\right)e^{-j(\omega_1 t - k_1 z)}$$

$$= -\frac{\omega_1^2 \varepsilon}{c^2} E_1(z)e^{-j(\omega_1 t - k_1 z)} - \frac{4\pi}{c^2}\left[-(\omega_3 - \omega_1)^2 4\overline{d}E_2^*(z)E_3(z)e^{-j[(\omega_3 - \omega_2)t - (k_3 - k_2)z]}\right]$$

<div align="right">3.51</div>

$$\omega_3 = \omega_1 + \omega \text{ and } \frac{\omega_1^2 \varepsilon}{c^2} = k_1^2$$

then

$$-2jk_1 \frac{dE_1}{dz}e^{-j(\omega_1 t - k_1 z)} = \frac{16\pi}{c^2}\left[\omega_1^2 \overline{d}E_2^*(z)E_3(z)e^{-j[(\omega_3 - \omega_2)t - (k_3 - k_2)z]}\right]$$

<div align="right">3.52</div>

$$\frac{dE_1}{dz} = -j\frac{8\omega_1^2 \overline{d}}{k_1 c^2}E_2^*(z)E_3(z)e^{-j\omega_1 t} \cdot e^{j\omega_1 t} \cdot e^{-jk_1 z} \cdot e^{j(k_3 - k_2)z}$$

<div align="right">3.53</div>

$$\frac{dE_1}{dz} = -j\frac{8\omega_1^2 \overline{d}}{k_1 c^2}E_2^*(z)E_3(z)e^{j(k_3 - k_2 - k_1)z}$$

<div align="right">3.54</div>

Similarly,

$$\frac{dE_2(z)}{dz} = -j\frac{8\pi\omega_2^2}{k_2 c^2}\overline{d}E_1^*(z)E_3(z)e^{j(k_3 - k_2 - k_1)z}$$

<div align="right">3.55</div>

and

$$\frac{dE_3(z)}{dz} = -j\frac{8\pi\omega_3^2}{k_3 c^2}\overline{d}E_1(z)E_2(z)e^{j(k_1 + k_2 - k_3)z}$$

<div align="right">3.56</div>

These are the basic equations, which describe non-linear parametric interactions. The three most common forms of which are

1.   Second harmonic generation in which part of the energy of an optical wave at frequency ω is converted to that of a wave at frequency 2ω.

2.   Parametric oscillation in which a strong pump at ω_3 causes the simultaneous generation in a nonlinear crystal of radiation at ω_1 and ω_2 such that $\omega_3 = \omega_1 + \omega_2$.

3.   Frequency up-conversion in which a weak signal of low frequency ω_1 is converted coherently to a signal of higher frequency ω_3 by mixing with a strong laser field at ω_2 such that $\omega_2 = \omega_3 - \omega_1$

It can be noted that they are coupled through the non-linear coefficient d. Each of the equations relates the rate of change of the amplitude at a particular frequency with distance with the rate of change of amplitude at the other two frequencies. They also show the phase difference between the polarisation wave and the electromagnetic wave, which can be written as

$$\Delta k = k_3 - k_2 - k_1 \qquad\qquad 3.57.$$

3.4   Optical Second Harmonic Generation

From the above amplitude equations, one can then obtain the equations governing sum frequency generation, difference frequency generation and second harmonic generation. Second harmonic generation is a special case of frequency mixing when it is considered that the two input frequencies are equal, thus $\omega_2 = 2\omega_1$. As before, the following equations can be derived:

$$\frac{dE_1(z)}{dz} = -j\frac{8\pi\omega_1^2}{k_1 c^2}\overline{d}E_1^*(z)E_2(z)e^{-j\Delta kz}$$ 3.58

$$\frac{dE_2(z)}{dz} = -j\frac{16\pi\omega_1^2}{k_2 c^2}\overline{d}E_1^2(z)e^{j\Delta kz}$$ 3.59

$$\Delta k = 2k_1 - k_2$$ 3.60

3.4.1 Classification of SHG

Principally, SHG can be broadly classified into two types (Hashizume, 1992); Type I in which there is a conversion from a fundamental guided mode into a second harmonic guided mode, known as the guided-guided SHG or second harmonic radiation mode. The guided-guided mode has four possible modes:

Guided TE(ω)	to	Guided TE(2ω)
Guided TE(ω)	to	Guided TM(2ω)
Guided TM(ω)	to	Guided TM(2ω)
Guided TM(ω)	to	Guided TE(2ω).

In this type of conversion, both the fundamental and the second harmonic waves are tightly confined in the guiding regions of the waveguide, hence making it ideal for use in integrated optics. It however requires critical control of the waveguide parameters for phase matching.

The conversion from a fundamental guided mode into a second harmonic radiation mode is also known as the Cerenkov type SHG. The possible modes of conversion are:

Guided TE(ω)   to   Radiation TE(2ω)

Guided TM(ω)	to	Radiation TE(2ω)
Guided TE(ω)	to	Radiation TM(2ω)
Guided TM(ω)	to	Radiation TM(2ω)

Type II conversion:

Guided (TE(ω) + TM(ω))	to	Radiation TE(2ω)
Guided (TE(ω) + TM(ω))	to	Radiation TM(2ω).

Unlike guided modes, which are discrete, radiation modes have a continuous spectrum. Phase matching is automatically satisfied as long as the phase velocity of the guided fundamental mode is faster than the SH wave in the substrate. A necessary condition for this being the effective index of the fundamental mode is smaller than the substrate refractive index of the SH, $n^{\omega} < n_s^{2\omega}$. This allows the SH to be radiated at a finite angle into the substrate.

In this work, we will consider the guided-guided type of conversion and mode I configuration of the Cerenkov type conversion.

3.4.2 Derivation of Second Harmonic Equation

In this section the second Harmonic wave equation is derived in a form suitable for solving using a numerical method, namely the finite element method.

Using the concept of the nonlinear polarization and assuming that this is related to the electric field of the electromagnetic wave by the scalar equation as shown previously,

$$P^{NL} = 2\varepsilon_o d E^2 \qquad\qquad 3.61$$

where d is a coefficient whose dimension is the inverse of the electric field.

It has also been shown previously that the physical origins of the non-linear polarisation can be attributed to the non-uniform deformation of the outer electrons of an atom or atomic system. If a monochromatic plane wave propagating through a non-linear crystal in the z direction is considered, then the electric field can be written as

$$E_\omega(z,t) = \frac{1}{2}\{E(z,\omega)\exp[j(\omega t - k_\omega z)] + c.c\},\qquad\qquad 3.62$$

where $c.c$ is the complex conjugate and $k_\omega = \dfrac{\omega}{c_\omega} = \dfrac{n_\omega \omega}{c_o}$.

In an anisotropic material, the above scalar relation between the non-linear polarisation and the electric field is not strictly valid. A tensor relation of the form $P^{NL} = \varepsilon_o[d]E^2$ can be established. It can be shown for an anisotropic material that, for a given direction of propagation, two different linearly polarised plane waves can propagate. Corresponding to these two different polarisation are two refractive indices, the ordinary and the extraordinary. Due to this phenomenon, the electric field, $E^\omega(r,t)$, of the electromagnetic wave at frequency ω and at a given point r and the non-linear polarisation at 2ω, $P_{NL}^{2\omega}(r,t)$ can be written in the form

$$E^\omega(r,t) = \frac{1}{2}\left[E^\omega(r,\omega)\exp(j\omega t) + c.c.\right]\qquad\qquad 3.63$$

$$P_{NL}^{2\omega}(r,t) = \frac{1}{2}\left[P^{2\omega}(r,2\omega)\exp(2j\omega t) + c.c.\right],\qquad\qquad 3.64$$

a tensor relation can be established between the non-linear polarisation at 2ω and the electric field at ω.

The second harmonic polarisation component in the j direction of the crystal is therefore

$$P_j^{2\omega} = \sum_{j,k=1,2,3} \varepsilon_o d_{ijk}^{2\omega} E_j^{\omega} E_k^{\omega} \qquad 3.65$$

Having derived an expression for the non-linear polarisation, it is now possible to derive equations describing the propagation the second harmonic wave through a crystal. Using Maxwell's equations as the starting point and by inserting the non-linear polarisation as a source term the following can be written

$$\nabla \times E = -\frac{\partial B}{\partial t} \qquad 3.66$$

$$\nabla \times H = \frac{\partial D}{\partial t} \qquad 3.67$$

$$B = \mu H \qquad 3.68$$

$$D = \varepsilon_o E + P^L + P^{NL} = \varepsilon_o [\varepsilon] E + \varepsilon_o P^{NL} \qquad 3.69$$

Substituting equation (3.68) into (3.66) and taking the curl of both sides of equation (3.66), the following is obtained

$$\nabla \times \nabla \times E = -\mu_o \frac{\partial}{\partial t}(\nabla \times H) \qquad 3.70$$

$$\nabla \times \nabla \times E = -\nabla^2 E \qquad 3.71a$$

$$\nabla \times H = \varepsilon_o [\varepsilon] \frac{\partial}{\partial t} E + \varepsilon_o [d] \frac{\partial}{\partial t} E^2 \qquad 3.71b$$

$$-\nabla^2 E = -\mu_o \frac{\partial}{\partial t} \left(\varepsilon_o [\varepsilon] \frac{\partial}{\partial t} E + \varepsilon_o [d] \frac{\partial}{\partial t} E^2 \right) \qquad 3.72a$$

$$-\nabla^2 E = -\mu_o \varepsilon_o [\varepsilon] \frac{\partial^2}{\partial t^2} E - \mu_o \varepsilon_o [d] \frac{\partial}{\partial t} E^2 \qquad 3.72b$$

$$\nabla^2 E - \mu_o \varepsilon_o [\varepsilon] \frac{\partial^2}{\partial t^2} E = \mu_o \varepsilon_o [d] \frac{\partial^2}{\partial t^2} E^2 \qquad \qquad 3.72c$$

$$\nabla^2 E - \frac{[\varepsilon]}{c^2} \frac{\partial^2}{\partial t^2} E = \frac{[d]}{c^2} \frac{\partial^2}{\partial t^2} E^2 \qquad \qquad 3.72d$$

$$\nabla^2 E + [\varepsilon] \frac{\omega^2}{c^2} E = -[d] \frac{\omega^2}{c^2} E^2 \qquad \qquad 3.72e$$

$$\nabla^2 E + [\varepsilon] k^2 E = -[d] k^2 E^2 \qquad \qquad 3.73$$

The above equation describes the propagation of waves in a crystal in the presence of a forcing function. It must be satisfied independently by each of the waves present in the crystal. For the second harmonic wave, therefore, we obtain the following,

$$\nabla^2 E_{2\omega} + [\varepsilon] k_{2\omega}^2 E_{2\omega} = -[d] k_{2\omega}^2 E_\omega^2 \qquad \qquad 3.74a$$

$$\nabla^2 E_{2\omega} + ([\varepsilon] k_{2\omega}^2 - \beta_{2\omega}^2) E_{2\omega} = -[d] k_{2\omega}^2 E_\omega^2. \qquad \qquad 3.74b$$

In a more general form, the above equation can be written as

$$\nabla^2 E_{2\omega} + ([\varepsilon] k_{2\omega}^2 - \beta_{2\omega}^2) E_{2\omega} = -\mu_o \omega_{2\omega}^2 P_{2\omega}^{NL}. \qquad \qquad 3.75$$

For different crystal cuts and orientations we will obtain different nonlinear polarization terms for which we solve for the second harmonic field. To solve this equation, we first set the right hand side to zero and find the field distribution at the fundamental frequency. Knowing the field we can find the nonlinear polarization at the harmonic frequency using the tensor relation. This is then inserted into the above equation to obtain the field at the harmonic frequency.

$$\nabla^2 E_{2\omega} + \left([\varepsilon] k_{2\omega}^2 - \beta_{2\omega}^2 \right) E_{2\omega} = P \qquad\qquad 3.76$$

where $\mathbf{P}$ is the calculated non-linear polarisation.

3.4.3 Variational expression for the S.H field equation

It can be shown that the functional which minimises the above equation is of the form

$$\wp = \iint \frac{1}{2} \left\{ \left(\frac{\partial E}{\partial x} \right)^2 + \left(\frac{\partial E}{\partial y} \right)^2 \, dxdy + \frac{\left([\varepsilon] k_{2\omega}^2 - \beta_{2\omega}^2 \right)}{2} \iint E^2 dxdy + \iint P \cdot E \, dxdy \right\}$$

3.77

An equation of the form $Lu = f$ is a deterministic problem, the solution of which is uniquely determined by the source term f. L is an operator and u is the function sought. One way of solving such a problem is to find a weak formulation of it, which satisfies certain specified conditions. This weak formulation is also known as the variational formulation the solution of which is also the solution of the original problem, provided that the specified conditions are satisfied.

If it is assumed that u_o is a solution of our deterministic problem, then the functional sought is of the form

$$Fu = \langle Lu, u \rangle - 2 \langle f, u \rangle \qquad\qquad 3.78$$

Since u_o is a solution we can say that $L u_o = f$. Substituting for f in the above we obtain

$$Fu = \langle Lu, u \rangle - 2\langle Lu_o, u \rangle \tag{3.79}$$

It is obvious however that

$$Fu = \langle Lu, u \rangle - \langle Lu_o, u \rangle - \langle u, Lu_o \rangle \tag{3.80a}$$

$$= \langle Lu, u \rangle - \langle Lu_o, u \rangle - \langle Lu, u_o \rangle \tag{3.80b}$$

$$= \langle Lu, u \rangle - \langle Lu_o, u \rangle - \langle Lu, u_o \rangle + \langle Lu_o, u_o \rangle - \langle Lu_o, u_o \rangle \tag{3.80c}$$

$$= \langle L(u - u_o), (u - u_o) \rangle - \langle Lu_o, u_o \rangle \tag{3.80d}$$

Assuming that the operator $L = -\nabla^2$, then

$$\langle Lu, v \rangle = -\int_\Omega v\nabla^2 u \, d\Omega \tag{3.81}$$

From Green's identity theorem the following is obtained

$$\int_\Omega v\frac{\partial u}{\partial n} ds = \int_\Omega \nabla u \nabla u \, d\Omega + \int_\Omega v\nabla^2 u \, d\Omega \tag{3.82}$$

so that

$$\rangle Lu, v \langle = \int_\Omega \nabla u \nabla u \, d\Omega - \int_s v\frac{\partial u}{\partial n} ds \tag{3.82}$$

If the operator is given explicitly by

$$L = \left(\nabla \times \nabla \times + \omega^2 \mu \varepsilon \right) \qquad\qquad 3.83$$

then

$$F = \left\langle \left(\nabla \times \nabla \times - \omega^2 \mu \varepsilon \right) E, E \right\rangle - 2 \left\langle P^{NL}, E \right\rangle \qquad\qquad 3.84$$

$$F = \left\langle \nabla \times \nabla \times E, E \right\rangle - \left\langle \omega^2 \mu \varepsilon\, E, E \right\rangle - 2 \left\langle P^{NL}, E \right\rangle \qquad\qquad 3.85$$

$$F = \iint_{\Omega} \left(\nabla \times E^* \right) \cdot \left([\mu]^{-1} \nabla \times E \right) d\Omega - \iint_{\Omega} E^* \omega^2 \varepsilon E d\Omega + 2 j \omega \iint_{\Omega} P^{NL} E^* d\Omega \qquad 3.86$$

$$\delta F = \iint_{\Omega} \left(\nabla \times \delta E^* \right) \cdot \left([\mu]^{-1} \nabla \times E \right) d\Omega - \iint_{\Omega} \delta E^* \omega^2 \varepsilon E d\Omega + 2 j \omega \iint_{\Omega} P^{NL} \delta E^* d\Omega \qquad 3.87$$

using the vector formula

$$\left(\nabla \times \delta E \right)^* \left(\nabla \times E \right) = \delta E^* \left[\nabla \times \nabla \times E \right] + \nabla \cdot \left[\delta E^* \times \nabla \times E \right] \qquad\qquad 3.88$$

$$\delta F = \iint_{\Omega} \delta E^* \left[\nabla \times \nabla \times E + k^2 E - 2 P^{NL} \right] d\Omega - \iint_{\Omega} \nabla \cdot \left[\delta E \times \nabla \times E \right] d\Omega \qquad\qquad 3.89$$

A minimisation of the above functional for first order triangular elements will yield

$$[S][E] + [C][E] = [T] \qquad\qquad 3.90$$

[S] is a real symmetric matrix, [C] is a complex symmetric matrix and [T] is the forcing function.

3.5   Phase Matching

The results from the previous section can be used to find the second harmonic conversion efficiency. The power per unit area can be defined with the relation

$$P^{2\omega} = \frac{\text{power}}{\text{Area}}$$ 3.91

which is the second harmonic output power density. From which the conversion efficiency for a crystal of length L, can be written as (Yariv, 1989)

$$\eta = \frac{P^{2\omega}}{P^{\omega}} = 8\left(\frac{\mu_o}{\varepsilon_o}\right)^{\frac{3}{2}} \frac{\omega^2 d^2 L^2}{n^3} \left(\frac{P^{\omega}}{Area}\right) \frac{\sin^2\left(\frac{\Delta k L}{2}\right)}{\left(\frac{\Delta k L}{2}\right)^2}$$ 3.92

This last result indicates that for efficient SHG

$$\Delta k = 0$$

or

$$\omega_3 = 2\omega, \ \omega_1 = \omega_2 = \omega$$

i.e.

$$k^{(2\omega)} = 2k^{(\omega)}$$

It follows that the output field is the coherent sum of the contributions generated along the length of the crystal. For equal phase velocities, the fundamental and the second harmonic radiation are equal and all the contributions add constructively and the output will be proportional to the crystal length. If this is the case, then it is said

to be phase matched. If, however, $\Delta k \neq 0$ as is generally the case, then the second harmonic wave generated at some point (say z_1) having propagated to another point (say z_2) will be out of phase with the second harmonic wave generated at the point (z_2). This will result in a destructive interference described by the factor

$$\frac{\sin^2\left(\dfrac{\Delta k L}{2}\right)}{\left(\dfrac{\Delta k L}{2}\right)^2}$$

The two adjacent peaks of the spatial interference are separated by the coherence length defined as

$$l_c = \frac{2\pi}{\Delta k} = \frac{2\pi}{k^{(2\omega)} - 2k^{(\omega)}} \qquad\qquad 3.93$$

This length l_c, is a measure of the maximum crystal length that is useful in producing second harmonic power. This useful length, l_c, can be attributed to the dispersion in the refractive indices of the non-linear crystal and only several microns for SHG of visible radiation. The efficiency of the non-phase-matched interactions is thus much smaller than of phase matched interactions and in practical applications is thus of no use.

Since the refractive index increases with frequency, equation 3.93 (above) could be rewritten in the following form for $k^{(\omega)} = \dfrac{\omega n^\omega}{c}$;

$$\Delta k = k^{(2\omega)} - 2k^{(\omega)} = \frac{2\omega}{c}\left(n^{2\omega} - n^\omega\right) \qquad\qquad 3.94$$

It follows that

$$l_c = \frac{\pi c}{\omega\left(n^{2\omega} - n^{\omega}\right)} = \frac{\lambda}{2\left(n^{2\omega} - n^{\omega}\right)} \qquad\qquad 3.95$$

where λ is the free space wavelength of the fundamental beam.

The phase matching requirement is that $\Delta k = 0$. By far the commonest technique for meeting this requirement makes use of the natural birefringence of anisotropic crystals, i.e. the difference between the refractive indices of orthogonally polarised waves. For some crystals there is a balance between the wavelength dependence of the refractive indices (dispersion) and the polarisation dependence of the refractive indices (birefringence). In such cases it is then possible for the phase velocity of the second harmonic wave polarised in one direction to equal that of the fundamental polarised wave in the orthogonal direction. Only a small number of crystals meet this criterion: however, until recently, birefringent phase matching has been the basis of almost all practical frequency conversion devices.

In phase matched devices, the efficiency will be proportional to the square of the non-linear susceptibility tensor and the length of the crystal but it varies linearly with input intensity. In typical non-linear materials, an efficiency of about 50% can be achieved with input intensities of $1 - 100$ MW/cm^2 (Fejer, 1994). Such intensities can be easily achieved in loosely focused pulsed laser beams with high peak powers. In continuous wave lasers, however, to achieve such intensities extremely tight focal spots will be required which in turn leads to diffraction. One way to overcome such shortcomings is to confine the crystal inside a resonator.

3.5.1 Angle phase matching

Fig 3.1 Angle Phase matching in KDP (Zernike and Midwinter, 1973)

True phase matching can be obtained by using the natural birefringence of uniaxial crystals. This method was first described by Maker *et al.*, (1962) and independently by Giordmaine, (1962). Given a negative uniaxial crystal in which the ordinary index is larger than the extraordinary index, equal refractive indices are required for the second harmonic and the fundamental. If it is required to convert a fundamental wave at 632.8 nm to a second harmonic at 316.4nm then, from Fig. 3.1 (Zernike and Midwinter, 1973), it can be seen that the ordinary index at 632.8nm is larger than the extraordinary index at the same wavelength. Changing the angle between the wave normal and the optic axis can be used to vary the index for the extraordinary wave. Using the ordinary ray as the fundamental and the extraordinary ray as the second harmonic, it is possible to transmit the wave at an angle θ to the optic axis, such that the refractive index for the input wave is exactly equal to that of the output second harmonic wave.

The main disadvantage of angle phase matching is that the extraordinary beam at an intermediate angle does not overlap the ordinary wave. It would follow that the output power would not be proportional to the square of the interaction length. This effect is more serious in type II interactions where the two fundamental beams do not

overlap completely. The polarisation wave thus simply disappears after a certain crystal length.

3.5.2 Quasi-Phase matching

To develop crystals that meet the phase matching requirements for efficient frequency conversion is a time consuming process, often requiring more than ten years between discovery and commercialisation (Fejer, 1994). Many attractive materials are excluded because of the very limited wavelength range over which birefringence phase matching can be achieved. In general therefore, the suitability of a material for frequency conversion applications is a complex function of its various optical parameters. A method to extend the range of usable materials and to obtain a significant increase in power would therefore be most welcome. If the phase difference between the polarisation wave and input electromagnetic wave could be changed, every coherence length by $\frac{\pi}{2}$ through the introduction of a structural periodicity, then it would be possible to correct the phase mismatch. This method of obtaining phase matching is known as quasi-phase matching (QPM) and was first proposed by Amstrong *et al.* (1962).

An efficient method of realising quasi-phase matching involves a sign change of the non-linear optical susceptibility tensor. This sign change resets the relative phase of the non-linear polarisation and the generated wave every time the phase slips by π. This will result in power flowing monotonically from the fundamental to the second harmonic field. Quasi-phase matching has major practical advantages in that it eliminates any dependence of device performance on the birefringence properties of the material. It is possible to use a non-linear material over its entire transparency range. The method also allows the use of the largest component of the non-linear susceptibility tensor.

The simplest way of achieving quasi-phase matching is to make thin plates of the crystal one coherence length thick and stacking them alternately such that the polarisation wave will undergo a 180° phase change from one plate to the other. The experimental difficulties of such an approach are obvious. The micro spatial scale required for plates makes this concept rather difficult to implement. The plates would also be required to be in optical contact.

3.6   Summary

This chapter has discussed the theory of second harmonic generation. The origin of nonlinearity in optical materials is examined. Following Zernike and Midwinter (1973), an attempt is made at a detailed derivation of the nonlinear interaction equation, which is at the heart of nonlinear phenomena. The classification of SHG is then considered. A finite element variational formulation of the nonlinear equation is then obtained from first principles. The chapter concludes with a look at methods used to increase the second harmonic output.

Chapter Four

Finite Element Analysis of Optical Waveguides

4.1.   Introduction

In this chapter the finite element method is applied to the analysis of optical waveguides. Results are presented for anisotropic waveguides, with an arbitrary permittivity tensor, being diffused in both the transverse directions and by using the finite element method with the vector **H**-field formulation for the analysis. The importance of considering the waveguide core dimensions to be greater than the diffusion depth in both the transverse directions, the use of extrapolation techniques and of a symmetry plane for anisotropic waveguides are also discussed. The modelling of asymmetric directional couplers is also considered.

Dielectric integrated optical channel waveguides are employed in a large number of optical devices, such as lasers (Webjörn *et al.*, 1997), switches (Wongcharoen *et al.*, 1997), modulators (Anwar *et al.*, 1999), phase-shifters (Bersiner *et al.*, 1991), amplifiers (Helmfrid *et al.*, 1993), parametric oscillators (Bava *et al.*, 1987) and cascaded non-linear devices (Ironside *et al.*, 1993). There is a growing interest in the accurate characterisation of advanced optical guided-wave devices for optimisation

of their design. Besides semiconductor waveguides, there has been considerable interest in guides formed by silver-sodium exchange, thermal back-diffusion of K^+ ions in soda lime glass, proton exchange in $LiNbO_3$ or in $LiTaO_3$, annealed proton exchange in $LiNbO_3$ and Ti indiffusion of $LiNbO_3$, which has received considerable attention. $Ti:LiNbO_3$ devices are particularly important because of their properties of low loss, their large electro-optic, piezo-electric, and elasto-optic coefficients and their high second-order nonlinearity (Strake *et al.* 1988). However due to the nature of the fabrication process, all of the above devices will result in a waveguide with a diffused refractive index profile and in any case, one which is anisotropic in nature.

Over the years, several methods have been developed for the analysis of waveguide devices. These can be classified broadly into two groups: approximate analytical methods and numerical methods. The first group includes such approaches as circular harmonic point-matching (Goell, 1969), the effective index method (Hocker and Burns, 1977), the spectral index method (Burke, 1990), the matrix method (Harrington, 1967) and the method of lines (Worm and Pregla, 1984). Some of the approximate methods provide very good results for the analysis of waveguides when operating far away from cut-off. Goell (1969) employed the method of circular harmonic point matching in the analysis of step index rectangular optical waveguides. The approximate method of Marcatili (1969), in which the field in the corner regions of the guide is ignored, has also been used for the analysis of step index guides. Many research workers, in view of its simplicity, have extensively used the effective index method, first introduced by Knox and Toulois (1970). However, many of these methods are not very suitable for the analysis of a wide range of important practical, arbitrarily shaped, graded index and anisotropic waveguides and often not so accurate particularly when operating as a single mode waveguide and when operating close to cutoff.

In the last two decades, numerical methods have been widely used in the study of optical guided-wave devices due to the availability of faster and cheaper computer power. A numerical method based on a vector integral equation has been used by

Pichot (1982) for the analysis of diffused channel waveguides. Sharma and Bindal (1992) have used a variational approach based on the Hermite-Gaussian trial functions to analyze diffused planar and channel waveguides. Schweig and Bridges (1984) and Lagu and Ramaswamy (1986) have employed the variational approach in the finite difference method (FDM) for the analysis of diffused channel waveguides. A method based on the direct solution of the vector wave equation, in terms of the transverse magnetic field, using a five-point finite difference scheme and which avoids spurious modes, has been used by Schulz *et al.* (1990). The beam propagation method (BPM) employed by Feit and Fleck (1978) is useful in the analysis of z-dependent guided wave devices for finding modal solutions, but with constraints on sampling points and refractive index changes.

However, for the modal solutions of z-independent waveguides, the finite element method (FEM) has established itself as a powerful, versatile and accurate method. Rahman and Davies (1984a,b) had developed and refined (Rahman and Davies, 1984c) the use of the vector **H**-field formulation for a wide range of optical waveguides based on the finite element method and this approach will be adopted and extended in this thesis.

In this section of the thesis, results are presented for waveguides diffused in both the transverse directions with isotropic, uniaxial and generally anisotropic refractive indices (Katsriku *et al.*, 1996). The importance of considering the case where the variable index waveguide core dimensions are greater than the diffusion depth in the transverse directions, which other workers neglect, is demonstrated and the validity of the application of the symmetry plane for anisotropic waveguides is also discussed.

The method developed in this section is in anticipation of work to be done in second harmonic generation in lithium niobate (LiNbO$_3$) guides. Since LiNbO$_3$ has a high nonlinear susceptibility tensor, it provides a useful material base for the design of guided wave devices. In such waveguides, it is possible to satisfy the phase matching

condition using the general anisotropy of the material and when this is not possible then the quasi-phase matching principle can be adopted. The ability to accurately model such waveguides is therefore of importance.

4.2. Waveguides

Two main categories of optical waveguides can be identified

a) waveguides for optical integrated circuits and

b) optical fibers.

Such waveguides are primarily for the guiding and processing of light. The technology relies on dielectric materials, a thin film of high refractive index sandwiched between a substrate of lower refractive index and an upper cladding (usually air) also of lower refractive index. This is achieved by using small amounts of titanium (Ti) to dope $LiNbO_3$ crystal and hence increase the index of refraction locally. Such an arrangement enables light to be trapped locally inside the film and hence achieving waveguiding. The higher the refractive index of the film, the more tightly confined is the light inside the guide. The refractive index in turn depends on the film thickness. The change in refractive index of the various sections of the waveguide can be classified as either step index or graded. In the step index guide, the refractive index changes in discrete steps at the boundaries of the sections. In graded index guides, the refractive index changes slowly throughout the guide.

Essentially these types of waveguides are the basis of electro-optic and acousto-optic technology; the optical signal is modulated by means of an electrically or acoustically induced change in the optical characteristics of the crystal, including phase, amplitude, polarisation, frequency and direction of propagation. This technology can be applied in the implementation of major devices including second harmonic devices.

4.2.1 Fabrication Techniques

Titanium diffused lithium niobate (Ti- LiNbO$_3$) waveguides were first fabricated by Schmidt and Kaminow, (1974). These early guides were multimode and planar but soon after single mode channel guides were also demonstrated (Schmidt and Kaminow, 1975). Using ultra violet exposure through a mask, the desired waveguide pattern is formed on LiNbO$_3$ substrate. Titanium, of carefully controlled thickness, is then deposited over the entire crystal by means of either electron beam or radio frequency sputtering. The undesired metal is then got rid off either by dissolving the photoresist or ecthing. To obtain diffusion, the guide is placed in a furnace with temperature ranging from 980°C to 1050°C for up to 12 hours.

The general schematic of the waveguide to be considered is shown in Fig 4.1. The guide refractive index given by $n(x, y)$ is slowly decreasing in both the x- and y-transverse directions. For a 2-D diffused guide, the diffusion profile can be expressed approximately as:

$$n(x, y) = n_s + (n_g - n_s) f(x) \cdot g(y) \qquad\qquad 4.1$$

where $f(x)$ and $g(y)$ are spatial functions of D$_x$ and D$_y$, the diffusion length in the x- and y-direction and n_g and n_s are the refractive indices of the guide core and substrate respectively. In a step index guide $n(x, y) = n_g$, a constant and the guide dimensions are defined by the width a and depth b. The width and height of the core for a diffused guide are often given by the diffusion width, D$_x$ and the diffusion depth, D$_y$ respectively. It is often assumed by other workers (Pichot, 1982, Sharma and Bindal, 1993, Lagu and Ramaswamy, 1986, Schulz et al., 1990 and Fleck and Feit, 1978), that outside the guide cross-section, defined by a and b, the refractive

index is constant and equal to n_s, which is not strictly correct. In this thesis initially a waveguide with uniform cross-section will be assumed. The guide is z-invariant and the refractive index does not change with the propagation direction. In the analysis of the propagation characteristics of practical waveguides, such an assumption is indispensable. Initially though, for the purpose of benchmarking, results will be obtained for planar waveguides with

   i)   step isotropic
   ii)   diffused isotropic
   iii)   step anisotropic and
   iv)   diffused anisotropic refractive indices.

Subsequently more realistic optical waveguides with optical energy confined in both transversve directions are considered.

Fig 4.1 Schematic showing the general structure of the waveguide under consideration.

The following two dimensional Helmholtz equation describes the propagation of the electromagnetic field in terms of the vector magnetic field **H**, in the guide:

$$\nabla^2 \mathbf{H} + \left(k^2 n^2 - \beta^2\right) * \mathbf{H} = 0 \qquad\qquad 4.2$$

where β is the propagation constant, n, the refractive index and k the free-space wavenumber.

In the FEM, the guide cross section is divided into a finite number of triangular elements to represent the problem. The FEM also allows each element to have a different but piecewise-constant refractive index constant refractive index. This property enables the FEM to be applied to the analysis of arbitrarily shaped diffused anisotropic waveguides.

In general, the permittivity tensor, $\hat{\varepsilon}$, which defines the anisotropy of the material may be written as

$$\hat{\varepsilon} = \begin{bmatrix} \varepsilon_{11} & \varepsilon_{12} & \varepsilon_{13} \\ \varepsilon_{21} & \varepsilon_{22} & \varepsilon_{23} \\ \varepsilon_{31} & \varepsilon_{32} & \varepsilon_{33} \end{bmatrix} \qquad\qquad 4.3$$

Two classes of anisotropic materials can be defined: those in which the natural modes of propagation are linearly polarised and those in which they are circularly polarised. For the first class of materials, the permittivity and permeability components respectively are symmetric, i.e. $\varepsilon_{ij} = \varepsilon_{ji}$ and $\mu_{ij} = \mu_{ji}$ (Ramo et al., 1994). The second group, known as gyrotropic materials, is those in which the natural modes of propagation are circularly polarised waves. In a loss-free gyrotropic material, the permittivity and permeability components are anti-symmetric, having $\varepsilon_{ij} = -\varepsilon_{ji}$ and $\mu_{ij} = -\mu_{ji}$. An anisotropic material is said to be uniaxial when the

elements above and below the principal diagonal are zero and two of the elements in the principal diagonal are equal. A biaxial material on the other hand has all off-diagonal elements equal to zero and all the three elements in the principal diagonal are unequal.

This chapter will be concerned with loss-less anisotropic media in which $\hat{\varepsilon}$ is a tensor with real components $\varepsilon_{ij} = \varepsilon_{ji}$. In particular, results for uniaxial anisotropic materials and anisotropic materials with off-diagonal terms in the x - y plane will be presented.

The full vector **H**-field formulation with the penalty term is given as

$$\omega^2 = \frac{\int (\nabla \times H)^* \, \hat{\varepsilon}^{-1}(x,y) \, (\nabla \times H) d\Omega + \alpha \int (\nabla \cdot H)^* \, (\nabla \cdot H) d\Omega}{\int H^* \cdot \hat{\mu} \cdot H d\Omega} \qquad 4.4$$

where α is the dimensionless penalty parameter, ω is the angular frequency and **H** is the vector magnetic field at the nodal points (Rahman and Davies, 1984c). It will be assumed that the material is loss-less and the usual time (t) and axial (z) dependence of the field in the form $\exp[j(\omega t - \beta z)]$ is considered throughout. However, waveguides with loss or gain can be characterised using the perturbation technique (Themistos $et\ al.$, 1995) or by using magnetic field formulation involving only the transverse components (Abid $et\ al.$, 1993).

Minimisation of the variational functional (4.4), with respect to each of the unknown nodal field components, H_x, H_y and H_z will yield a stationary solution in the form of a set of linear algebraic eigenvalue equations, i.e.

$$[A]\{x\} - \omega^2 [B]\{x\} = 0 \qquad 4.5$$

where [A] is a complex Hermitian matrix, [B] is a real symmetric and positive definite matrix, ω^2 is the eigenvalue, and $\{x\}$ is the eigenvector. For the loss-less case, a general phase difference of 90° between the axial and transverse components of H allows the transformation of A into a real symmetric matrix (Rahman and Davies, 1984b). A solution of the above eigenvalue equation for a given value of β will yield a set of eigenvalues (ω^2) with a corresponding eigenvector $\{x\}$ set representing the three components of the H-field at each of the nodes. To obtain the complete ω / β dispersion curves, a set of values of ω and β are obtained for each mode. If it is necessary to obtain the propagation constant, β, for a given wavelength, then this can be achieved by using 2 to 3 iterations.

4.3.   Results

In this section, results for various types of waveguides are presented. Using the FEM, results are given and compared for planar diffused waveguides with isotropic and anisotropic refractive indices. Results are also presented for the channel waveguide diffused in both transverse directions. The diffusion profiles in the x and y directions could be defined by any arbitrary function, and both isotropic and anisotropic channel waveguides are considered.

4.3.1.   Planar waveguides

Initially, the accuracy of the finite element method is demonstrated by comparing with the exact analytical solution for a simple slab waveguide. This is the simplest of all optical waveguides. It confines the light only in the direction of the guide thickness. In a three layer asymmetric step index slab waveguide the following condition is true: $n_c \le n_s < n_g$. A symmetric waveguide is considered here, the parameters of which are defined as follows, where the wavelength, $\lambda = 1.3\mu m$ and

the refractive indices of the cover, film guide and substrate are $n_c = 1.4$, $n_g = 1.5$, n_s = 1.4 respectively. The finite element solutions using different mesh divisions are shown in Table 4.1. The exact effective index $(n_e = \beta/k_o)$ for the waveguide is 1.457728, which has been obtained by solving the transcendental equation. It can be seen, from Table 4.1, that the accuracy of the finite element solution depends on the mesh refinement, in a similar way to most of the other numerical methods. In many practical waveguides an analytical solution is not available and a numerical technique has to be considered. The computational resources available could therefore limit the accuracy of finite element solutions, like many other numerical methods. For such problems, it is often necessary to extrapolate the results as the limits of computational facilities available are reached. Here two different extrapolation techniques, Aitken's extrapolation method (Rahman and Davies, 1985) and an extrapolation method given by Koshiba (Koshiba, 1992) are compared.

In Aitkens' method, the extrapolated result is obtained from three successive mesh divisions with a fixed geometric ratio, using the following equation

$$x_{\infty} = x_{r+1} - \frac{(x_{r+1} - x_r)^2}{x_{r+1} - 2x_r + x_{r-1}}$$ 4.6

where x_{∞} is the extrapolated result and x_{r-1}, x_r and x_{r+1}, are results obtained from three successive mesh divisions. In using the above formula, it is important to maintain a constant ratio of proportionality.

The extrapolation procedure suggested by Koshiba (1992) is as follows

$$k_{0\infty}^2 = \frac{k_{02}^2 - q^2 k_{01}^2}{1 - q^2}$$ 4.7

where $k_{0\infty}^2$ is the extrapolated solution and k_{01}^2 and k_{02}^2 are solutions obtained using N_{E1}, and N_{E2} elements respectively with $N_{E1} < N_{E2}$, and $q \cong \sqrt{N_{E1}/N_{E2}}$. In this approach, results for only two mesh divisions are required with any arbitrary ratio.

Mesh	FEM	Aitken's Extrapolation	Koshiba's Extrapolation
50	1.457614	-	-
100	1.457707	-	-
200	1.457723	1.457726	1.457759
400	1.457727	1.457728	1.457734
800	1.457728	1.457728	1.457730
1600	1.457728	1.457728	1.457728

Table 4.1. Comparison of the effective index values obtained using the FEM with different extrapolation techniques. The exact analytical solution is $n_e = 1.457728$

The raw finite element results are shown in column 2 of Table 4.1, and in columns 3 and 4 the extrapolated results are shown using Aitkens' (Rahman and Davies, 1985) and Koshiba's, (Koshiba, 1992) approaches respectively. The extrapolated results using Aitkens' approach is shown in column 3, where any of its values in any row is obtained by using the three successive raw FEM results of column 2, including the two previous rows and the present row. The extrapolated results using Koshiba's approach is shown in column 4 and its value in any row is obtained by using the raw FEM of the present row and the previous row. Although, Aiken's extrapolation required three sets of results with constant geometric ratio, it can be seen from the table that this approach converges faster than the approach given by Koshiba, as such, in this work Aitkens' method of extrapolation has been used.

4.3.2.   Diffused Planar Isotropic Waveguide

Next the accuracy of the finite element method is tested for diffused planar waveguides. Many fabrication processes lead to a graded index of the film. The refractive index profile for such waveguides can be described using the following

$$n^2(y) = n_s^2 + 2n_s \cdot \Delta n \cdot g(y) \qquad\qquad y > 0 \qquad\qquad 4.8a$$

$$n^2(y) = n_c^2 \qquad\qquad\qquad\qquad y < 0 \qquad\qquad 4.8b$$

In the above, $g(y)$ is the distribution function which describes the diffusion profile of the refractive index in the guide. The particular profile assumed will depend on the fabrication process used. Various distribution functions are used to approximate the refractive index in the core of the waveguide. Results for a waveguide having the following diffusion profiles: exponential, Gaussian and complimentary error function (CEF), in the y direction, are shown in Table 4.2 for various approaches taken. In this example, the wavelength $\lambda = 1.3\mu m$, the refractive indices of the cover and substrate are $n_c = 1.0$, and $n_s = 2.177$ respectively and $\Delta n = 0.043$ is the maximum change in the refractive index between the core and the substrate. The normalized frequency, V, is defined as $V = k_o b \sqrt{2n_s \Delta n}$, where b is waveguide depth and k_o the wavenumber. For a diffused waveguide, the diffusion depth D_y, can be considered as the waveguide depth b for defining the normalized frequency. The propagation constants may be computed for various values of V. From the results presented in Table 4.2, it can be observed that the finite element (FE) solutions compare very well with those obtained by Sharma and Bindal (1993) and are better than those obtained by the Hermite-Gaussian (HG), Evanescent Hermite-Gaussian (EHG) and the cosine-exponential methods (CE) (Sharma and Bindal, 1993). It is believed that the finite element approach using 800 mesh points is more accurate than the results of Sharma and Bindal, using a numerical approach, which they have referred to as 'exact'. It should be noted that most practical waveguides have 2-D confinement, for which analytical solutions are not possible. In such cases numerical methods of evaluation have to be employed.

g(y)	V	Sharma	FEM	CE	EHG	HG
$\exp\left(-\left(\dfrac{b}{D_y}\right)^2\right)$	2.0	0.082	0.081	0.078	0.044	0.005
	3.0	0.275	0.272	0.270	0.263	0.216
	4.0	0.413	0.409	0.408	0.408	0.370
$\exp\left(-\dfrac{b}{D_y}\right)$	2.0	0.105	0.104	0.100	0.087	0.066
	3.0	0.229	0.227	0.223	0.218	0.193
	4.0	0.321	0.318	0.316	0.313	0.289
$\text{erfc}\left(\dfrac{b}{D_y}\right)$	3.0	0.068	0.067	0.064	0.041	0.015
	4.0	0.169	0.168	0.164	0.154	0.121

$$V = k_o a \sqrt{2 n_s \Delta n};\ n_c = 1.0,\ n_s = 2.177,\ \Delta n = 0.043,\ \lambda = 1.3 \mu m$$

Table 4.2. Normalized propagation constant, $B = [(\beta / k_o)^2 - n_s^2]/2n_s\Delta n$, for diffused planar waveguides obtained by different methods.

4.3.3.   Diffused Planar Anisotropic Waveguide

The Y-cut, X-propagation LiNbO$_3$ planar anisotropic optical waveguide with the optical axis in the x-y plane at an optical angle θ to the x-axis has also been studied. The refractive index profiles for both the ordinary and extraordinary rays in the guide core may be defined respectively as:

$$n_0(y) = n_{os} + \Delta n_o \cdot g(y) \qquad\qquad y > 0 \qquad\qquad 4.9a$$

$$n_e(y) = n_{es} + \Delta n_e \cdot g(y) \qquad\qquad y > 0 \qquad\qquad\qquad 4.9b$$

where n_{os} and n_{es} are the substrate refractive indices, Δn_o and Δn_e are the maximum changes in refractive indices between the core and the substrate for the ordinary and extraordinary rays respectively and $g(y)$ has a Gaussian profile. It is assumed that the top cladding layer is air with an isotropic refractive index $n_c = 1.0$. The non-zero elements of the relative permittivity tensor in the guide region are given by

$$\varepsilon_{xx} = n_o^2(y)\cos^2\theta + n_e^2(y)\sin^2\theta \qquad\qquad\qquad 4.10a$$

$$\varepsilon_{yy} = n_o^2(y) \qquad\qquad\qquad 4.10b$$

$$\varepsilon_{zz} = n_e^2(y)\cos^2\theta + n_o^2(y)\sin^2\theta \qquad\qquad\qquad 4.10c$$

$$\varepsilon_{xy} = \varepsilon_{yx} = \left[n_e^2(y) - n_o^2(y)\right]\sin\theta\cos\theta \qquad\qquad\qquad 4.10d$$

The effective indices for the first four modes when $D_y = 5$ μm and the first two modes when $D_y = 3$ μm, are calculated using the FEM and compared in Table 4.3 with results available in the literature (Koshiba, 1992). In this example, the guide parameters are defined as follows: $\theta = 0^o$, $\lambda = 0.6328\mu m$, $n_{os} = 2.286$, $n_{es} = 2.2$ and $\Delta n_e = \Delta n_o = 0.01$. In Table 4.3, results obtained in this work are compared with those obtained by Koshiba (1992) using the FEM, the differential numbered solution (DNS), the multilayer approximation method (MAM), and the WKB method (Yamanouchi et al., 1978). The results obtained show very good agreement with those obtained previously (Koshiba, 1992). The results presented by the authors would be expected to be more accurate than those of Koshiba (1992) since in this calculation 800 first order elements are used, which represents a much finer mesh

compared to the 20 second order elements used by Koshiba. The computational time required for our mesh is approximately 8s on a SUN Sparc2 workstation. These FEM results have been tested using Aitken's extrapolation and have shown excellent convergence.

D_y	Mode	FEM	Koshiba	DNS	MAM	WKB
3.0	0	2.20582	2.20581	2.20581	2.20583	2.20577
	1	2.20159	2.20158	2.20159	2.20160	2.20155
5.0	0	2.20736	2.20734	2.20734	2.20738	2.20735
	1	2.20427	2.20426	2.20430	2.20430	2.20426
	2	2.20184	2.20184	2.20184	2.20187	2.20184
	3	2.20028	2.20027	2.20028	2.20027	2.20027

Table 4.3 Effective index results for a diffused anisotropic planar waveguide

4.3.4.   Diffused Channel Isotropic Waveguides

It is possible to represent accurately any waveguide with an arbitrary cross-section and refractive index profile, which may arise as a result of the complex diffusion chemistry using the finite element method. However, to test the utility of the FEM and to compare our results with other reported results, the index profile is considered to be the simple product of two functions, $f(x)$ and $g(y)$, where $f(x)$ and $g(y)$ can be defined by any two given functions. The form of these functions is determined by the fabrication method of the device. In Ti:LiNbO$_3$, the refractive index profile has been empirically approximated by Gaussian, exponential or complimentary error functions by various authors. However, it should be noted that in practical waveguides, the index profiles might not be a simple product of the two transverse

direction profiles. The FEM can model any such arbitrary variations, which other methods will not be able to tackle.

In this section, the FEM method is applied to the analysis of 2-D diffused channel waveguides with various refractive index distributions. The index distribution in the x and y direction, $f(x)$ and $g(y)$, is defined by any one of the following functions:

$$f(x) = \begin{cases} \exp(-x^2 / D_x^2) \\ \exp(-x / D_x) \\ \mathrm{erfc}(x / D_x) \end{cases}$$

4.11a

$$g(y) = \begin{cases} \exp(-y^2 / D_y^2) \\ \exp(-y / D_y) \\ \mathrm{erfc}(y / D_y) \end{cases}$$

4.11b

In the next example, it is assumed that $\varepsilon_o = 1$, $\varepsilon_2 = 2.1$, $\varepsilon_{max} = 1.05^2 \cdot \varepsilon_2$ and $a/b = 1$. The normalized frequency is defined as $V = k_o a \sqrt{\varepsilon_{max} - \varepsilon_2}$, wavenumber, $k_o = 2\pi / \lambda_o$, where a is the guide width, b is the guide depth and a/b is the aspect ratio. In this example, the available one-fold symmetry has been exploited and an irregular mesh (a greater number of divisions in the guide core and lesser number in the cladding) has been used to represent one half of the guide cross-section. In the first example $a = 2D_x$ since one fold symmetry has been used and $b = D_y$. In Fig. 4.2, results for a Gaussian-Gaussian diffused index profile are compared with those obtained by Lagu et al. (1986), Schulz et al. (1990) and Sharma and Bindal (1992). These results show very good agreement with those obtained by Schulz et al. (1990) who have used a vector finite difference formulation. The present results differ slightly from those obtained by Lagu et al. (1986) who used a scalar formulation, which did not take into consideration the hybrid nature of the modes. These results differ significantly from those obtained by Sharma and Bindal (1992). However, it should be noted that the normalized frequency as defined by them, $V = k_o W \sqrt{2n_s \, \Delta n}$,

differs from that used by Schulz *et al.* (1990), Lagu *et al.* (1986) and as was defined in the present work, being $V = k_o a \sqrt{\varepsilon_{\max} - \varepsilon_2}$, where $2W$ is the initial metal strip width. The results of Sharma and Bindal therefore cannot be directly compared with those of Schulz *et al.* (1990) and Lagu *et al.* (1986). Their claim (Sharma and Bindal, 1992), therefore, of presenting a better method can be attributed to the discrepancy in defining V and therefore, in our opinion, may not be valid.
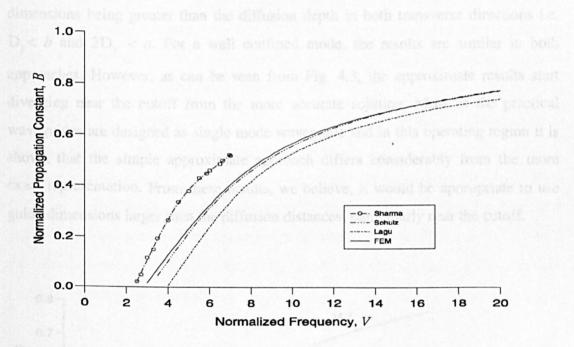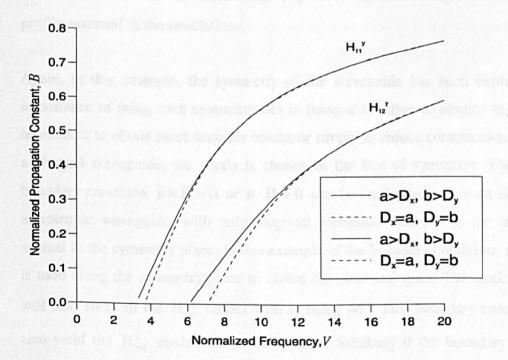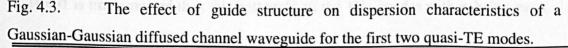

Fig. 4.2   The variation of the normalised propagation constant with the normalised waveguide dimension for a gaussian-gaussian diffused waveguide.

The effect of considering waveguide dimensions, which are greater than the diffusion depth, has also been studied in this work. In most of the literature, the region of the guide core generally considered to have a diffused profile is defined by a and b which are equal to $2D_x$ and D_y respectively (see Fig. 4.1). Outside this region, the refractive index is assumed to be constant, equal to the substrate index. In Fig. 4.3, the dispersion characteristics of the H_{11}^y and H_{12}^y modes are shown for a guide with Gaussian index profiles in both the transverse directions. In this case the refractive indices of the substrate and the core region are given as $\varepsilon_2 = 2.1$, $\varepsilon_{\max} = 1.05^2 \varepsilon_2$,

respectively. In the example, the diffusion depth and the diffusion width are taken as $D_y = 2D_x = 6\mu m$. In the first approach, the guide core is defined by the diffusion depth and width, i.e. $D_y = b$, and similarly, $2D_x = a$. This is the approach adopted by most of the other research workers, whereas in reality, the refractive index profiles do not suddenly become uniform beyond the distances D_y and D_x. Thus the inaccuracy due to the first approach is tested by considering the effect of the guide dimensions being greater than the diffusion depth in both transverse directions i.e. $D_y < b$ and $2D_x < a$. For a well confined mode, the results are similar in both approaches. However, as can be seen from Fig. 4.3, the approximate results start diverging near the cutoff from the more accurate solution. Most of the practical waveguides are designed as single mode waveguide and in this operating region it is shown that the simple approximate approach differs considerably from the more exact representation. From these results, we believe, it would be appropriate to use guide dimensions larger than the diffusion distances, particularly near the cutoff.

Fig. 4.3.   The effect of guide structure on dispersion characteristics of a Gaussian-Gaussian diffused channel waveguide for the first two quasi-TE modes.

133

4.3.5.   Anisotropic diffused channel waveguides

Next, anisotropic waveguides with diffused refractive index profiles in both transverse directions are considered. In this example, it is assumed that the optical axis is in the direction of the x-axis and hence the relative permittivity tensor will have only diagonal elements. In the general expression relating to the permittivity tensor equation (4.10), this is equivalent to $\theta = 0^0$. In the example, various parameters involved may be defined as $n_{es} = 2.20$, $n_{os} = 2.286$, $n_{eg} = 2.21$, $n_{og} = 2.296$, $D_x = 3.0 \mu m$ and $D_y = 6.0 \mu m$. In Fig. 4.4, the dispersion characteristics of a waveguide with a Gaussian diffusion profile in the x-direction and different diffusion profile namely, Gaussian, exponential and complimentary error functions (CEF) in the y-direction are shown. It should be noted that any other function of x and y could have been used to represent the diffusion in the guide. It can be seen that the effective index of the fundamental H_{11}^x mode depends strongly on the diffusion profile assumed in the simulation.

Again, in this example, the symmetry of the waveguide has been exploited. The importance of using such symmetry lies in being able either to employ higher mesh refinement to obtain more accurate results or simply to reduce computational time. In a channel waveguide, the y-axis is chosen as the line of symmetry. The required boundary condition $\mathbf{n} \times \mathbf{H} = 0$ or $\mathbf{n} \cdot \mathbf{H} = 0$ can be easily realised in an isotropic or anisotropic waveguide, with only diagonal elements, where $\mathbf{n}$ is the unit vector normal to the symmetry plane. In this example, if the boundary condition, $\mathbf{n} \times \mathbf{H} = 0$, is used along the symmetry plane to obtain the dominant quasi TM mode, then this will also yield all the H_{mn}^x modes with m being odd. This boundary condition will also yield the H_{mn}^y mode with m being even. Similarly if the boundary condition $\mathbf{n} \cdot \mathbf{H} = 0$ is implemented then this will yield all the H_{mn}^x modes with m being even.
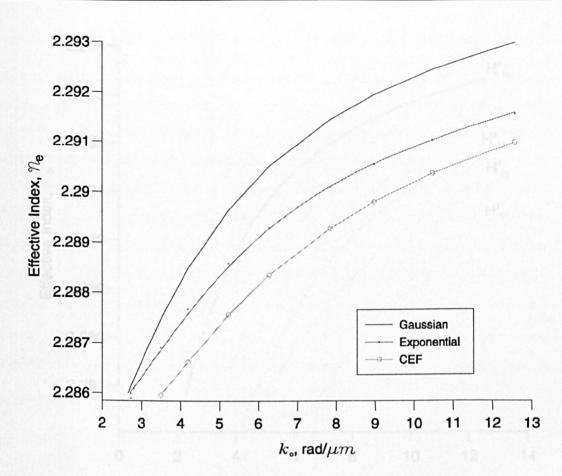
Fig.4.4.   Dispersion characteristics of a rotated y-cut LiNbO$_3$ waveguide with Gaussian index in the x-direction and various index profiles in the y-direction.

Again, a waveguide with only diagonal elements in its relative permitivity tensor but with $\theta = 90^0$ has been studied. The other waveguide parameters are $n_{es} = 2.20$, $n_{os} = 2.286$, $n_{eg} = 2.21$, $n_{og} = 2.296$, $D_x = 3.0\mu m$ and $D_y = 6.0\mu m$. The diffusion profile in the y-direction is an exponential function and in the x-direction, a Gaussian function. The dispersion curves for the first four H_{mn}^y modes of the waveguide are shown in Fig. 4.5. With $\theta = 90^0$, the optical axis is in the direction of the y-axis. It can be seen that, for this crystal orientation, the H_{mn}^y (quasi-TE) modes see the ordinary refractive index of the guide. The boundary condition $\mathbf{n} \cdot \mathbf{H} = 0$ has been used along the symmetry plane, giving the H_{mn}^y mode with m as odd.
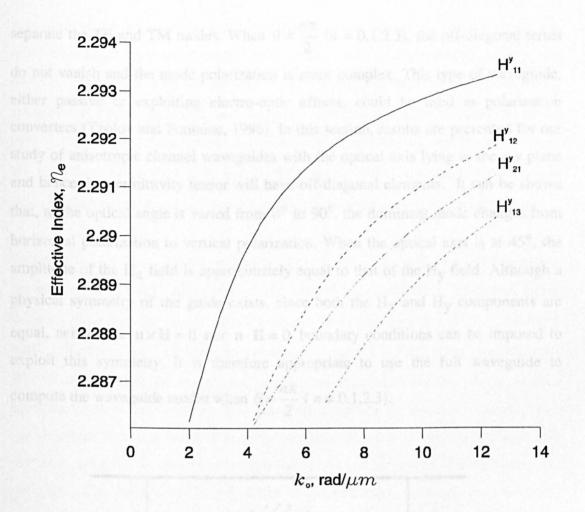
Fig. 4.5.   Dispersion characteristics of a diffused anisotropic waveguide with optical axis at 90°.

4.3.6   Anisotropic   diffused   waveguides   with   arbitrary permittivity tensor

From the permittivity relations given in equation (4.10), it is clear that at $\theta = 0^0$ or 90^0, the permittivity tensor will reduce to one with only diagonal elements and modes will be dominantly either vertically or horizontally polarised. A waveguide having such a permittivity tensor could therefore be used as a mode discriminator, to

separate the TE and TM modes. When $\theta \neq \dfrac{n\pi}{2}$ ($n = 0,1,2,3$), the off-diagonal terms do not vanish and the mode polarization is more complex. This type of waveguide, either passive or exploiting electro-optic effects, could be used as polarisation converters (Tzolov and Fontaine, 1996). In this section, results are presented for our study of anisotropic channel waveguides with the optical axis lying in the x-y plane and hence the permittivity tensor will have off-diagonal elements. It can be shown that, as the optical angle is varied from 0^0 to 90^0, the dominant mode changes from horizontal polarization to vertical polarization. When the optical axis is at 45^0, the amplitude of the H_x field is approximately equal to that of the H_y field. Although a physical symmetry of the guide exists, since both the H_x and H_y components are equal, neither the $\mathbf{n} \times \mathbf{H} = 0$ nor $\mathbf{n} \cdot \mathbf{H} = 0$ boundary conditions can be imposed to exploit this symmetry. It is therefore appropriate to use the full waveguide to compute the waveguide modes when $\theta \neq \dfrac{n\pi}{2}$ ($n = 0,1,2,3$).

Fig. 4.6. The relative strength and orientation of the **H** field for anisotropic waveguide with optical axis at 45^0.

The orientation and relative strength of the vector **H**-field in a full waveguide at $\theta = 45^0$ is shown in Fig. 4.6 when $\lambda = 0.6328 \mu m$. The field amplitude is a

maximum at the centre of the guide and reduces along the transverse directions. The other waveguide parameters are the same as are given in the example for Figs. 4.4 and 4.5. It has been checked that the H_x and H_y field components are individually symmetrical about the y-axis and the total vector magnetic is directed along the optical axis (see Fig 4.8). For the dominant modes, both the H_x and H_y components are maximum along the y-axis, and $H_x \cong H_y$, that is both are even functions and in this case neither the $\mathbf{n} \times \mathbf{H} = 0$ nor the $\mathbf{n} \cdot \mathbf{H} = 0$ boundary condition is applicable.

It would appear from the above results that for $\theta = 0^o$ or 90^0, it is best to impose symmetry to take full advantage of the reduced computational time and higher accuracy. The full waveguide should be used for cases when $\theta \neq 0^o, 90^0$, to obtain both accurate and physically meaningful results. For other angles, say $\theta = 30^o$ or 60° both H_x and H_y components are maxima along the y-axis but their maximum values are different. The boundary condition of $\mathbf{n} \times \mathbf{H} = 0$ or $\mathbf{n} \cdot \mathbf{H} = 0$ can therefore be easily realized in an isotropic or anisotropic waveguide, with only diagonal elements, because of the dominance of one of the modes and the absence of the other. The dispersion characteristics of the first two modes of the waveguide considered are shown in Fig 4.7 for $\theta = 45^0$.
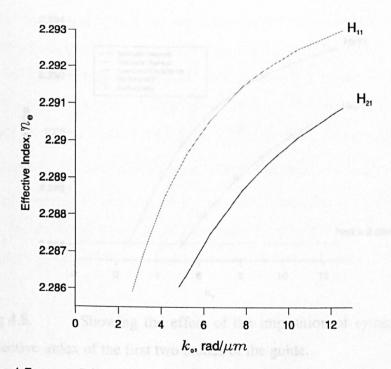
Fig. 4.7.   Dispersion characteristics of the first two modes of a diffused anisotropic waveguide with optical axis at 45°.

In Fig 4.8, the results from the numerical simulation, which checks the symmetry condition, are presented for two different modes. In the simulation, steps were taken to ensure that, in the waveguide region, a proportionately equal number of elements were used. The results show very good agreement, an indication that for the same number of elements, it did not matter whether symmetry was imposed. It must be noted however that the use of symmetry will allow the use of a greater number of mesh divisions, hence leading to an improvement in accuracy.
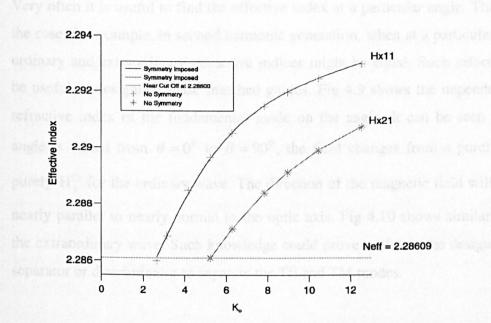
Fig 4.8.   Showing the effect of the imposition of symmetry condition on the effective index of the first two modes of the guide.
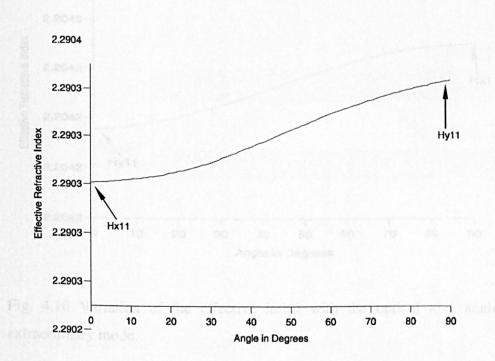

Fig. 4.9.   Variation of the effective index with the optical axis angle, for the ordinary mode.

Very often it is useful to find the effective index at a particular angle. This might be the case, for example, in second harmonic generation, when at a particular angle, the ordinary and extraordinary refractive indices might be equal. Such information will be useful in designing phase matched guides. Fig 4.9 shows the dependence of the refractive index of the fundamental mode on the angle. It can be seen that as the angle is varied from $\theta = 0^0$ to $\theta = 90^0$, the field changes from a purely H_x^{11} to a purely H_y^{11} for the ordinary wave. The direction of the magnetic field will vary from nearly parallel to nearly normal to the optic axis. Fig 4.10 shows similar results for the extraordinary wave. Such knowledge could prove useful in the design of a mode separator or discriminator to separate the TE and TM modes.
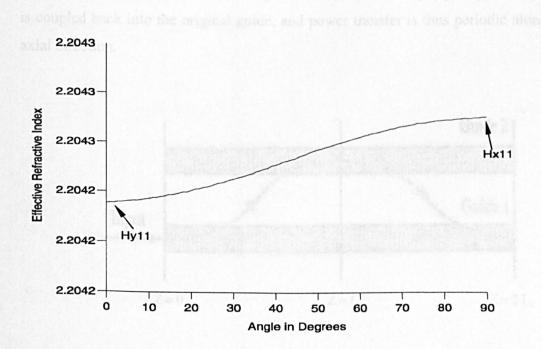

Fig. 4.10 Variation of the effective index with the optical axis angle, for the extraordinary mode.

4.4. Asymmetric Directional Couplers

This section briefly explores the application of the finite element method to coupled mode devices. These devices are important in the design of compact photonic systems. These devices (directional couplers) belong to a class of passive devices in which power exchange takes place between two modes, which are in close proximity to each other. A directional coupler is made up of two waveguides parallel to each other such that the evanescent field of one guide penetrates the other and optical power is coupled into the propagating mode of the latter guide. The coupling length, L_c, is defined as the distance over which maximum power transfer occurs. This depends on the structure and refractive indices of the waveguides making up the directional coupler and the distance of separation between the guides. Fig 4.11 illustrates the coupling between two guides. Beyond the coupling length, the power is coupled back into the original guide, and power transfer is thus periodic along the axial direction.
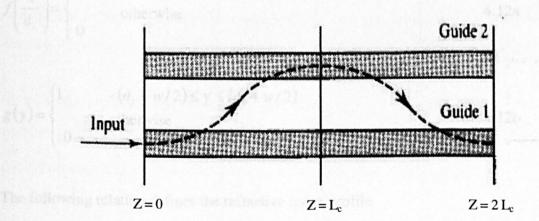

Fig 4.11 Diagrammatic representation of a directional coupler

Directional couplers are used in a variety of integrated optical devices including power dividers (Hotta *et al.*, 1994), input-output couplers (Rajarajan *et al.*, 1999),

modulators (Anwar *et al.*, 1999), filters, switches (Jenkins *et al.*, 1994), polarisers (Tzolov and Fontaine, 1996) and spot size expanders, (Rajarajan *et al.*, 1998). More recently they have been used in the enhancement of the second harmonic power output (Hempelmann, 1999). An accurate knowledge of the propagation characteristics is thus essential. For illustrative purposes, the FEM developed here is applied to the characterisation of such a device. Guide one is formed by field assisted $K^+ - Na^+$ exchange. It is assumed that the refractive index profile is step index in both the lateral and transversal dimensions. It is assumed that there is as much side-diffusion as depth diffusion such that $d_l \approx d_t$ and w is the guide width. Due to stress, the guide will be anisotropic with the following parameters:

TE-polarisation: $\Delta n = 1.0 \times 10^{-2}$

TM-polarisation: $\Delta n = 1.2 \times 10^{-2}$

$$f\left(\frac{x}{d_t}\right) = \begin{cases} 1 & 0 \le x \le d_t \\ & \text{otherwise} \\ 0 & \end{cases} \qquad\qquad 4.12a$$

$$g(y) = \begin{cases} 1 & -(d_l + w/2) \le y \le (d_l + w/2) \\ & \text{otherwise} \\ 0 & \end{cases} \qquad\qquad 4.12b$$

The following relation defines the refractive index profile

$$n(x, y) = n_s + (n_g - n_s) f(x/d_t) \cdot g(y) \qquad\qquad 4.13$$

The second guide is formed by thermal $Ag^+ - Na^+$ exchange. The refractive index change at the surface is given by $\Delta n = 1.0 \times 10^{-2}$. No anisotropy is assumed for this waveguide. The refractive index is approximated by the complementary error function in the x-direction. Such an approximation is valid and has been verified

experimentally for planar waveguides. The refractive index in the y-direction is represented by sum of error functions.

$$f\left(\frac{x}{d}\right) = erfc\left(\frac{x}{d}\right)$$

4.14a

$$g\left(\frac{2y}{w}\right) = \frac{1}{2}\left\{erf\left[\frac{w}{2d}\left(1+\frac{2y}{w}\right)\right] + erf\left[\frac{w}{2d}\left(1-\frac{2y}{w}\right)\right]\right\}$$

4.14b

$$n^2(x, y) = n_s^2 + (n_g^2 - n_s^2)f(x/d)\cdot\frac{g(2y/w)}{g(0/w)}$$

4.15

The denominator $g(0/w)$ has been included for the purpose of normalising the refractive index change. The diffusion depth is $d = d_{erfc} = 0.636^{-1} \times d_{1/e}$.

The dispersion characteristics of the individual waveguides are calculated at first. The modal fields of both individual guides may then be used to design the asymmetrical coupler approximately using simple coupled mode theory or improved coupled mode theory. The following parameters are common to both waveguides:

for both guides the substrate index is $n_s = 1.512$,

for both guides the upper cladding index is $n_c = 1.0$,

the wavelength region of interest is between $\lambda = (0.55 \text{ to } 0.70)\mu m$, and

the mask has widths between $w = (1.8 \text{ to } 4.0)\mu m$.

A comparison of the results obtained using the finite element method with the effective index method (Gwneuch, 1995), are shown in Table 4.4 for both Gaussian and complimentary error function index profiles. In this case the refractive index profile is unnormalised. The refractive index at the core of the film is 1.522 and the aspect ratio is given as $\frac{w}{d} = 1$. Table 4.5 shows the relative error between the FEM

and the EIM near to cutoff. It can be seen from the table that as the mode approaches cutoff, the relative error also increases. This can also be deduced from table 4.4

| $V = \dfrac{2\pi d}{\lambda}\sqrt{n_f^2 - n_s^2}$ | Propagation constant | | | |
| | FEM | | EIM | |
	Erfc	Gaussian	Erfc	Gaussian
8	0.09828	0.21795	0.0963	0.2117
10	0.14695	0.26944	0.1443	0.2630
12	0.18478	0.30612	0.1820	0.2996

Table 4.4 A comparison of the FEM with the EIM for complimentary error function and Gaussian function in a directional coupler.

| $V = \dfrac{2\pi d}{\lambda}\sqrt{n_f^2 - n_s^2}$ | Propagation constant (with normalised refractive index profile) | | |
| | FEM | EIM | |
	Erfc	Erfc	Rel. error %
4.5	0.08649	0.0919	+5.9
5	0.12967	0.1318	+1.6
5.97	0.20545	0.2040	-0.7

Table 4.5   Showing the relative error in the normalised refractive index between the FEM and the EIM for the complimentary error function.

4.5.   Summary

Using the vector **H**-field finite element formulation, waveguides with an arbitrary index distribution in both the transverse directions have been investigated, as were waveguides with an arbitrary permittivity tensor. The effect of anisotropy on the symmetry of the guide has been reported. To test the accuracy of the FEM initially some planar examples were considered where a FEM solution was obtained for a simple planar waveguide and compared with the exact solution obtained by solving the transcedental equation. Since computational resources can limit the accuracy of the FEM, two extrapolation techniques used in improving the accuracy of the finite element solution were tested. It was shown that Aitkens' extrapolation technique converges faster than the approach adopted by Koshiba. So far, many workers have assumed that in diffused waveguides, the diffusion parameters are equal to the guide dimensions. In this chapter, it has also been shown that for waveguides with diffused index profiles, better results are obtained near cut off if the waveguide dimensions are assumed to be greater than the diffusion parameters. Anisotropy of the waveguide was investigated and results were presented for a two dimensional diffused waveguide with an arbitrary permittivity tensor. It has been shown that in analyzing anisotropic waveguides with an off-diagonal refractive index tensor, it is not possible to exploit the physical symmetry of the guide to achieve computational efficiency. In the simulation and optimization of second harmonic generators where phase matching is achieved due to the birefringence of the material or in an electrooptic modulator where the applied modulating potential introduces off-diagonal tensor refractive indices, cascaded nonlinear devices or erbium doped amplifiers, the adoption of the above analysis technique would be of particular value.

Chapter Five

Numerical Modelling of Second Harmonic Generation in Optical Waveguides Using the Finite Element Method

I. Introduction

A numerical study of Second Harmonic Generation in optical waveguides is presented using the finite element method and the Crank-Nicholson split-step procedure. Results are given for a Cerenkov radiation scheme in both planar and channel waveguides. Also presented are results obtained on frequency doubling for guided modes in both planar and channel waveguides, using the quasi-phase matching scheme.

The demand for compact and robust solid-state sources, emitting coherent blue radiation for data storage and laser printing as well as all-optical switching applications has intensified the search for appropriate materials from which they may be fabricated. This is evident from the number of recent publications in the field, (Hashizume *et al.*, 1992, Li *et al.*, 1990, Hayata and Koshiba, 1991, Suhara and Nishiahara, 1990, Mizuuchi *et al.*, 1994, Delacourt *et al.*, 1994). Reliable coherent

radiation on this wavelength band is still difficult to obtain directly, and second harmonic generation (SHG) is one convenient alternative method of obtaining a compact, coherent source of blue radiation. This has the potentially of offering high conversion efficiencies (Suhara and Nishiahara, 1990, Mizuuchi *et al.*, 1994, Reneger and Sohler, 1988, Kinkata *et al.*, 1996, Leo *et al.*, 1992, Fluck *et al.*, 1996). As a phenomenon, SHG was first observed in the early 1960s, yet its exploitation has been rendered difficult by technological problems as well as finding materials that meet the phase matching requirements. The need to model such devices accurately and efficiently becomes even more urgent as a means of cutting down on developmental costs, thus enhancing the productivity of the search. It is quite difficult to model non-linear devices accurately using analytical methods, and so several numerical methods have been proposed and developed (Masoudi and Arnold, 1995, Yevick, 1994, Krijnen *et al.*, 1996, Hayata and Koshiba, 1991, Mahalakshmi *et al.*, 1996). The difficulties encountered in modelling such devices accurately has meant that approximations, such as a reduced geometry, or a planar representation of a two dimensional structure are often employed (Hayata and Koshiba, 1991, Mahalakshmi *et al.*, 1996). The FEM has previously been shown to be a very powerful, accurate and versatile method (Rahman and Davies, 1984a), useful in obtaining the modal solution of any waveguide medium with an arbitrary diffusion profile and anisotropic properties. Waveguides structures having such characteristics are particularly suitable for SHG. In this section of the thesis, results are presented on the SHG process in optical waveguides using the finite element-based beam propagation method (FE-BPM) and the split-step Crank-Nicholson procedure, where both planar and channel waveguides are considered. Two major schemes for obtaining second harmonic radiation are studied, these being the birefringent phase matching and the quasi-phase matching techniques.

5.2   Theoretical Background

When electromagnetic radiation propagates through certain a class of crystals, the non-linear dielectric properties of the material induce in it a polarisation. It is well known that the mathematical representation of this induced polarisation in the crystal contains a higher order term, proportional to the quadratic of the non-linear susceptibility and to the square of the applied electric field. The non-linear response of the material may lead to an exchange of energy between the electromagnetic fields propagating at different frequencies Yariv (1989). One important application of such a phenomenon is in second harmonic generation in which part of the energy of the input field, at a frequency, ω, is transferred to a field at double that frequency, 2ω. The non-linear susceptibility term is the index of proportionality between the induced polarisation and the propagating fields and is defined as

$$P = 2d\,E \cdot E \qquad\qquad 5.1$$

where P is the non-linear polarisation, E is the field and d is the non-linear susceptibility tensor.

However, due to symmetry requirements, only materials from the non-centrosymmetric point group have a quadratic non-linear susceptibility term Fejer (1994) *i.e.* they posses a non-vanishing tensor term. In general, the induced polarisation can be written as follows (Yariv, 1989):

$$
\begin{vmatrix} P_x \\ P_y \\ P_z \end{vmatrix} =
\begin{vmatrix}
d_{11} & d_{12} & d_{13} & d_{14} & d_{15} & d_{16} \\
d_{21} & d_{22} & d_{23} & d_{24} & d_{25} & d_{26} \\
d_{31} & d_{32} & d_{33} & d_{34} & d_{35} & d_{36}
\end{vmatrix}
\begin{vmatrix}
E_x^2 \\ E_y^2 \\ E_z^2 \\ 2E_zE_y \\ 2E_zE_x \\ 2E_xE_y
\end{vmatrix} \qquad 5.2
$$

where P_x, P_y, and P_z are the components of the non-linear polarisation expressed in terms of the non-linear coefficient tensor, d_{mn} $(m = 1...3, n = 1...6)$ and E_x, E_y and E_z are the amplitudes of the fundamental electric fields. The specific form of the tensor depends on the point-group symmetry to which the crystal belongs. The small magnitude of the non-linear susceptibility tensor and phase velocity dispersion does not enable high output powers of the generated second harmonic radiation to be obtained.

5.2.1   Coupled Wave Equations

From Maxwell's equation, the propagation of an optical field in a given material can be written as

$$\nabla^2 \Phi - p_z \beta^2 \Phi + q k_o^2 \Phi = P_{NL} \qquad 5.3$$

and considering two fields propagating at two different frequencies in the material, the total optical field, Φ, can be written as (Weitzman and Osterberg, 1993)

$$\Phi(x, y, z, t) = \frac{1}{2}\left\{\Phi_1(x,y)\exp\left[j(\omega t - \beta z)\right] + \Phi_2(x,y,z)\exp\left[j(2\omega t - 2\beta z)\right] + c.c\right\} \quad 5.4$$

where Φ_2 is the slowly varying amplitude of the generated second harmonic field, Φ_1 is the input field of the fundamental wave, P_{NL} is the non-linear polarisation, q and p_z relate to the refractive index of the guide, k_o is the wave number, ω is the angular frequency and β is the propagation constant of the fundamental wave and c.c. is the complex conjugate. From the above equations, making the assumptions that the fundamental field is independent of the direction of propagation z, and that

$P_{NL} = 0$ for the fundamental field, the following coupled non-linear parabolic equations can be derived:

$$P_{x1}\frac{\partial^2 \Phi_1}{\partial x^2} + P_{y1}\frac{\partial^2 \Phi_1}{\partial y^2} - P_{z1}\beta^2\Phi_1 + q_1 k_o^2 \Phi_1 = 0 \qquad 5.5$$

$$-j4\beta p_{z2}\frac{\partial \Phi_2}{\partial z} + P_{x2}\frac{\partial^2 \Phi_2}{\partial x^2} + P_{y2}\frac{\partial^2 \Phi_2}{\partial y^2} - 4 p_{z2}\beta^2\Phi_2 + q_2 k_o^2 \Phi_2 = P_{NL} \qquad 5.6$$

The subscripts 1 and 2 denote the fundamental and second harmonic respectively. For the TE modes, $\Phi = E_x$, $p_x = n_x/n_y$, $p_y = p_z = 1, q = n_x^2$ and for TM modes $\Phi = E_y$, $p_x = 1/n_y^2$, $p_y = 1/n_z^2, p_z = 1/n_y^2, q = 1$. For $c//y$, $n_x = n_z = n_o$, the ordinary refractive index and $n_y = n_e$, the extraordinary refractive index, for a planar waveguide $\frac{\partial}{\partial x} = 0$.

5.2.2   Phase Matching Techniques

The magnitude of the second harmonic power generated depends critically on the waveguide parameters and on the non-linear tensor. As mentioned earlier, the small magnitude of the non-linear tensor and the phase velocity dispersion affect the level of output power generated. Research in the area of second harmonic generation is therefore mainly directed at finding new materials with a high non-linear susceptibility tensor and at ways of reducing phase velocity dispersion and hence obtaining phase matching. This study uses the latter methods.

To obtain acceptable conversion efficiency, a high input intensity and large nonlinearity are required. High pump power density may be obtained through the use of appropriate optical resonator geometry. This however requires the accurate

matching of pump laser and resonator wavelength. This can be done by employing, for example, mode-locking techniques. High pump power density can also be obtained by confining the pump light within the nonlinear part of the optical waveguide, rather than focus it into the bulk material. This can, however, lead to a narrow tolerance in pump wavelength and it might be difficult to achieve in semiconductor lasers with an extended temperature range.

The efficiency of the second harmonic generation depends critically on the waveguide parameters, thus requiring tight control of the guide thickness. A number of techniques exist for obtaining phase matching and these include birefringent phase matching and quasi-phase matching (QPM). Birefringent phase matching is a frequently used technique. It is based on the anisotropic properties of crystals, in which it is possible to make, as a fundamental input, an ordinary wave and for the output, an extraordinary wave or vice versa, depending on whether the crystal has negative or positive birefringence (Harvey, 1970). The phase velocities can be matched by choosing the particular angle between the direction of propagation and the optical axis. This results in the two waves 'seeing' different refractive indices. Birefringent phase matching is thus based on the difference between the refractive indices of the orthogonally polarised waves in the medium. Due to this difference, it is possible to have a situation where the phase velocity of the second harmonic wave equals that of the orthogonally polarised fundamental wave, because the refractive index, as 'seen' by the fundamental wave, is different from that of the generated second harmonic wave. The second harmonic field is thus radiated into the substrate at a known angle with respect to the propagation direction. This angle at which the second harmonic field is radiated is defined by $\cos\theta = \dfrac{n_{eff}(\omega)}{n_{sub}(2\omega)}$ where $n_{eff}(\omega)$ is the effective fundamental refractive index and $n_{sub}(2\omega)$ is substrate index of second harmonic. The bandwidth over which this occurs is very narrow, thereby limiting the transparency range of the material. Until recently, all frequency conversion devices were based on this method, despite the fact that only a few materials meet this

requirement. Since the generated second harmonic wave is radiated, special steps must be taken to ensure its efficient collection.

In isotropic media with normal dispersion, the phase matching conditions cannot be satisfied as in anisotropic materials since the refractive index is frequency dependent (Harvey, 1970). Other methods are therefore used to obtain phase matching. In quasi-phase matching (QPM), the non-linear coefficient is modulated by the periodic reversal of the ferroelectric domains after each coherence length. The effect of this is to negate any build-up of the phase mismatch. The device performance is therefore not dependent on the anisotropic properties of the material, hence making it possible to use the material over its entire transparency range. Another technique is domain disordering in which the non-linear susceptibility tensor is periodically destroyed in alternate half periods of the waveguide structure (Masoudi *et al.*, 1995). Generation of the second harmonic wave by this method is ideal for use in integrated optics due to its narrow confinement. It also requires, however, that the waveguide parameters are tightly controlled.

5.2.3 Propagation in Linear medium

For the purpose of comparison, equations describing the propagation of the TE wave profile in planar waveguides are derived. The waveguide was assumed to be linear and isotropic and capable of single mode operation. The initial wave profile was obtained by solving the eigenvalue problem using the well-developed FEM. The equation describing the propagation of a wave profile in an isotropic is given as

$$- j2\beta p \frac{\partial \phi}{\partial z} + \frac{\partial^2 \phi}{\partial x^2} + \frac{\partial^2 \phi}{\partial y^2} - \beta^2 \phi + k_o^2 n^2 \phi = 0 \qquad 5.7$$

Application of the finite element method (Appendix 4) to the above yields the following matrix equation

$$-j2\beta[B]\frac{\partial\{\phi\}}{\partial z}+\left([A]-\beta^2[B]\right)\{\phi\}=0 \qquad\qquad 5.8$$

where

$$[A]=\sum_e\iint\left[k_o^2n^2\{N\}\{N\}^T-\{N_x\}\{N_x\}^T\right]dxdy \quad\text{and} \qquad\qquad 5.9a$$

$$[B]=\sum_e\iint\left[k_o^2n^2\{N\}\{N\}^T\right]dxdy \qquad\qquad 5.9b$$

where $\{N\}$ and $\{N_x\}$ have been defined earlier as the element shape function and its derivative. The element shape function and its derivative for second order linear elements are given as follows

$$\int_e\{N\}\{N\}^T\,dxdy=\frac{l_e}{30}\begin{bmatrix}4 & -1 & 2\\ -1 & 4 & 2\\ 2 & 2 & 16\end{bmatrix} \qquad\qquad 5.10$$

and

$$\int_e\{N_x\}\{N_x\}^T\,dxdy=\frac{1}{3l_e}\begin{bmatrix}7 & 1 & -8\\ 1 & 7 & -8\\ -8 & -8 & 16\end{bmatrix} \qquad\qquad 5.11$$

respectively.

For propagation analysis, the finite difference method is applied to equation (5.1) over the small interval $i\Delta z\le z\le(i+\Delta z)$ along the direction of propagation. This will yield a matrix equation for the evolution of the wavefront in the form

$$-j2\beta[B]\frac{(\{\phi\}_{i+1}-\{\phi\}_i)}{\Delta z}+\left([A]-\beta^2[B]\right)\left[\theta\{\phi\}_{i+1}+(1-\theta)\{\phi\}_i\right]=\{0\} \qquad\qquad 5.12$$

This equation can be transformed into an equivalent matrix equation of the form $Ax = b$ by carrying out the following algebraic manipulations

$$- j2\beta[B]_i(\{\phi\}_{i+1} - \{\phi\}_i) + \Delta z([A]_i - \beta^2[B]_i)[\theta\{\phi\}_{i+1} + (1-\theta)\{\phi\}_i] = \{0\}$$ 5.13

multiplying out the above and rearranging the terms the following is obtained

$$- j2\beta[B]_i\{\phi\}_{i+1} + \Delta z([A]_i - \beta^2[B]_i)\theta\{\phi\}_{i+1} + j2\beta[B]_i\{\phi\}_i$$

$$+ \Delta z([A]_i - \beta^2[B]_i)(1-\theta)\{\phi\}_i = \{0\}$$ 5.14

The above can be rearranged to give

$$(- j2\beta[A]_i + \Delta z([A]_i - \beta^2[B]_i)\theta)\{\phi\}_{i+1} =$$

$$(- j2\beta[B]_i - \Delta z([A]_i - \beta^2[B]_i)(1-\theta))\{\phi\}_i$$ 5.15

Making the following substitutions

$$L(\theta) = - j2\beta[B]_i + \Delta z\theta([A]_i - \beta^2[B]_i)$$ 5.16a

and

$$L(1-\theta) = - j2\beta[B]_i + \Delta z(1-\theta)([A]_i - \beta^2[B]_i)$$ 5.16b

equation (5.15) can be written as

$$[L(\theta)]_i\{\phi\}_{i+1} = [L(1-\theta)]_i\{\phi\}_i$$ 5.17

The wavefront at each $(i+1)^{th}$ step is given by

$$\{\phi\}_{i+1} = [L(\theta)]_i^{-1}[L(1-\theta)]_i\{\phi\}_i$$
                                                                    5.18

The artificial parameter θ determines which propagation scheme is being used. If equal to zero, the forward difference scheme is obtained and equation (5.16) will be reduced to the following

$$L(\theta) = -j2\beta\{B\}_i$$
                                                                    5.19a

$$L(1-\theta) = -j2\beta[B]_i + \Delta z([A]_i - \beta^2[B]_i)$$
                                                                    5.19b

The backward difference scheme can be obtained by equating $\theta = 1$, in which case equation (5.16) becomes

$$L(\theta) = -j2\beta[B]_i + \Delta z([A]_i - \beta^2[B]_i)$$
                                                                    5.20a

and

$$L(1-\theta) = -j2\beta\{B\}_i$$
                                                                    5.20b

In the Crank-Nicolson scheme, theta is assigned the value of 0.5. It has been shown that with $\theta = 0.5$, the numerical stability of the solution is guaranteed. Equation (5.16) can then be written as

$$L(\theta) = -j2\beta[B]_i + 0.5\Delta z([A]_i - \beta^2[B]_i)$$
                                                                    5.21a

and

$$L(\theta - 1) = -j2\beta[B]_i - 0.5\Delta z([A]_i - \beta^2[B]_i)$$
                                                                    5.21b

5.2.4 Power Calculation

In second harmonic generation, a wave at a fundamental frequency, ω_1, is converted into a second harmonic wave at a frequency, ω_2. In this process, the main interest is in finding the amount of power at the fundamental wavelength that has been transferred to the second harmonic wavelength. In second harmonic analysis, therefore, an input field profile at the fundamental frequency is obtained and the energy or power contained in that field profile is calculated using the relation $E_{\omega 1}^* \times H_{\omega 1}$. The fundamental field is then used as a source term to find the second harmonic field. The power contained in the second harmonic field is calculated using the relation $E_{\omega 2}^* \times H_{\omega 2}$. In the following, an outline is given of how the power within the guide cross-section can be calculated using the element shape functions of the finite element formulation.

The power in an electromagnetic field can be defined using the Pyonting vector

$$E^* \times H = \begin{vmatrix} \overline{a}_x & \overline{a}_y & \overline{a}_z \\ E_x^* & E_y^* & E_z^* \\ H_x & H_y & H_z \end{vmatrix} = a_x\left(E_y^* H_z - E_z^* H_y\right) - a_y\left(E_x^* H_z - E_z^* H_x\right) + a_z\left(E_x^* H_y - E_y^* H_x\right)$$

$$5.22$$

$$S = \int E^* \times H d\Delta \qquad 5.23$$

In the above the integration is carried out over each element cross section; the interest is in the propagation direction and hence the following is obtained

$$\int E^* \times H d\Delta = \int_\Delta \left(E_x^* H_y - E_y^* H_x \right) d\Delta \qquad\qquad 5.24$$

To simplify the above, a relation is established between the **E** and the **H** components so that the final expression is in one variable only. From Maxwell's equations it is found that:

$$\nabla \times H^* = j\omega\varepsilon E^* = \begin{vmatrix} \overline{x} & \overline{y} & \overline{z} \\ \partial_x & \partial_y & \partial_z \\ H_x^* & H_y^* & H_z^* \end{vmatrix} \qquad\qquad 5.25$$

from which the following is obtained

$$j\varepsilon\omega\left(E_{x\overline{x}}^* + E_{y\overline{y}}^* + E_{z\overline{z}}^* \right) = \left(\frac{\partial H_z^*}{\partial y} - \frac{\partial H_y^*}{\partial z} \right)\overline{x} - \left(\frac{\partial H_z^*}{\partial x} - \frac{\partial H_x^*}{\partial z} \right)\overline{y} + \left(\frac{\partial H_y^*}{\partial x} - \frac{\partial H_x^*}{\partial y} \right)\overline{z} \quad 5.26$$

Equating terms with equal coefficients;

$$j\varepsilon\omega E_{x\overline{x}}^* = \left(\frac{\partial H_z^*}{\partial y} - \frac{\partial H_y^*}{\partial z} \right)\overline{x} \qquad\qquad 5.27a$$

$$j\varepsilon\omega E_{y\overline{y}}^* = -\left(\frac{\partial H_z^*}{\partial x} - \frac{\partial H_x^*}{\partial z} \right)\overline{y} \qquad\qquad 5.27b$$

The $\frac{\partial}{\partial z}$ component can be replaced with $-j\beta$

$$j\varepsilon\omega E_x^* = \frac{\partial H_z^*}{\partial y} + j\beta H_y^* \Rightarrow E_x^* = -\frac{1}{j\varepsilon\omega}\frac{\partial H_z^*}{\partial y} + \frac{\beta}{\omega\varepsilon}H_y^* \qquad\qquad 5.28a$$

$$j\varepsilon\omega E_y^* = \frac{\partial H_z^*}{\partial x} + j\beta H_x^* \Rightarrow E_y^* = \frac{1}{j\varepsilon\omega}\frac{\partial H_z^*}{\partial x} - \frac{\beta}{\omega\varepsilon}H_x^* \qquad\qquad 5.28b$$

Substituting the above in the Pyonting vector, the following is obtained

$$\int_\Delta \frac{1}{\omega\varepsilon}\left(\beta H_y^* - j\frac{\partial H_z^*}{\partial y}\right)H_y - \frac{1}{\omega\varepsilon}\left(-\beta H_x^* + j\frac{\partial H_z^*}{\partial x}\right)H_x d\Delta \qquad\qquad 5.29$$

$$\int_\Delta \left[\frac{1}{\omega\varepsilon}\left(\beta H_y^* H_y + \beta H_x^* H_x\right) - \frac{1}{\omega\varepsilon}\left(j\frac{\partial H_z^*}{\partial x}H_x + j\frac{\partial H_z^*}{\partial y}\right)H_y\right]_x d\Delta \qquad\qquad 5.30$$

From the representation of the field in triangular elements using shape functions, the following can be written

$$H = [N]\{H\} \text{ and } H^* = \{H\}^T[N]^T \text{ where } [N] = (N_1 \quad N_2 \quad N_3) \text{ and } \{H\} = \begin{pmatrix} H_1 \\ H_2 \\ H_3 \end{pmatrix}.$$

Making use of the above and their corresponding transpositions, equation (5.30) becomes

$$\int_\Delta \left[\frac{\beta}{\omega\varepsilon}\left(\{H_y\}^T[N]^T[N]\{H_y\} + \{H_x\}^T[N]^T[N]\{H_x\}\right) - \frac{j}{\omega\varepsilon}\left(\{H_z\}^T\frac{\partial[N]^T[N]}{\partial x}\{H_x\} + \{H_z\}^T\frac{\partial[N]^T[N]}{\partial y}\{H_y\}\right)\right]_x d\Delta$$

$$5.31$$

$$[N]^T[N] = \begin{vmatrix} N_1^2 & N_1N_2 & N_1N_2 \\ N_2N_1 & N_2^2 & N_2N_3 \\ N_3N_1 & N_3N_2 & N_3^2 \end{vmatrix} = \begin{bmatrix} \dfrac{\Delta}{6} & \dfrac{\Delta}{12} & \dfrac{\Delta}{12} \\ \dfrac{\Delta}{12} & \dfrac{\Delta}{6} & \dfrac{\Delta}{12} \\ \dfrac{\Delta}{12} & \dfrac{\Delta}{12} & \dfrac{\Delta}{6} \end{bmatrix} \qquad\qquad 5.32$$

$$\frac{\partial [N]^T[N]}{\partial x} = \begin{vmatrix} \dfrac{\partial N_1 N_1}{\partial x} & \dfrac{\partial N_1 N_2}{\partial x} & \dfrac{\partial N_1 N_3}{\partial x} \\ \dfrac{\partial N_2 N_1}{\partial x} & \dfrac{\partial N_2 N_2}{\partial x} & \dfrac{\partial N_2 N_3}{\partial x} \\ \dfrac{\partial N_3 N_1}{\partial x} & \dfrac{\partial N_3 N_2}{\partial x} & \dfrac{\partial N_3 N_3}{\partial x} \end{vmatrix} \qquad 5.33$$

From equation (2.57) the following can be obtained

$$\frac{\partial N_1}{\partial x} = a_2; \quad \frac{\partial N_2}{\partial x} = a_5; \quad \frac{\partial N_3}{\partial x} = a_8 \quad \text{such that}$$

$$\frac{\partial [N]^T[N]}{\partial x} = \begin{vmatrix} a_2 N_1 & a_2 N_2 & a_2 N_3 \\ a_5 N_1 & a_5 N_2 & a_5 N_3 \\ a_8 N_1 & a_8 N_2 & a_8 N_3 \end{vmatrix} \qquad 5.34$$

Similarly,

$$\frac{\partial [N]^T[N]}{\partial y} = \begin{vmatrix} \dfrac{\partial N_1 N_1}{\partial y} & \dfrac{\partial N_1 N_2}{\partial y} & \dfrac{\partial N_1 N_3}{\partial y} \\ \dfrac{\partial N_2 N_1}{\partial y} & \dfrac{\partial N_2 N_2}{\partial y} & \dfrac{\partial N_2 N_3}{\partial y} \\ \dfrac{\partial N_3 N_1}{\partial y} & \dfrac{\partial N_3 N_2}{\partial y} & \dfrac{\partial N_3 N_3}{\partial y} \end{vmatrix} \qquad 5.35$$

and making the following substitutions $\dfrac{\partial N_1}{\partial y} = a_3; \quad \dfrac{\partial N_2}{\partial y} = a_6; \quad \dfrac{\partial N_3}{\partial y} = a_9$

$$\frac{\partial [N]^T[N]}{\partial y} = \begin{vmatrix} a_3 N_1 & a_3 N_2 & a_3 N_3 \\ a_6 N_1 & a_6 N_2 & a_6 N_3 \\ a_9 N_1 & a_9 N_2 & a_9 N_3 \end{vmatrix} \qquad 5.36$$

A substitution of the above in equation (5.31), and noting that

$$\int N_1 d\Delta = \int N_2 d\Delta = \int N_3 d\Delta = \frac{\Delta}{3} \text{ results in the power equation becoming}$$

$$\frac{\beta}{\omega\varepsilon}\left(\{H_y\}^T \frac{\Delta}{6} \begin{vmatrix} 1 & \frac{1}{2} & \frac{1}{2} \\ \frac{1}{2} & 1 & \frac{1}{2} \\ \frac{1}{2} & \frac{1}{2} & 1 \end{vmatrix} \{H_y\} + \{H_x\}^T \frac{\Delta}{6} \begin{vmatrix} 1 & \frac{1}{2} & \frac{1}{2} \\ \frac{1}{2} & 1 & \frac{1}{2} \\ \frac{1}{2} & \frac{1}{2} & 1 \end{vmatrix} \{H_x\} \right)$$

$$-\frac{1}{\omega\varepsilon}\left(\{H_z\}^T j\frac{\Delta}{3} \begin{vmatrix} a_2 & a_2 & a_2 \\ a_5 & a_5 & a_5 \\ a_8 & a_8 & a_8 \end{vmatrix} \{H_x\} + \{H_z\}^T j\frac{\Delta}{3} \begin{vmatrix} a_2 & a_2 & a_2 \\ a_5 & a_5 & a_5 \\ a_8 & a_8 & a_8 \end{vmatrix} \{H_y\} \right)$$

5.37

5.3   Results of the Simulation

In this section, the numerical method developed in this research project will be applied to the simulation of various types of nonlinear waveguides. Initially the one-dimensional planar structure will be considered. The method will then be extended to two-dimensional structures. A number of schemes for improving the output power will also be examined.

5.3.1 Planar Waveguides

The finite element method (FEM) has previously been shown to be useful in the analysis of optical waveguides, particularly in obtaining a modal solution (Rahman and Davies, 1984a). In this section, the finite element method is applied to the analysis of the second order non-linear process of second harmonic generation in planar waveguides. To test the accuracy of the present method, results obtained are first compared with those previously published. Applying the FEM to equation (5.5)

and assuming a stationary analysis, the following matrix equation is obtained for the *modal* analysis model (Rahman and Davies, 1984b)

$$[\mathbf{A}]\{\Phi\} + \omega^2[\mathbf{B}]\{\Phi\} = 0 \qquad\qquad 5.38$$

where [**A**] is a complex Hermitian matrix, [**B**] is a real symmetric and positive definite matrix, ω^2 is the eigenvalue, and $\{\Phi\}$ is the eigenvector.

Applying the FEM to equation (5.6) will yield the following matrix equation for the propagation model:

$$-j4\beta[\mathbf{B}]\frac{d\{\Phi\}}{dz} + \left([\mathbf{A}] - 4\beta^2[\mathbf{B}]\right)\{\Phi\} = \{\psi_{\mathrm{NL}}\} \qquad\qquad 5.39$$

Equation (5.39) may be solved using a split-step procedure; the propagation step in which the finite difference method is applied within a short interval and the non-linear step where the effect of the non-linear term is considered. Such a procedure will yield a matrix equation of the form (Hayata *et al.*, 1991)

$$\{\Phi_2\}_{i+1} = [L(\theta)]^{-1}[L(\theta-1)]\{\Phi_2\}_i + j\frac{\Delta z}{4\beta p_{z2}}\{\psi_{\mathrm{NL}}\} \qquad\qquad 5.40$$

where

$$L(\theta) = -j4\beta[\mathbf{B}] + \theta\Delta z\left([\mathbf{A}] - 4\beta^2[\mathbf{B}]\right) \qquad\qquad 5.41$$

and θ, as stated previously, is an artificial parameter which controls stability of solution. For the Crank-Nicholson scheme, $\theta = 0.5$, which provides a stable solution unconditionally.

5.3.1.1   The non-linear Tensor for TE mode

In equation (5.40), the profile of the non-linear polarisation can be written as Koshiba (1992)

$$\psi_{NL} = -\frac{2k_o^2}{\varepsilon_o}(i_x \cdot P_{NL})$$

5.42

for the TE mode, where i_x is the unit vector in the x-direction. For the direction under consideration, the electric fields of the TE mode can be approximated as follows

$$e_{x1} = \phi_1, \qquad e_{y1} = 0 \qquad e_{z1} = 0$$

Making this substitution in equation (5.2), the following is obtained

$$P_{NL} = \begin{vmatrix} P_x \\ 0 \\ 0 \end{vmatrix} = \varepsilon_o \begin{vmatrix} d_{11}e_{x1}^2 \\ d_{21}e_{x1}^2 \\ d_{31}e_{x1}^2 \end{vmatrix}$$

5.43

The non-linear tensor d is different for different crystal orientations. In LiNbO$_3$ when $c//x$, $d_{11} = d_{33}$, $d_{21} = 0$, and $d_{31} = 0$ and the non-linear polarisation becomes

$$P_{NL} = P_x = \varepsilon_o d_{33} e_{x1}^2$$

5.44

The refractive indices for this orientation are also given by the following

$$n_x = n_e, \; n_y = n_z = n_o$$

For $c//y$, the following tensor values are obtained

$d_{11} = 0$, $d_{21} = d_{31}$, and $d_{31} = -d_{22}$

Making this substitution in equation (5.2) the following is obtained

$$P_{NL} = \begin{vmatrix} P_x \\ 0 \\ 0 \end{vmatrix} = \varepsilon_o \begin{vmatrix} 0 \\ d_{31}e_{x1}^2 \\ -d_{22}e_{x1}^2 \end{vmatrix} \qquad 5.45$$

This shows that no polarisation term is obtained for the TE mode in a crystal cut with
$c//y$.

Similarly when $c//z$ the following is obtained

$d_{11} = 0$, $d_{21} = -d_{22}$, and $d_{31} = d_{13}$

$$P_{NL} = \begin{vmatrix} P_x \\ 0 \\ 0 \end{vmatrix} = \varepsilon_o \begin{vmatrix} 0 \\ -d_{22}e_{x1}^2 \\ d_{31}e_{x1}^2 \end{vmatrix} \qquad 5.46$$

Again no polarisation is generated in a crystal cut with $c//z$.

5.3.1.2   The non-linear Tensor for TM mode

For the TM mode, the source field is given by the following

$$\psi_{NL} = \frac{k_o}{\varepsilon_o z_o} \left[\frac{2\beta(i_y \cdot P_{NL})}{n_y^2} - j\frac{1}{n_z^2}\frac{\partial(i_z \cdot P_{NL})}{\partial y} \right] \qquad 5.47$$

where i_y and i_z are unit vectors in the y and z directions respectively. The approximate values of the fundamental electric fields can be expressed as

$$e_{x1} = 0, \qquad e_{y1} = -\frac{z_o \beta}{n_y^2 k_o} \phi_1 \qquad e_{z1} = j \frac{z_o}{n_z^2 k_o} \frac{\partial \phi_1}{\partial y}$$

Using these values in the second order non-linear polarisation term, the following equation is obtained

$$\begin{vmatrix} P_x \\ P_y \\ P_z \end{vmatrix} = \varepsilon_o \begin{vmatrix} d_{11} & \cdots & d_{16} \\ d_{21} & \cdots & d_{26} \\ d_{31} & \cdots & d_{36} \end{vmatrix} \begin{vmatrix} 0 \\ e_y^2 \\ e_z^2 \\ 2e_z e_y \\ 0 \\ 0 \end{vmatrix} \qquad 5.48$$

It follows that

$$\begin{vmatrix} P_x \\ P_y \\ P_z \end{vmatrix} = \varepsilon_o \begin{vmatrix} d_{12}e_y^2 + d_{13}e_z^2 + 2d_{14}e_y e_z \\ d_{22}e_y^2 + d_{23}e_z^2 + 2d_{24}e_y e_z \\ d_{32}e_y^2 + d_{33}e_z^2 + 2d_{34}e_y e_z \end{vmatrix} \qquad 5.49$$

Different crystal orientations will give different values of the non-linear polarisation since a different tensor is operative.

For $c//x$, the non-linear polarisation is as follows

$$\begin{vmatrix} P_x \\ P_y \\ P_z \end{vmatrix} = \varepsilon_o \begin{vmatrix} d_{31}e_y^2 + d_{31}e_z^2 \\ d_{22}e_y^2 - d_{22}e_z^2 \\ -2d_{22}e_y e_z \end{vmatrix} \qquad 5.50$$

For $c//y$, the non-linear polarisation is as follows

$$
\begin{vmatrix} P_x \\ P_y \\ P_z \end{vmatrix} = \varepsilon_o \begin{vmatrix} 0 \\ d_{33}e_y^2 + d_{31}e_z^2 \\ d_{22}e_z^2 + 2d_{15}e_y e_z \end{vmatrix}
\qquad\qquad 5.51
$$

For c//z, the non-linear polarisation is as follows

$$
\begin{vmatrix} P_x \\ P_y \\ P_z \end{vmatrix} = \varepsilon_o \begin{vmatrix} 0 \\ d_{22}e_z^2 + 2d_{15}e_y e_z \\ d_{31}e_y^2 + d_{33}e_z^2 \end{vmatrix}
\qquad\qquad 5.52
$$

For a TM mode with c//y, equation (5.51) is substituted in (5.47) to give

$$
\Psi_{NL} = \frac{k_o}{\varepsilon_o z_o} \left[\frac{2\beta\varepsilon_o \left(d_{33}e_y^2 + d_{31}e_z^2 \right)}{n_y^2} - j\frac{\varepsilon_o}{n_z^2} \frac{\partial\left(d_{22}e_z^2 + 2d_{15}e_y e_z \right)}{\partial y} \right]
\qquad 5.53
$$

5.3.2   Cerenkov radiation scheme

The first extensive theoretical treatment of Cerenkov radiation scheme was provided by Sanford and Connors (1989). As in such other work, the model makes the following assumptions

- a quasi slab approximation
- no depletion of the pump beam by losses
- no depletion of the pump beam by second harmonic conversion
- a simple TE or TM polarisation

The Cerenkov radiation scheme makes use of the phase matching existing between the fundamental guided mode and the second harmonic radiation mode. In this type of scheme, the generated second harmonic wave in the non-linear medium travels with a phase velocity faster than that in the substrate. As a result of this, the

generated second harmonic wave is radiated into the substrate at an angle satisfying the phase matching condition (see Fig 5.1).
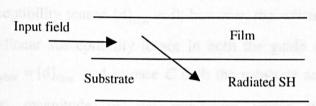
Input field   Film

Substrate

Radiated SH

Fig 5.1 Schematic representation of the Cherenkov scheme in planar waveguide.

The wavelength (λ) dependencies of the ordinary and extraordinary refractive indices n_o and n_e, respectively of the material substrate (LiNbO$_3$) are given as follows (Smith *et al.*, 1976)

$$n_o^2 = 4.9048 - \frac{0.11768}{0.04750 - \lambda^2} - 0.027169\lambda^2 \qquad \text{5.54a}$$

$$n_e^2 = 4.5820 - \frac{0.099169}{0.044432 - \lambda^2} - 0.021950\lambda^2 \qquad \text{5.54b}$$

In this study the orientation of the crystalline axis is assumed to be *c//y* for the TM mode, which is considered here. The explicit form of the second order nonlinear optical tensor for such a crystalline orientation is given as

$$[d] = \begin{bmatrix} 0 & 0 & 0 & 0 & -d_{22} & d_{15} \\ d_{31} & d_{33} & d_{31} & 0 & 0 & 0 \\ -d_{22} & 0 & d_{22} & d_{15} & 0 & 0 \end{bmatrix} \qquad \text{5.55}$$

The values of the non-linear tensor terms used in this simulation are given as

$d_{15} = d_{33} = -5.9 \times 10^{-12} m/V$, $\qquad d_{22} = -4.0 \times 10^{-12} m/V$, $d_{33} = -34 \times 10^{-12} m/V$

(Hayata and Koshiba, 1991). The guide dimensions considered in this work are $y_{film} = 0.525 \mu m$, where y_{film} is the height of the guide and y_{subst} is the height of the substrate. Three cases labelled *A, B* and *C*, with respect to the non-linear term are considered, where in case *A*, the guide is assumed to be linear, and the non-linear susceptibility tensor $[d]_{film} = 0$; however, the substrate is non-linear. In case *B*, the non-linear susceptibility tensor in both the guide and the substrate are equal *i.e.*, $[d]_{subst} = [d]_{film}$ and in case *C* both the substrate and guide are non-linear with the same magnitude of the non-linear tensor but with different signs *i.e.* $[d]_{subst} = -[d]_{film}$. The above three cases may occur depending on the actual manufacturing process.

Fig 5.2. Profile of the input field.

The field profile of the fundamental TM mode at $\lambda = 1.06 \mu m$ is obtained by way of a modal analysis using the FEM procedure. The profile of this field, which is launched at the input to the guide, is shown in Fig. 5.2. The guide core is within the following

limits $0.8 \leq y \leq 1.325 \mu m$. It can be observed that the field profile penetrates only slightly into the top air-cladding region but, however, decays much more slowly into the lower substrate region. This fundamental field generates the second harmonic field and its evolution along the optical structure is followed by the step-by-step solution of equation (5.9).
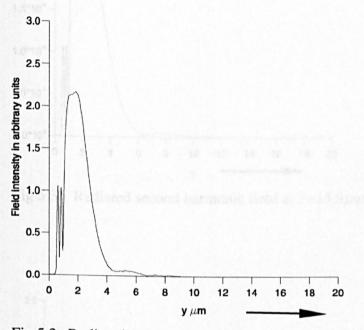

Fig 5.3a Radiated second harmonic field at Z=10.6μm

The evolution of the second harmonic field profile as it propagates in the z-direction is shown in Figure 5.3 for five different propagation distances (Z=10.6μm, 15.9μm, 26.5μm, 30.6μm and 47.7μm), for case A, when the substrate is nonlinear.

Fig 5.3b. Radiated second harmonic field at $Z=15.9\mu m$

Fig 5.3c. Radiated second harmonic field at $Z=26.5\mu m$
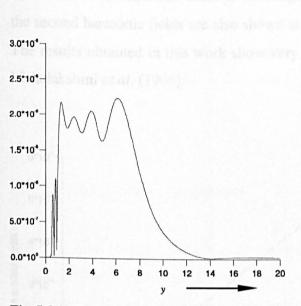
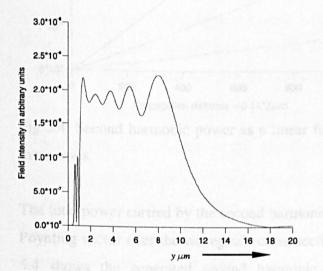Fig 5.3d. Radiated second harmonic field at Z=30.6μm

Fig 5.3e. Radiated second harmonic field at Z=47.7μm

The continuous spectrum of the radiated mode as it radiates into the substrate can be observed. From Fig. 5.3a, it can be observed that the second harmonic field has penetrated a distance of up to 4μm into the substrate. It can also be seen from Fig. 5.3b, at Z=15.9μm that the second harmonic field has penetrated further into the substrate region. Fig. 5.3c shows the second harmonic field at Z=26.5μm and although it has penetrated well into the substrate region, it can be noticed that the

maximum field amplitude remains unchanged in all three cases. In Figs 5.3d and e, the second harmonic fields are also shown at $Z=30.6\mu m$ and $Z=47.7\mu m$, respectively. The results obtained in this work show very close agreement with those obtained by Mahalakshmi *et al.* (1996).
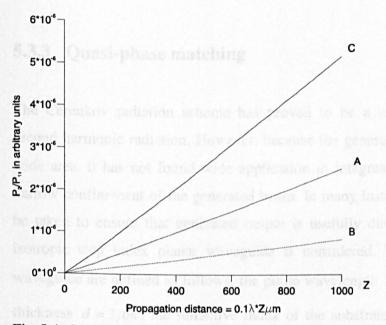

Fig 5.4. Second harmonic power as a linear function of propagation distance for all three cases.
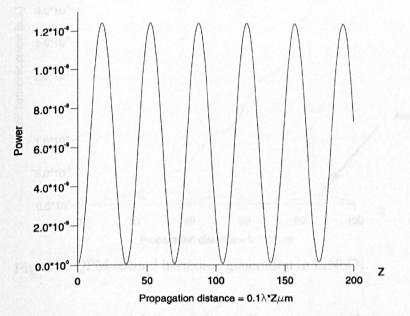
The total power carried by the second harmonic wave is calculated by integrating the Poynting vector over the waveguide cross-section for each longitudinal position. Fig. 5.4 shows the generated second harmonic power as a linear function of the propagation distance, for all three cases. In case *C*, when the magnitude of the tensor terms in the guide and in the substrate are equal but of opposite sign, the intensity of the generated second harmonic radiation is higher than that of cases *A* and *B* at any given longitudinal distance. The significant increase in the radiated power in case *C* might be attributed to phase matching due to domain inversion (similar to quasi-phase matching in guided structures), as the radiated wave propagates in the *yz* plane. This will suggest that a substantial increase in second harmonic output could be obtained by carefully considering the phase matching requirements along the *y*-axis
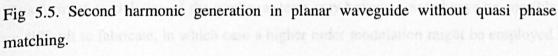
in a Cerenkov radiation scheme. The results obtained in this work show very close agreement with those obtained by Hayata and Koshiba (1991). It should be noted, however, that second order line elements were used in the work of Hayata and Koshiba (1991), whilst first order linear elements have been employed in these simulations.

5.3.3 Quasi-phase matching

The Cerenkov radiation scheme has proved to be a useful source of generating second harmonic radiation. However, because the generated wave is radiated over a wide area, it has not found wide application in integrated optics, which requires a narrow confinement of the generated beam. In many instances, special steps have to be taken to ensure that generated output is usefully directed. In the next case, an isotropic step index planar waveguide is considered. The parameters of such a waveguide are defined as follows: the pump wavelength $\lambda_\omega = 0.84 \mu m$, the waveguide thickness $d = 3 \mu m$, the refractive index of the substrate at λ_ω is $n_s^\omega = 2.172$, the refractive index of substrate at the second harmonic wavelength, $n_s^{2\omega} = 2.309$, and the index step between guide and substrate is $\Delta n = 0.01$. In this simulation, it is assumed that the index change, Δn, is the same at both wavelengths and the value of the nonlinear susceptibility is as previously defined. The effective indexes of the fundamental wave and the second harmonic have been found to be 2.1790 and 2.3181 respectively. Fig.5.5 shows the evolution of the second harmonic power without any phase matching. The fundamental and the second harmonic wave will travel at different velocities due to normal dispersion in the material. The direction of flow of power between the two waves is dependent on their relative phases. A continuous change in the direction of flow of power is therefore obtained as a result of the continuous change in phase velocity between the two waves. Since the fundamental and the second harmonic waves are not phase matched, an efficient and complete exchange of power between them is not possible and, as expected, the

power builds up to a maximum (over the coherence length) and then dissipates due to the phase mismatch.

Fig 5.5. Second harmonic generation in planar waveguide without quasi phase matching.

Modulating the non-linear term can, substantially increase the second harmonic power generated. Depending on the periodicity of modulation, different orders can be identified. Fig 5.6 shows QPM second harmonic generation using first order modulation, i.e. periodically modulating the nonlinear term in alternate half-periods. As expected, the second harmonic power is seen to build up. During the simulations, it was tested and found that the integrity of the second harmonic field profile is preserved during the period of propagation.
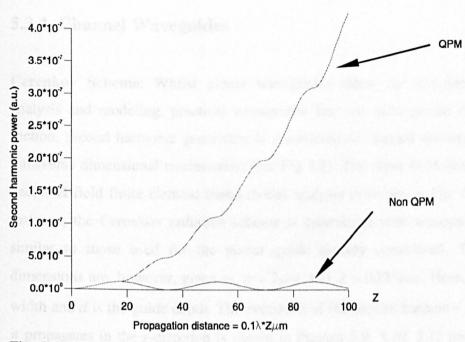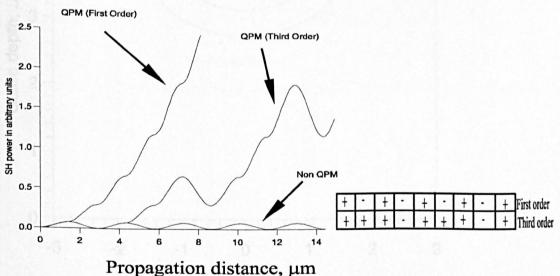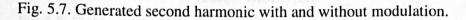
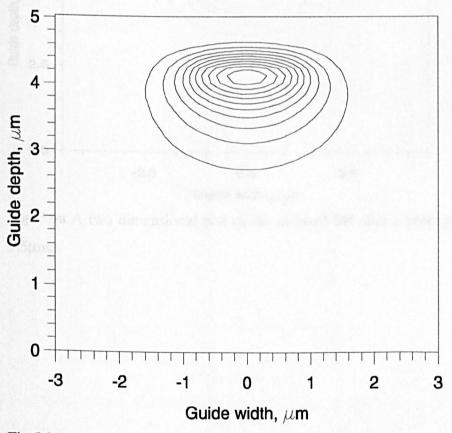Fig. 5.6. QPM second harmonic generation in LiNbO$_3$.

This form of modulation of the nonlinear term may however, not always be possible or difficult to fabricate, in which case a higher order modulation might be employed. The first and third order modulations are shown in Fig. 5.7. For the higher order modulation, the period of modulation is longer and hence easier to fabricate. It must be noted however that the first order modulation achieves the most rapid growth in output power.
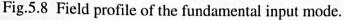

Fig. 5.7. Generated second harmonic with and without modulation.

5.3.4 Channel Waveguides

Cerenkov Scheme: Whilst planar waveguides allow for a comparatively easy analysis and modeling, practical waveguides are two dimensional devices. In this section, second harmonic generation is considered in channel waveguides with two transverse dimensional confinement (see Fig 4.1). The input field obtained from the vector **H**-field finite element based modal analysis is shown in Fig. 5.8. In the first instance, the Cerenkov radiation scheme is considered with waveguide parameters similar to those used for the planar guide already considered. The waveguide dimensions are, however, given as $w = 2\mu m$ and $d = 0.525\mu m$. Here, w is the guide width and d is the guide depth. The evolution of the second harmonic field profile as it propagates in the z-direction is shown in Figures 5.9, 5.10, 5.11 and 5.12 for four different propagation distances ($z=1.5\mu m$, $2.65\mu m$, $3.82\mu m$ and $4.77\mu m$), for case A, when the substrate is nonlinear.

Fig.5.8 Field profile of the fundamental input mode.

From Fig. 5.9a, it can be observed that the second harmonic (SH) field has penetrated slightly into the substrate but its peak however is still in the guiding layer. Fig 9b shows a three dimensional view of the same field plot. It can be observed from Fig 5.10a that a substantial amount of the second harmonic field has now penetrated further into the substrate region, this is after a propagation distance of $2.65\mu m$. Fig. 5.11 shows the second harmonic field at $z=3.82\mu m$, the peak having moved almost totally into the substrate. Fig. 5.12 shows the second harmonic field at $z=4.77\mu m$, in this case the field now being wholly in the substrate.
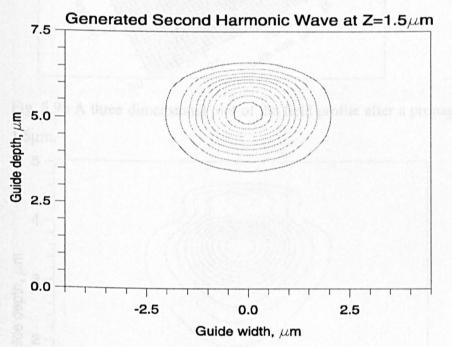
Fig. 5.9a A two dimensional plot of the radiated SH after a propagation distance of 1.5μm.

Generated Second Harmonic Wave at Z=1.5μm
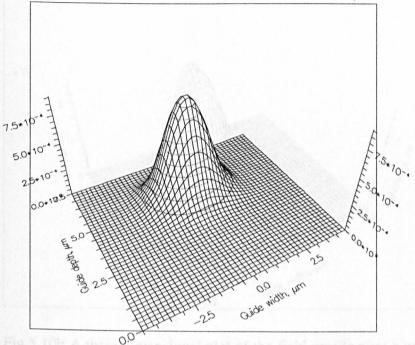

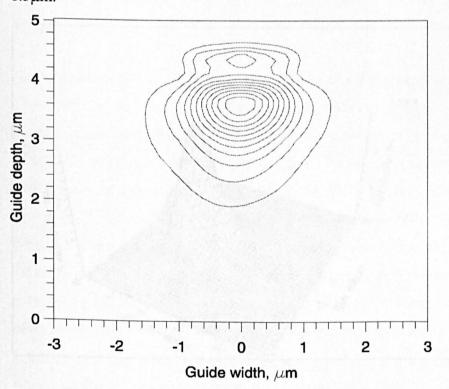Fig. 5.9b A three dimensional plot of the field profile after a propagation distance of 1.5µm.

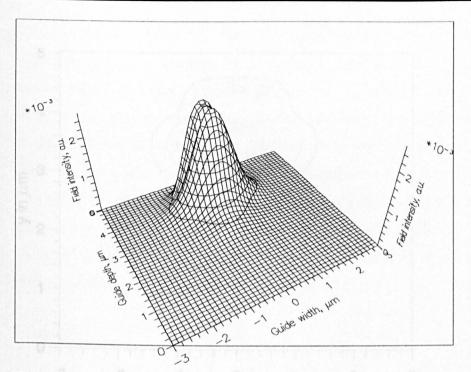Fig. 5.10a A two dimensional plot of the field penetration after a propagation of 2.65μm

Fig.5.10b A three dimensional plot of the field profile after a propagation distance of 2.65μm.
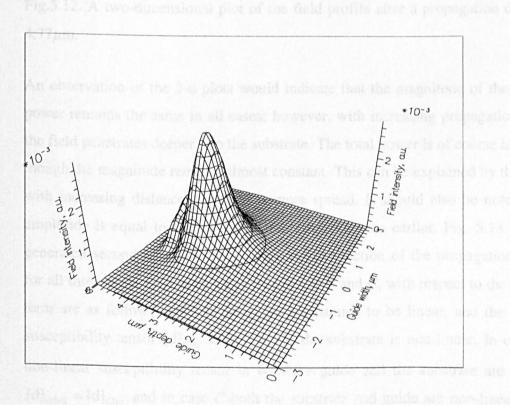

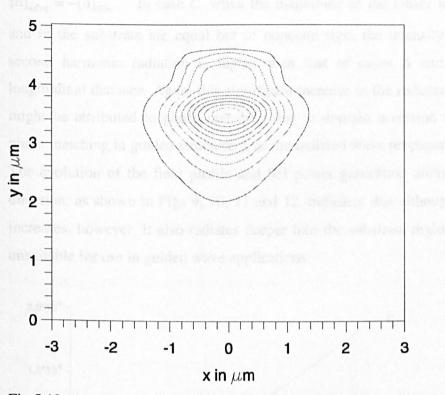Fig.5.11 A three dimensional plot of the field profile after a propagation distance of 3.82μm.

Fig.5.12. A two-dimensional plot of the field profile after a propagation distance of 4.77μm.

An observation of the 3-d plots would indicate that the magnitude of the generated power remains the same in all cases; however, with increasing propagation distance the field penetrates deeper into the substrate. The total power is of course higher even though the magnitude remains almost constant. This can be explained by the fact that with increasing distance, the field is more spread. It should also be noted that the amplitude is equal to that of the planar structure seen earlier. Fig. 5.13 shows the generated second harmonic power as a linear function of the propagation distance, for all three cases. The three cases labelled A, B and C, with respect to the non-linear term are as follows: case A, the guide is assumed to be linear, and the non-linear susceptibility tensor $[d]_{film}$ =0; however, the substrate is non-linear. In case B, the non-linear susceptibility tensor in both the guide and the substrate are equal i.e., $[d]_{subst} = [d]_{film}$ and in case C both the substrate and guide are non-linear with the same magnitude of the non-linear tensor but with different signs i.e.

$[d]_{subst} = -[d]_{film}$. In case C, when the magnitude of the tensor terms in the guide and in the substrate are equal but of opposite sign, the intensity of the generated second harmonic radiation is higher than that of cases A and B at any given longitudinal distance. Again this significant increase in the radiated power in case C might be attributed to phase matching due to domain inversion (similar to quasi-phase matching in guided structures), as the radiated wave propagates in the yz plane. The evolution of the field profile and SH power generation along the longitudinal direction, as shown in Figs 9, 10, 11 and 12, indicates that although the total power increases, however, it also radiates deeper into the substrate region which makes it unsuitable for use in guided wave applications.
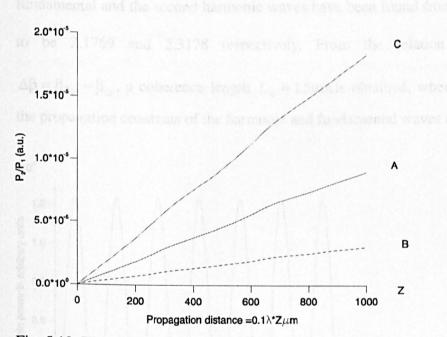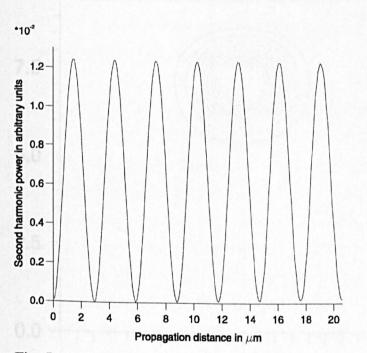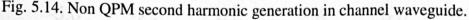

Fig. 5.13. The second harmonic power as a linear function of propagation distance.

5.3.5 Quasi-phase matching scheme

For quasi-phase matching scheme, an isotropic waveguide is now considered, of the type given in earlier work (Delacourt *et al.*, 1994). The waveguide parameters are as follows; $\lambda_f = 0.84 \mu m$, waveguide thickness $d = 3\mu m$, guide width $w = 3\mu m$,

refractive index of substrate at fundamental wavelength, λ_f, $n_s^\omega = 2.172$, refractive index of substrate at second harmonic wavelength, $n_s^{2\omega} = 2.309$ and the index step between guide and substrate is $\Delta n = 0.01$. For simplicity, it is assumed that this index change, Δn, is the same at both wavelengths and the value of the nonlinear susceptibility as previously defined are given by $d_{15} = d_{33} = -5.9 \times 10^{-12} m/V$, $d_{22} = -4.0 \times 10^{-12} m/V$, $d_{33} = -34 \times 10^{-12} m/V$ (Hayata and Koshiba, 1991). The numerical method adopted in this work can be used to consider any realistic index profile, for the fundamental and second harmonic waves. In this case, the guide is first considered without quasi-phase matching. The effective indices of the fundamental and the second harmonic waves have been found from a modal solution to be 2.1769 and 2.3178 respectively. From the relation $L_c = \dfrac{\pi}{\Delta\beta}$, with $\Delta\beta = \beta_{2\omega} - \beta_\omega$, a coherence length $L_c \approx 1.5\mu m$ is obtained, where $\beta_{2\omega}$ and β_ω are the propagation constants of the harmonic and fundamental waves respectively.

Fig. 5.14. Non QPM second harmonic generation in channel waveguide.

This result agrees very closely with what was obtained by Delacourt *et al.* (1994). This is also confirmed in our numerical analysis using the BPM. It can be observed in Fig. 5.14 that the maximum harmonic power is attained after propagating $1.5\mu m$, which is equal to the coherence length, and which also agrees with the modal solution. Since the fundamental and the second harmonic waves are not phase matched, an efficient exchange of power between them is not possible and as expected, the power builds up to its maximum over the coherence length and then dissipates due to the phase mismatch.

Fig.5.15a shows the second harmonic field profile at maximum power *i.e.* after propagating a distance equal to one unit of coherence length. This figure clearly shows the field is well confined within the guiding section of the waveguide. It will be noticed that the integrity of the input field has not been compromised. A three dimensional representation of the field is shown in Fig. 5.15b.
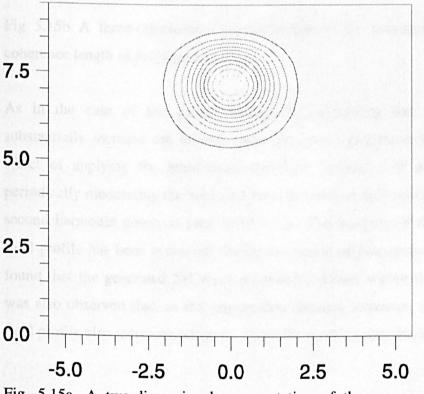

Fig. 5.15a. A two-dimensional representation of the propagating field after one coherence length of propagation.
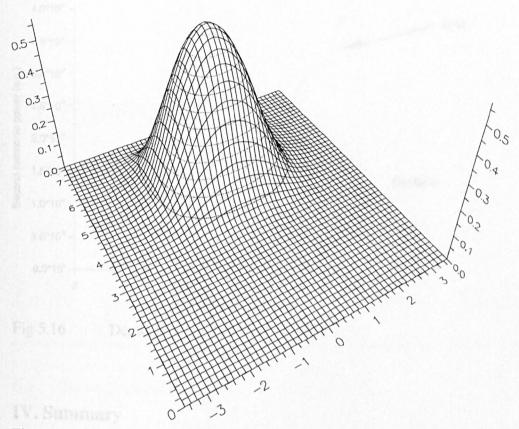
Fig 5.15b A three-dimensional representation of the propagating field after one coherence length of propagation.

As in the case of the planar waveguide, modulating the nonlinear term can substantially increase the second harmonic power generated. Fig. 5.16 shows the effect of applying the quasi-phase matching technique of domain reversal, *i.e.* periodically modulating the nonlinear term in alternate half-periods. As expected, the second harmonic power is seen to build up. The integrity of the second harmonic field profile has been preserved during the period of propagation. It was tested and found that the generated SH wave remained confined within the guiding region. It was also observed that, as the propagation distance increases, the magnitude of the field profile also increases however, its profile remain quite similar.

Fig 5.16   Demonstrating the effect of QPM

IV. Summary

In this section of the thesis, results for second harmonic generation by the Cerenkov and QPM approaches have been shown in optical waveguides with both 1-D and 2-D confinement. The evolution of the second harmonic for various cases and the generation of second harmonic power are also illustrated. In the simulation, the vector finite element method is used to find the modal solutions following which the FEM-based BPM program has been used to study the evolution of the second harmonic waves along the waveguide structure. The numerical approach developed here is accurate, computationally efficient and also very versatile. It allows both practical and realistic waveguide structures with anisotropic material properties, diffused in both the transverse directions and with 2-D confinement to be considered. This approach can be used to optimise device designs for any particular operation. It could also be extended to the study of the phenomenon of cascaded second harmonic generation.

Chapter Six

Finite Element Analysis of Second Harmonic Generation in AlGaAs Waveguides

6.1   Introduction

The rigorous and efficient FEM based beam propagation method is used to model SHG in semiconductor waveguides. The effect of material loss on the overall efficiency of SHG is also analysed. It is shown that under certain conditions, GaAlAs based devices with a lower non-linear susceptibility tensor could be more efficient than GaAs with a higher non-linear susceptibility tensor due to their low material loss. Numerical results are also presented, of the effect of domain fabrication error, in the case of quasi phase matched devices on the efficiency of SHG.

The prospect of building compact and robust solid state devices emitting short and coherent wavelengths which are important in data storage, laser printing and all-optical switching applications has been given considerable impetus by recent advances in semiconductor fabricating technology. It has been difficult to exploit fully the phenomenon of second harmonic generation (SHG) due to both technological problems as well as the need to find suitable materials that meet the required phase matching conditions (Fujimura *et al.*, 1993), particularly in isotropic crystals due to the normal dispersion of the material. Earlier work had therefore

focused on achieving phase matching using the natural birefringence of the material; however, for a given material, the wavelength range over which birefringent phase matching can be achieved practically is very narrow, thereby limiting the use of materials which could otherwise be attractive.

With recent progress in semiconductor fabrication technology, these formerly rejected materials are now being examined with renewed interest. Materials such as GaAs are reported to have a high non-linear coefficient, several orders higher than in most anisotropic materials, making them suitable candidates for all-optical switching applications as well as a source of blue light. In such materials, because of normal dispersion, the phase matching conditions cannot be satisfied since the refractive index is frequency dependent (Harvey, 1970). It is therefore necessary to correct the phase mismatch at regular intervals. One technique used to achieve this (as discussed in the previous chapter) is known quasi-phase matching (QPM), where the phase difference between the two interacting waves is corrected at regular intervals by means of a structural periodicity built into the nonlinear material at the stage of fabrication (Yoo et al., 1995). Quasi-phase matched second harmonic generation has been achieved in such materials as $LiNbO_3$, $LiTaO_3$ and KTP. Among the suggested methods for phase matching are domain inversion, domain disordering and wafer bonding. In domain inversion, the sign of the nonlinear tensor is reversed in alternate domains of the waveguide structure. In $LiNbO_3$ for example, the technique of ferroelectric domain inversion has been well studied and developed and is at the stage of commercial exploitation. However, when domain inversion is not possible then an alternative technique, domain disordering could be employed. Under this technique, the non-linear susceptibility tensor is periodically destroyed in alternate half periods of the waveguide structure (Jones-Bey, 1998). In general, the output power from this method is lower than that achieved in domain reversal. In wafer bonding of GaAs material, wafers grown by metalorganic chemical vapour deposition (MOCVD) are bonded such that the [110] directions of neighbouring wafers are parallel to each other (Yoo et al., 1995).

If shorter wavelengths can be obtained by means of second harmonic generation in semiconductor materials, then monolithically integrating the source wave and the generated second harmonic wave becomes a real possibility. In integrated optical semiconductor waveguides the high index difference between the substrate and the core leads to tightly confined modes, which enhances second harmonic generation by this method. However, GaAs is also known to have very high absorption loss, particularly at shorter wavelengths. The role of numerical simulation in the study, development and evaluation of such GaAs based systems, particularly in the effect of material loss, can be immensely important for design optimisation.

The powerful, accurate and versatile finite element method with the vector **H**-field (Rahman and Davies, 1985) has previously been used to find modal solutions for semiconductor optical waveguides, and later on for waveguides with diffused index profile and arbitrary guide parameters (Katsriku *et al.*, 1996). It has also proved useful in obtaining modal fields for the modelling of second harmonic generation in LiNbO$_3$ waveguides, which is an important material for SHG parameters (Katsriku *et al.*, 1997). However for the study of the evolution of the harmonic field, the finite element-based beam propagation method (BPM) parameters (Katsriku *et al.*, 1996, Hayata and Koshiba, 1991) is the most suitable, when compared to the modal solution approach which only provides a static solution.

GaAs is a reliable source of high power infrared wavelengths, having a high non-linear susceptibility tensor and providing good confinement of the waveguide modes, and thus, could provide a useful source of second harmonic power. However, it also suffers from high absorption loss, with the loss factor strongly dependent on wavelength. On the other hand, although AlGaAs has a smaller non-linear susceptibility value compared to GaAs, to compensate that, it has a much lower loss factor. Given the characteristics of these materials, it is important to evaluate numerically the opportunity and scope provided by devices built on such material systems. For such an analysis, a rigorous model is required. In this Chapter the use of the numerically efficient finite element-based BPM to model second harmonic

generation in a waveguide of practical interest is reported. In particular, using this modelling approach, the effect of loss on the overall efficiency of the generated second harmonic power is reported. It is also shown that a better efficiency is achieved by use of $Ga_xAl_{1-x}As$ as the core material, rather than GaAs.

6.2 Theoretical Background

Optical waveguiding in any material requires a controlled variation of the refractive index in the plane perpendicular to the direction of power flow. In semiconductor materials, just as in any other material, there must be a region of higher refractive index than its surroundings. In the group III-V compounds, the index can be varied by means of changing the electrical properties. Strain and/or electric fields could also be applied to alter the refractive index locally. Epitaxial growth techniques can be used to obtain alloy compositions of graded or step types, where the refractive index of such materials is a function of the alloy composition. A good lattice match between the epitaxial layer and the substrate is required in order to avoid the formation of dislocations and strains at the interface. $Al_{1-x}Ga_xAs$ is found to be lattice matched to GaAs over the entire range, from GaAs to AlAs. The optical properties of the $Al_{1-x}Ga_xAs$ alloy have been previously reported (Adachi, 1985, 1988, 1989; Jenkins, 1990). Following the approach of Jenkins, the refractive index of $Al_{1-x}Ga_xAs$ is obtained as a function of the aluminium concentration for different wavelengths by developing a computer code to find the contribution of each energy band structure to the refractive index. In the model, the real and imaginary parts of the dielectric function are approximated by several terms, which are explicit functions of energy. The index of refraction is then obtained as a function of energy and aluminium composition in $Al_{1-x}Ga_xAs$. Fig 6.1 shows the plot of refractive index against fractional aluminium for various wavelengths of interest.

It has previously been stated that when electromagnetic radiation propagates through a certain class of crystals, the non-linear dielectric properties of the material induce

in it a polarisation. It is well known that the mathematical representation of this induced polarisation in the crystal contains a higher order term, proportional to the quadratic of the non-linear susceptibility and to the square of the applied electric field. The non-linear response of the material may lead to an exchange of energy between the electromagnetic fields propagating at different frequencies. An important application of this is in SHG in which part of the energy of the input field at an angular frequency, ω, is transferred to a field at double that frequency, 2ω. In general due to lack of phase matching, the wave at 2ω will propagate at a velocity not equal to that of the fundamental wave. As a result, the amplitude of the second harmonic builds up to a maximum and then dissipates. The distance over which the amplitude of the second harmonic reaches its first maximum is the coherence length, l_c and is given by

$$l_c = \frac{2\pi}{\Delta\beta}$$ 6.1

where $\Delta\beta = 2\beta_\omega - \beta_{2\omega}$

β_ω and $\beta_{2\omega}$ are the normalised propagation constants at the fundamental and harmonic wavelengths respectively.

In the case of index matched second harmonic generation, the coherence length is infinite and the amplitude of the second harmonic wave builds up continuously. However, in most cases, the two fields are not index matched and the generated wave periodically builds up and dissipates unless special phase matching conditions are considered.
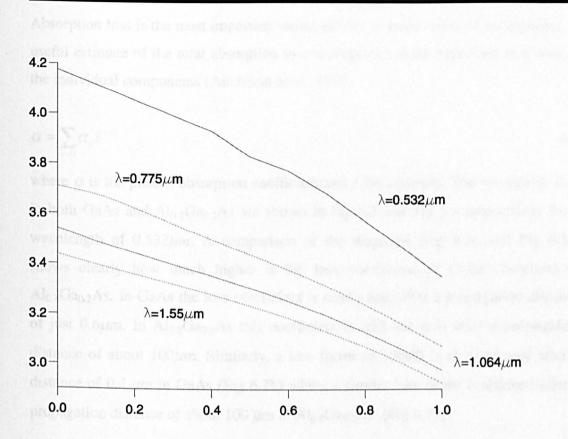
Fig 6.1 Dependence of refractive index on fractional aluminium concentration, $1-x$

In order to obtain phase matching, a number of techniques are employed. In isotropic media with normal dispersion, the quasi phase matching (QPM) technique is used. In this technique, the non-linear coefficient is modulated by the periodic reversal of the domain structure. A variation on this technique is domain disordering in which the non-linear susceptibility tensor is periodically destroyed in alternate half periods. These techniques are particularly useful in cubic crystals, which would otherwise not be viable candidates for second harmonic generation.

An important characteristic of an optical waveguide to be considered is the loss or attenuation. Loss in semiconductor waveguides can be attributed primarily to scattering, radiation and absorption. Radiation loss is a significant factor in bent waveguides whilst scattering losses are predominant in dielectric waveguides.

Absorption loss is the most important source of loss in semiconductor waveguides. A useful estimate of the total absorption in a waveguide can be expressed as a sum of the individual components (Aitchison *et al.*, 1997)

$$\alpha = \sum_{r=0} \alpha_r I^{r-1} \qquad\qquad 6.2$$

where α is the photon absorption coefficient and I the intensity. The waveguide loss in both GaAs and $Al_{0.8}Ga_{0.2}As$ are shown in Fig 6.2 and Fig 6.3 respectively for a wavelength of $0.532\mu m$. A comparison of the diagrams (Fig 6.2a and Fig 6.3a) shows clearly how much higher is the loss coefficient of GaAs compared to $Al_{0.8}Ga_{0.2}As$. In GaAs the loss coefficient is nearly zero after a propagation distance of just $0.6\mu m$. In $Al_{0.8}Ga_{0.2}As$ this coefficient is still not zero after a propagation distance of about $100\mu m$. Similarly, a loss factor of $-30dB$ is attained only after a distance of $0.4 \mu m$ in GaAs (Fig 6.2b) whilst a similar loss factor is attained after a propagation distance of about $100 \mu m$ in $Al_{0.8}Ga_{0.2}As$ (Fig 6.3b).
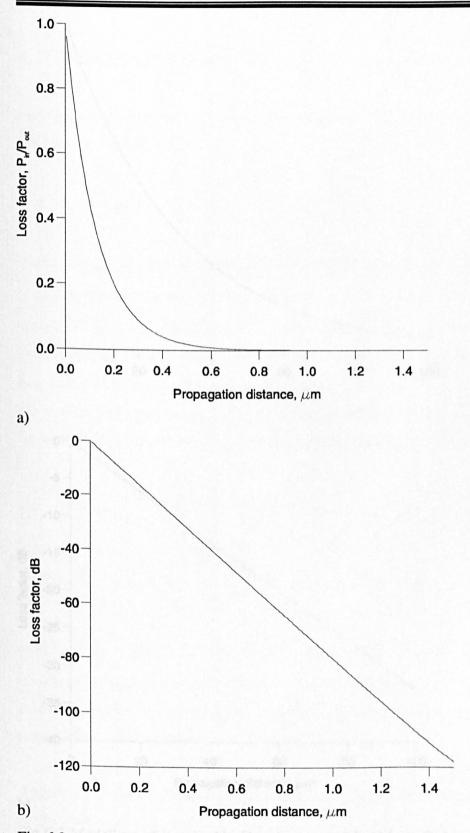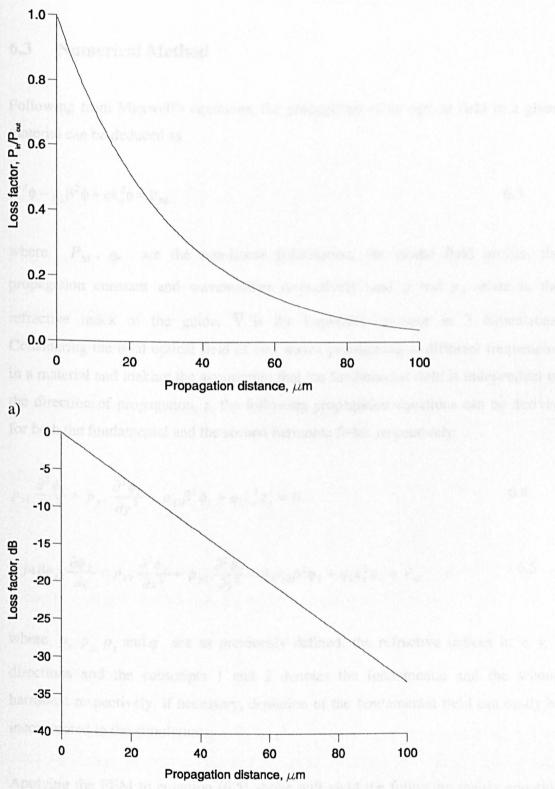
a)

b)

Fig 6.2 Modelling of loss in a GaAs waveguide a) Loss factor as a function of propagation distance b) Loss factor as a function of propagation distance.

a)

b)

Fig 6.3 Modelling of loss in $Al_{0.8}Ga_{0.2}As$ waveguide a) Loss factor as a function of propagation distance b) Loss factor as a function of propagation distance.

6.3   Numerical Method

Following from Maxwell's equations, the propagation of an optical field in a given material can be deduced as

$$\nabla^2 \phi - p_z \beta^2 \phi + q k_o^2 \phi = P_{NL}$$ 6.3

where P_{NL}, ϕ, are the non-linear polarisation, the modal field profile, the propagation constant and wavenumber respectively, and q and p_z relate to the refractive index of the guide. ∇ is the Laplacian operator in 3 dimensions. Considering the total optical field of two waves propagating at different frequencies in a material and making the assumption that the fundamental field is independent of the direction of propagation, z, the following propagation equations can be derived for both the fundamental and the second harmonic fields respectively:

$$p_{x1} \frac{\partial^2 \phi_1}{\partial x^2} + p_{y1} \frac{\partial^2 \phi_1}{\partial y^2} - p_{z1} \beta^2 \phi_1 + q_1 k_o^2 \phi_1 = 0$$ 6.4

$$-j4\beta p_{z2} \frac{\partial \phi_2}{\partial z} + p_{x2} \frac{\partial^2 \phi_2}{\partial x^2} + p_{y2} \frac{\partial^2 \phi_2}{\partial y^2} - 4 p_{z2} \beta^2 \phi_2 + q_2 k_o^2 \phi_2 = P_{NL}$$ 6.5

where p_x, p_y, p_z and q are as previously defined, the refractive indices in x, y, z directions and the subscripts 1 and 2 denotes the fundamental and the second harmonic respectively. If necessary, depletion of the fundamental field can easily be incorporated in the simulations.

Applying the FEM to equation (6.5) above will yield the following matrix equation for the propagation model:

$$-j4\beta[B_{2\omega}]\frac{d\{\phi\}}{dz} + \left([A_{2\omega}] - 4\beta^2[B_{2\omega}]\right)\{\phi\} = \{P_{NL}\} \qquad\qquad 6.6$$

where

$$[A_{2\omega}] = \sum_e \iint \left[q_{2\omega}k_o^2\{N\}\{N\}^T - p_{x2\omega}k_o^2\{N_x\}\{N_x\}^T - p_{y2\omega}k_o^2\{N_y\}\{N_y\}^T\right]dxdy$$

$$[B_{2\omega}] = \sum_e \iint \left[p_{z2\omega}k_o^2\{N\}\{N\}^T\right]dxdy$$

This equation may be solved using a split-step procedure: the propagation step in which the finite difference method is applied within a short interval and the non-linear step where the effect of the nonlinear term is considered. Such a procedure will yield a matrix equation of the form

$$\{\Phi_2\}_{i+1} = [L(\theta)]^{-1}[L(\theta-1)]\{\Phi_2\}_i + j\frac{\Delta z}{4\beta\, p_{z2}}\{P_{NL}\} \qquad\qquad 6.7$$

where

$$[L(\theta)] = -j4\beta[B_{2\omega}] + \theta\Delta z\left([A_{2\omega}] - 4\beta^2[B_{2\omega}]\right)$$

and θ is an artificial parameter which controls stability of solution. For the Crank-Nicholson scheme, $\theta = 0.5$ provides unconditionally a stable solution.

6.4   Results

The waveguide under consideration, shown in Fig.6.4, has an air cladding and, the substrate is made of AlAs with a core of $Ga_xAl_{1-x}As$. Here, W is the guide width, h is the height of the rib and t is the height of the slab waveguide underneath. The waveguide core and substrate refractive indexes for such a device with GaAs as the core at a wavelength of $\lambda = 1.064\mu m$ is given by $n_{g1} = 3.48$ and $n_{s1} = 2.93$,

respectively, and by $n_{g2} = 4.13$ and $n_{s2} = 3.23$, respectively at a wavelength of $\lambda = 0.532 \mu m$. At a fractional aluminium concentration of $x = 0.2$ and a fundamental wavelength of $1.064 \mu m$, the substrate and core indexes are $n_{s1} = 2.93$ and $n_{g1} = 3.05$, respectively and the respective index values at second harmonic wavelength of $0.532 \mu m$ are $n_{s2} = 3.23$ and $n_{g2} = 3.50$. These values of the refractive indices were calculated following Jenkins (1990) and compared with values given by Whitbread and Robson (1994). Fig. 6.4 also shows the H_y field profile for the fundamental quasi-TE field profile obtained from the modal analysis using the vector $\mathbf{H}$-field formulation for the $Ga_{0.2}Al_{0.8}As$ waveguide. The waveguide is assumed to have the following dimensions, $W = 1.0 \mu m$, $h = 1.0 \mu m$ and $t = 0.2 \mu m$. At the fundamental frequency, such a guide will support two quasi-TE modes.
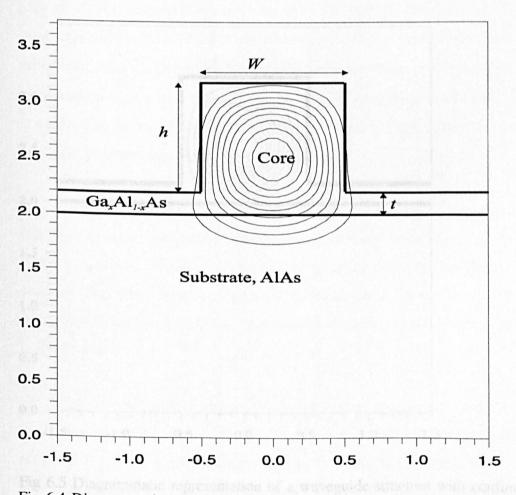

Fig 6.4 Diagrammatic representation of a waveguide structure with confinement of the fundamental wave.

The spot size of the fundamental mode has been calculated to be $0.326 \, \mu m^2$ with a confinement factor of 88.43%. It can be observed that, for the fundamental mode, the field spreads just slightly outside the waveguide region. The peak of the field, however, is confined within the guide core. The input power is assumed to be 20 W for the SHG simulation. Fig. 6.5 illustrates the confinement of the generated second harmonic field after one coherence length of propagation. At this shorter wavelength, the confinement factor has increased to 99.88% and the spot size reduced to $0.26 \, \mu m^2$. At the second harmonic wavelength, the guide is capable of supporting seven modes. This field plot was obtained using the finite element-based BPM and, as can be observed, the field is much better confined than the fundamental wave.
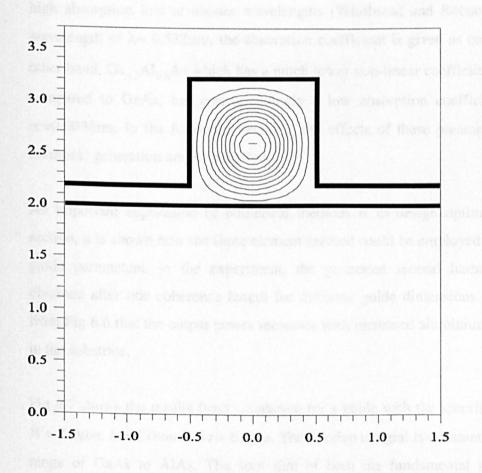

Fig 6.5 Diagrammatic representation of a waveguide structure with confinement of the second harmonic wave.
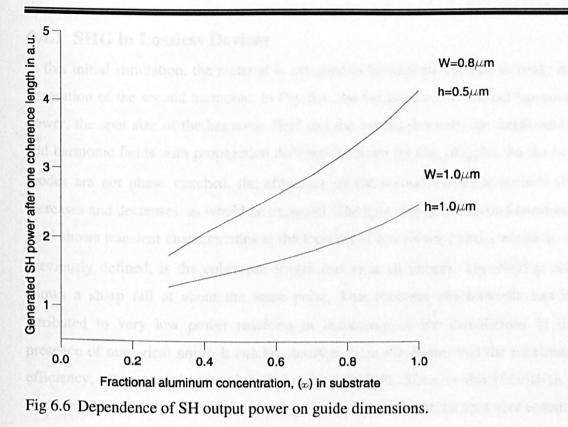
On the other hand, a guide with a GaAs core would support 5 modes at the fundamental wavelength, and the fundamental mode will have a confinement factor 99.55% and a spot size of $0.265\,\mu m^2$. At the harmonic wavelength, this guide could support nine modes where the fundamental has a confinement factor of 99.98% and a spot size $0.248\,\mu m^2$. The index change (Δn) between the substrate and the core at the harmonic wavelength is much greater and also the waveguide dimensions are now twice those of the wavelength, which results in a much better field confinement.

GaAs has a high non-linear coefficient (565pm/V), thereby making it a suitable candidate for second harmonic generation. However, it has one major drawback, its high absorption loss at shorter wavelengths (Whitbread and Robson, 1994). At a wavelength of λ= 0.532μm, the absorption coefficient is given as $\alpha = 8/\,\mu m$. On the other hand, $Ga_{0.2}Al_{0.8}As$ which has a much lower non-linear coefficient of 113pm/V, compared to GaAs, has correspondingly a low absorption coefficient, quoted at α =0.009/μm. In the following sections, the effects of these parameters on second harmonic generation are investigated.

An important application of numerical methods is in design optimisation. In this section, it is shown how the finite element method could be employed to optimise the guide parameters. In the experiment, the generated second harmonic power is obtained after one coherence length for different guide dimensions. It can be seen from Fig 6.6 that the output power increases with increased aluminium concentration in the substrate.

Fig 6.7 shows the results from simulation for a guide with the specified dimensions, $W = 1.0\mu m$, $h = 1.0\mu m$ and $t = 0.2\mu m$. The overlap integral is constant throughout the range of GaAs to AlAs. The spot size of both the fundamental and the second harmonic are seen to decrease slightly with increased aluminium concentration.
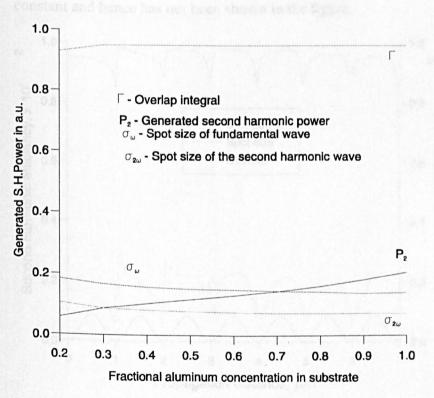
Fig 6.6 Dependence of SH output power on guide dimensions.

Fig 6.7. SH power, Overlap integral and spot size as a function of aluminium concentration.

6.4.1 SHG in Lossless Devices

In this initial simulation, the material is assumed to be lossless in order to study the generation of the second harmonic. In Fig. 6.8, the variation of the second harmonic power, the spot size of the harmonic field and the overlap between the fundamental and harmonic fields with propagation distance is shown for $Ga_{0.2}Al_{0.8}As$. As the two modes are not phase matched, the efficiency of the second harmonic periodically increases and decreases, as would be expected. The spot size of the second harmonic field shows transient characteristics at the location of low power $z=ml_C$, where l_C, as previously defined, is the coherence length and m is an integer. The overlap also shows a sharp fall at about the same point. This transient characteristic can be attributed to very low power resulting in inaccuracy in the calculations in the presence of numerical noise. It can be observed from this figure that the maximum efficiency, after one coherence length, is about 0.001%. Since in this simulation it has been assumed that the fundamental power is not depleted, its spot size remains constant and hence has not been shown in the figure.
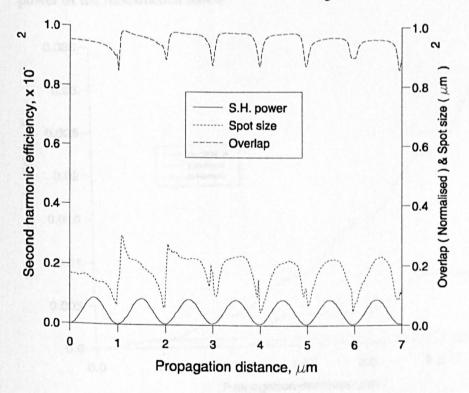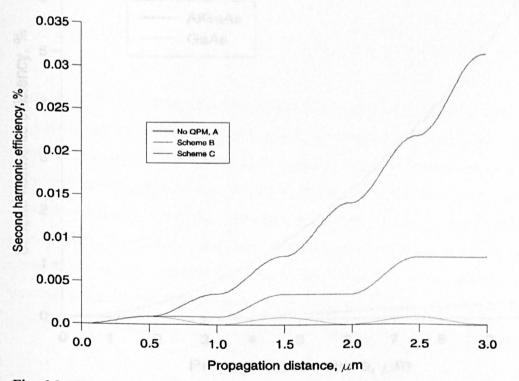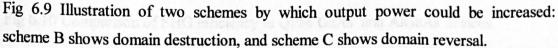

Fig 6.8 SHG in lossless AlGaAs , the variation of output power, spot size and overlap with propagation distance.
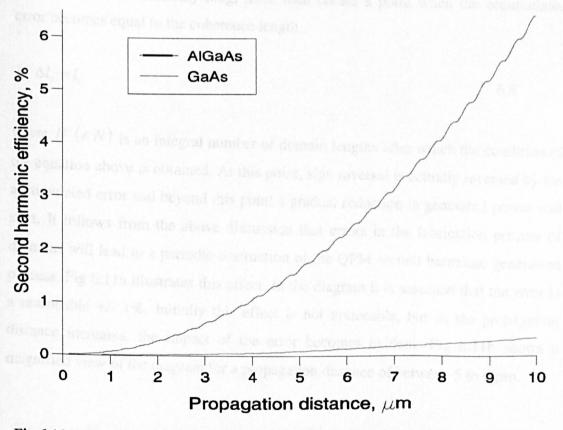
In Fig. 6.9 two schemes are illustrated by which greater second harmonic efficiency can be achieved in a semiconductor waveguide. The cyclic build up and dissipation of the second harmonic wave when phase matching is not employed is labelled as **A**. In the first scheme, labelled **B**, the non-linear coefficient is destroyed in alternate half periods of the waveguide. In this instance, since the non-linear susceptibility tensor d = 0, in the alternate half period no second harmonic wave is generated and hence no phase mismatch takes place, and as a result, the power already generated remains undepleted. In semiconductor waveguides, a periodic reversal of the non-linear coefficient has been demonstrated by use of wafer bonding (Yoo *et al.*, 1995), and the SHG signal produced by this scheme is labelled as **C** in this figure. In this case, a reversal of the sign of the non-linear susceptibility results in the correction of the phase mismatch therefore enabling the generated power to grow. It can be seen that the latter method achieves a much greater efficiency than the former and very high efficiency can be obtained, either by increasing the device length or by increasing the power of the fundamental mode.

Fig 6.9 Illustration of two schemes by which output power could be increased: scheme B shows domain destruction, and scheme C shows domain reversal.
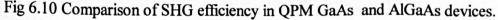
6.4.2 Perfectly Phase Matched Devices without Loss

As noted earlier, GaAs has a high non-linear coefficient. It will be illustrative therefore to compare the second harmonic generation in a lossless, perfectly phase matched, GaAs device with that of $Ga_xAl_{1-x}As$. As can be observed from Fig. 6.10, in the absence of absorption losses, the efficiency of GaAs is very high, thereby implying that it is the more suitable material for second harmonic generation than $Ga_xAl_{1-x}As$. After a propagation distance of $10\mu m$, the efficiency of a GaAs based device has grown to over 6% whilst that of a $Ga_xAl_{1-x}As$ based device is still less than 0.5%. Such growth in output power can be attributed entirely to the higher nonlinear susceptibility tensor of GaAs. However it will be shown later on that high absorption losses reduce the efficiency to such a level that $Ga_xAl_{1-x}As$ becomes more efficient.

Fig 6.10 Comparison of SHG efficiency in QPM GaAs and AlGaAs devices.

6.4.3 Effect of Inaccuracy in Phase Matching due to Fabrication

In this section, results are presented on the effect of fabrication errors, which can build up during quasi phase matching. As is well known, during quasi phase matching, the sign of the non-linear susceptibility tensor is reversed in alternate domains. Perfectly periodic alternating domain structures are difficult, if not impossible, to fabricate. In a perfect QPM structure, the sign reversal occurs after a length defined by l_C, the coherence length. Assuming an error $\Delta l_c = l_c - l'_c$ during fabrication, where l'_c is the actual designed value and l_c is the desired value and assuming also that the device is of N domains, then over the entire device length the accumulated error is given by $N\Delta l_c$.

If the device is sufficiently long, there then comes a point when the accumulated error becomes equal to the coherence length

$$N'\Delta l_c = l_c \qquad\qquad\qquad\qquad\qquad 6.8$$

where $N'(\neq N)$ is an integral number of domain lengths after which the condition of the equation above is obtained. At this point, sign reversal is actually reversed by the accumulated error and beyond this point a gradual reduction in generated power will start. It follows from the above discussion that errors in the fabrication process of domains will lead to a periodic destruction of the QPM second harmonic generation process. Fig 6.11a illustrates this effect. In the diagram it is assumed that the error is a reasonable +/- 1%. Initially this effect is not noticeable, but as the propagation distance increases, the impact of the error becomes evident. Fig 6.11b shows a magnified view of the diagram for a propagation distance of between 5 to 6 μm.
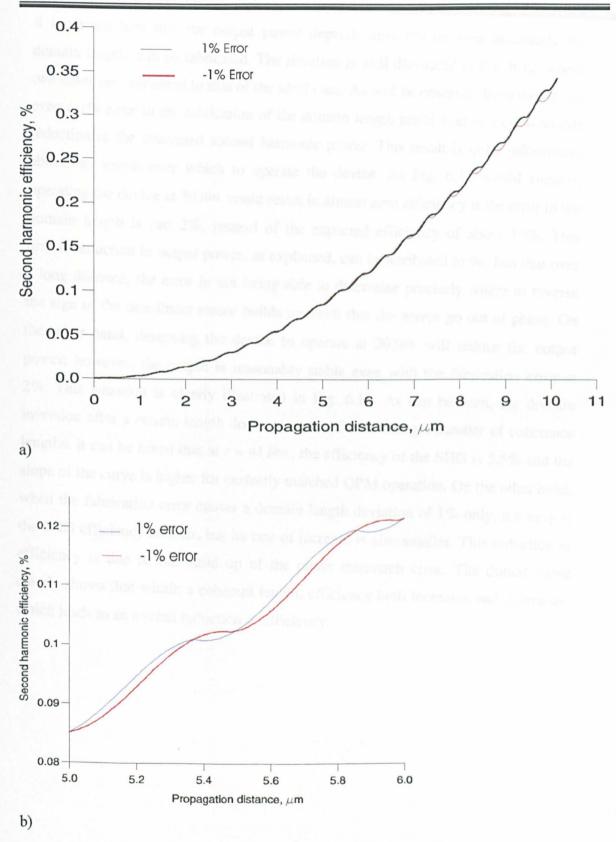
a)

b)

Fig 6.11. Showing the effect of fabrication error on QPM.

It is shown here that the output power depends critically on how accurately the domain lengths can be fabricated. The situation is well illustrated in Fig. 6.12, where two cases are compared to that of the ideal case. As will be observed from the figure, even a 1% error in the fabrication of the domain length could lead to a considerable reduction in the generated second harmonic power. This result is quite informative about the length over which to operate the device. As Fig. 6.12 would suggest, operating the device at $50\,\mu m$ could result in almost zero efficiency if the error in the domain length is just 2%, instead of the expected efficiency of about 10%. This drastic reduction in output power, as explained, can be attributed to the fact that over a long distance, the error in not being able to determine precisely where to reverse the sign of the non-linear tensor builds up, such that the waves go out of phase. On the other hand, designing the device to operate at $20\,\mu m$ will reduce the output power; however, the output is reasonably stable even with the fabrication error at 2%. This situation is clearly illustrated in Fig. 6.13. As can be seen, the domain inversion after a certain length does not occur after an integer number of coherence lengths. It can be noted that at $z = 41\,\mu m$, the efficiency of the SHG is 5.5% and the slope of the curve is higher for perfectly matched QPM operation. On the other hand, when the fabrication error causes a domain length deviation of 1% only, not only is the SHG efficiency smaller, but its rate of increase is also smaller. This reduction in efficiency is due to the build up of the phase mismatch error. The dotted curve clearly shows that within a coherent length, efficiency both increases and decreases, which leads to an overall reduction in efficiency.
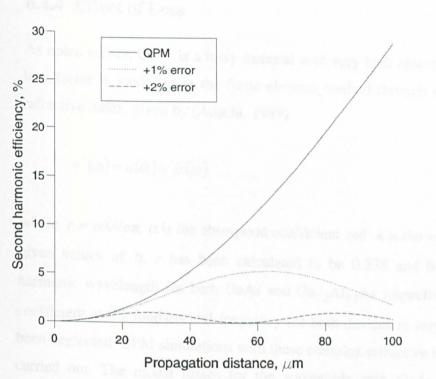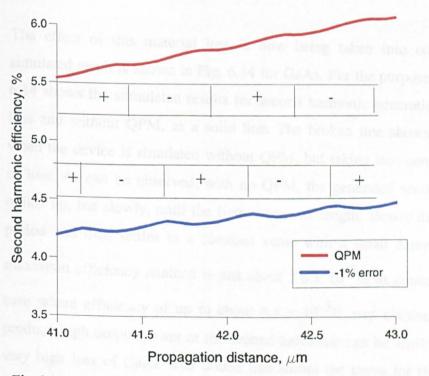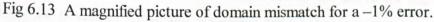
6.4.4 Effect of Loss

As noted earlier, GaAs is a lossy material with very high absorption coefficient. This ... factor is included in the finite element method through the use of a complex refractive index, given by (Adachi, 1989,

$$n^*(\omega) = n(\omega) + i\kappa(\omega)$$

... $\kappa = \alpha\lambda/4\pi$, α is the absorption coefficient and λ is the wavelength. Using the ... values of α, κ has been calculated to be 0.338 and 0.0017 at the second harmonic wavelength ... both GaAs and Ga ... Al ... respectively. The absorption coefficient ... fundamental frequency ... wavelength ... is very low and hence has been neglected. QPM simulations with these complex refractive index data have been carried out. The modal losses for the waveguide with GaAs as core layer coefficient at the second harmonic frequency of λ=0.532 μm is ~90487 /μm, and for a $Ga_{0.x}$ GaAs core, the loss has been calculated to be only ~0.3486 /μm.

The effect of this material loss ... now being taken into consideration and the simulated results are shown in Fig. 6.14 for GaAs. For the purpose of comparison, Fig ... shows the simulated results for second harmonic generation in GaAs, without ... and without QPM, as a solid line. The broken line shows the curve obtained ... the device is simulated without QPM, but taking into consideration the effect ... losses ... can be observed with no QPM, the generated second harmonic power ... up but slowly, until the first coherence length, slowly dissipates at the next period and then settles to a constant value with a small damped oscillation. The maximum efficiency attained is just about 0.5 ... % as compared to the loss-less case where efficiency of up to about ... can be ... obtained. The inability to produce high output power at the second harmonic can be attributed entirely to the very high loss of GaAs. The broken line shows the curve for the device incorporating ... and taking into consideration ... losses. With the effect of loss. An

Fig 6.12 Effect of fabrication error on second harmonic output power, a comparison of idealised QPM with assumed error.

Fig 6.13 A magnified picture of domain mismatch for a −1% error.

6.4.4 Effect of Loss

As noted earlier, GaAs is a lossy material with very high absorption coefficient. This loss factor is modelled in the finite element method through the use of a complex refractive index, given by (Adachi, 1989)

$$n^*(\omega) = n(\omega) + jr(\omega) \qquad\qquad 6.9$$

where $r = \alpha\lambda/4p\pi$, α is the absorption coefficient and λ is the wavelength. Using the given values of α, r has been calculated to be 0.338 and 0.0017 at the second harmonic wavelength for both GaAs and $Ga_{0.2}Al_{0.8}As$ respectively. The absorption coefficient at the fundamental frequency for both devices is very low and hence has been neglected. BPM simulations with these complex refractive index data have been carried out. The modal losses for the waveguide with GaAs as core have been calculated at the second harmonic frequency of λ=0.532μm, as –90dB/ μm, and for a $Ga_{0.2}Al_{0.8}As$ core, the loss has been calculated to be only –0.3dB/ μm.

The effect of this material loss is now being taken into consideration and the simulated result is shown in Fig. 6.14 for GaAs. For the purpose of comparison, Fig. 6.14 shows the stimulated results for second harmonic generation in GaAs, without loss and without QPM, as a solid line. The broken line shows the curve obtained when the device is simulated without QPM, but taking into consideration the effect of loss. As can be observed, with no QPM, the generated second harmonic power builds up, but slowly, until the first coherence length, slowly dissipates in the next period and then settles to a constant value with a small damped oscillation. The maximum efficiency attained is just about 2.8 x 10^{-3}% as compared to the lossless case where efficiency of up to about 8.4 x 10^{-3}% was obtained. The inability to produce high output power at the second harmonic can be attributed entirely to the very high loss of GaAs. The dotted line shows the curve for the power generated when the device is QPM and simulated taking inot account the effect of loss. An

attempt at introducing QPM does not lead to any appreciable increase in the efficiency of the generated second harmonic power. As can be seen from Fig. 6.14, the efficiency curve of the generated second harmonic power assumes a periodic nature after the first coherence length.
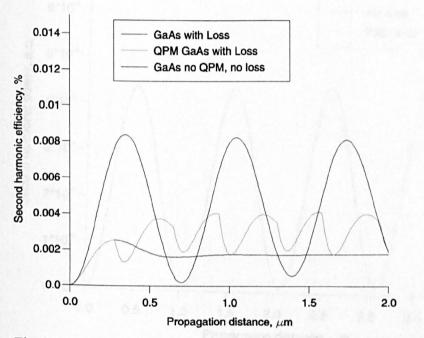

Fig 6.14 The effect of loss on SHG in GaAs with and without QPM.

The maximum efficiency obtained is 4×10^{-3}%. As is seen in the figure, without QPM the power generated is attenuated very rapidly. With the introduction of QPM however, some form of periodicity is maintained. This periodicity can be directly attributed to the absorption loss, which effectively nullifies the effect of QPM.

Fig. 6.15 and Fig 6.16 compares SHG in $Ga_{0.2}Al_{0.8}As$ for both lossy and lossless cases. In this case the maximum power generated after one l_c is about 4.5×10^{-4}% (without loss), which is about 20 times smaller than a comparative case in lossless GaAs (8.4×10^{-3}%). However it can be observed that the introduction of loss factor does not lead to any appreciable attenuation of the generated power. As can also be seen, the loss is small and the difference between this and case of no loss is hardly noticeable over very short distances. The reduction in generated power becomes

evident only after about $1.5\mu m$, the maximum power attained as will be expected is lower than in the case of GaAs.

Fig 6.15 The effect of loss on second harmonic power in AlGaAs without QPM

In Fig. 6.16 quasi phase matched second harmonic generation in a lossy device is compared with that of the lossless case. The results show that over very short distances, hardly any differences are observed.
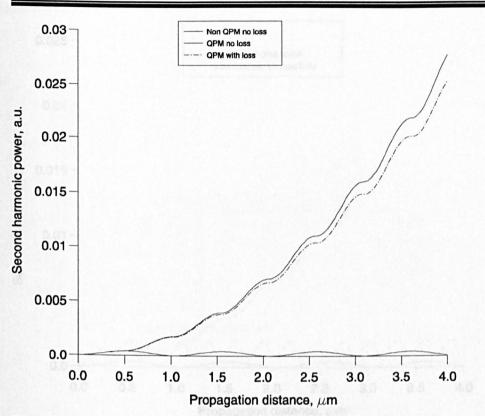
Fig 6.16 A comparison of second harmonic output power in a lossless QPM AlGaAs device with second harmonic power in a lossy QPM AlGaAs device.

In Fig. 6.17, SHG in a lossy $Ga_{0.2}Al_{0.8}As$ with QPM is compared with SHG in a lossy GaAs, and also with QPM. It can be seen that initially, within the first half of the coherence length, the power generated by the GaAs device builds up more rapidly than that of $Ga_{0.2}Al_{0.8}As$. However as the propagation distance increases, the effect of high absorption losses in GaAs become evident and the power generated by $Ga_{0.2}Al_{0.8}As$ device becomes greater. In a perfectly quasi phase matched device, the efficiency will continue to increase with distance. It can be seen, therefore, that although GaAs has a higher non-linear coefficient, its high loss makes it less efficient than $Ga_{0.2}Al_{0.8}As$.

Fig 6.17   A comparison of QPM second harmonic output power in lossy GaAs and AlGaAs devices.

The loss factor assumed for GaAs in the present simulation shows that not much second harmonic power is generated. If, however, the loss factor can be reduced by some novel growth technique, then the device could become more efficient. Fig. 6.18a shows the efficiency of second harmonic generation in GaAs for various assumed values of the absorption coefficient, without QPM. It will be observed that the lower the loss, the more efficient the device. The effect of loss is still noticeable in the damped oscillation. With lower loss factor, the oscillation lasts longer and the average output is also slightly higher. With a high loss factor, the oscillation is strongly damped.

a)

b)

Fig 6.18 Numerical simulation of various assumed loss values in a) non-QPM GaAs device and b) QPM GaAs device.

Fig 6.18b shows SHG in GaAs with QPM for the different values of the absorption coefficient considered in Fig 6.9a. It is possible, therefore, to increase the efficiency

of the device by reducing the loss factor. As would be observed, reducing the loss by a factor of 2 leads to a corresponding increase in efficiency over the coherence length. Over very short distances, this could still be more efficient than for $Ga_{0.2}Al_{0.8}As$, but it settles down to much lower values than can be achieved in GaAlAs over longer distances.

It is well known that increasing the input power could increase the efficiency of the output second harmonic power. Fig. 6.19 shows the variation of efficiency with input power for a perfectly quasi phase matched $Ga_{0.2}Al_{0.8}As$ device, at a distance of $10\mu m$. The figure also shows results when the device is assumed to have 1% and 2% error in fabrication. Fig. 6.20 compares the generated power for different input values of power over a fixed device length. When the input power is increased by a factor of 10, the efficiency also increases by the same factor and hence the overall power output is increased by 100 times.

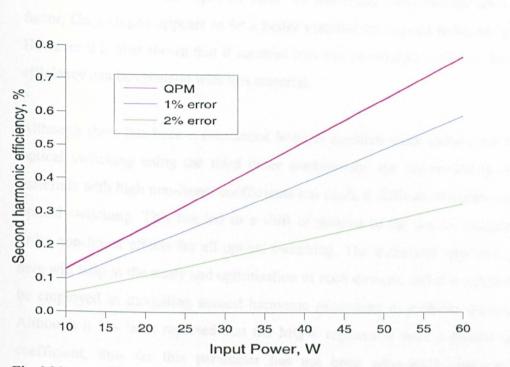Fig 6.19   The effect of increased input power on efficiency of generated power.

Fig 6.20   The variation of efficiency with input power for different fabrication errors calculated at a distance of $10 \mu m$

6.5   Summary

An accurate and efficient numerical method has been described for the study of second harmonic generation in semiconductor waveguides. The monolithic integration of the fundamental source with the second harmonic is possible in semiconductor waveguides. It is shown that fabrication tolerances leading to errors in the domain length could result in a substantial reduction in the generated power. GaAs has a high nonlinear susceptibility compared to AlGaAs: it has, however, a much higher loss factor. In an accurate model therefore, it is important to incorporate this loss factor.

In this chapter, numerically simulated results have been presented for second harmonic generation, after taking into consideration this loss factor. These results

demonstrate that for the reported values of non-linear susceptibility tensor and loss factor, $Ga_{0.2}Al_{0.8}As$ appears to be a better material for second harmonic generation. However it is also shown that if material loss can be reduced in GaAs, then a greater efficiency can be obtained with this material.

Although there has been a substantial level of research work carried out to achieve optical switching using the third order nonlinearity, the unavailability of suitable materials with high non-linear coefficients has made it difficult to achieve low power optical switching. This has led to a shift of interest to the use of cascaded second order non-linear effects for all optical switching. The numerical approach presented here will help in the study and optimisation of such devices, and this method can also be employed in modelling second harmonic generation in multiple quantum wells. Although it has been reported that the MQW region can have a greater non-linear coefficient, thus far this parameter has not been adequately characterised. As fabrication technology improves and material data become available, the device parameters can be optimised and the model is seen to be capable of incorporating important features such as material anisotropy, loss factor and diffused index profiles.

Chapter Seven

Cascaded Second Harmonic Generation

7.1   Introduction

Integrated all-optical switching devices will form a fundamental component in future communication systems. Many important applications of the second order nonlinear process are well known and documented. Research activity in this field has focused primarily on the generation of new frequencies as well as finding materials with high nonlinear term (Aitchison 1997, 1998). Advances in second harmonic generation, particularly the enhancement of the magnitude of the second order nonlinearity has led to a renewed interest in the cascaded process, having great potential for use in all optical switches, all optical transistors, wavelength division multiplexing, directional couplers and intensity-dependent phase modulation (Torruellas 1994, Kelaidis 1994, Aitchison, 1995, 1997, 1998). In second harmonic generation, for example, the focus has been on the production of a second harmonic wavelength and the maximisation of the efficiency of the process. In this, the wave of interest has been the generated second harmonic beam and the focus has been on how to achieve phase matching in order to maximise the transfer of power from the fundamental to the harmonic

(Stegeman, 1996). Various schemes have therefore been designed to ensure that the beams are phase matched, the necessary condition for the maximum transfer of power between the fundamental and the second harmonic. In this, often it is assumed that the fundamental beam is not affected by the harmonic. At very low intensities such an assumption may be valid. The source beam is, however, provided by a highly focused laser beam with high intensity. Under such a condition, the said assumption will not be valid and hence the need is to study the effect of the generated second harmonic on the fundamental. This is known as the cascaded effect and has found application in all-optical switching. The theoretical predictions for the cascaded process have been known since the early days of second harmonic generation. It has been known that, far from phase matching and in the presence of an intense source, the generated second harmonic can interfere with the fundamental, resulting in the mimicking of the third order processes. This cascaded process can now produce effects several orders of magnitude larger than the traditional third order process (Torruellas 1994). The need to model such devices accurately and efficiently is thus urgent, and will serve in cutting down developmental costs, thus enhancing productivity. The difficulty in modelling such devices accurately has meant that approximations such as reduced geometry or an undepleted pump beam are often employed. The undepleted pump approximation assumes that the depletion of energy from the pump beam is minimal and can therefore be neglected. In second harmonic generation, high input intensities are required. From the theory of nonlinear optics (Bloembergen, 1965), it is known that such an assumption is only valid at low input intensities. In other words the assumption fails for cases of particular interest.

7.2   Numerical Formulation

Using Maxwell's equations for the propagation of an optical field in a given medium, then

$$\nabla^2 \Phi - p_z \beta^2 \Phi + q k_o^2 \Phi = P_{NL} \qquad\qquad 7.1$$

where P_{NL} is the nonlinear polarization, ϕ is the modal field profile, β is the propagation constant and k_o is the wavenumber. The indices of refraction of the guide are defined through q and p_z. If the total field of two waves propagating at different frequencies is now considered, then the following coupled propagation equations can be derived for both the fundamental and second harmonic fields respectively:

$$p_{x1}\frac{\partial^2\Phi_1}{\partial x^2} + p_{y1}\frac{\partial^2\Phi_1}{\partial y^2} - p_{z1}\beta^2\Phi_1 + q_1 k_o^2\Phi_1 = P_{NL}^1 \qquad 7.2$$

$$-j4\beta p_{z2}\frac{\partial\Phi_2}{\partial z} + p_{x2}\frac{\partial^2\Phi_2}{\partial x^2} + p_{y2}\frac{\partial^2\Phi_2}{\partial y^2} - 4p_{z2}\beta^2\Phi_2 + q_2 k_o^2\Phi_2 = P_{NL}^2 \qquad 7.3$$

The subscripts 1 and 2 denote the fundamental and second harmonic respectively. For the TE modes, $\Phi = E_x$, $p_x = n_x/n_y$, $p_y = p_z = 1, q = n_x^2$ and for TM modes $\Phi = E_y$, $p_x = 1/n_y^2$, $p_y = 1/n_z^2, p_z = 1/n_y^2, q = 1$. For $c//y$, $n_x = n_z = n_o$, the ordinary refractive index and $n_y = n_e$, the extraordinary refractive index, for a planar waveguide $\frac{\partial}{\partial x} = 0$.

The nonlinear polarization is defined for both the fundamental and harmonic fields as $P_{NL}^1 = 2dE_1E_2$ and $P_{NL}^2 = 2dE_1E_1$ respectively.

Application of the finite element method to the equations above will yield the following matrix equation for the propagation models of both the fundamental and harmonic fields:

$$-j2\beta_\omega[B_\omega]\frac{\partial\{\phi_\omega\}}{\partial z} + ([A_\omega] - \beta_\omega^2[B_\omega])\{\phi_\omega\} = \{\psi_{NL}^1\} \qquad 7.4$$

$$-j4\beta_{2\omega}[B_{2\omega}]\frac{\partial\{\phi_{2\omega}\}}{\partial z} + ([A_{2\omega}] - 4\beta_{2\omega}^2[B_{2\omega}])\{\phi_{2\omega}\} = \{\psi_{NL}^2\} \qquad 7.5$$

where

$$[A_\omega] = \sum_e \iint \left[k_o^2 q_\omega \{N\}\{N\}^T - p_{x\omega}k_o^2\{N_x\}\{N_x\}^T - p_{y\omega}k_o^2\{N_y\}\{N_y\}^T \right] dxdy$$

$$[B_\omega] = \sum_e \iint \left[k_o^2 p_{z\omega}\{N\}\{N\}^T \right] dxdy$$

$$[A_{2\omega}] = \sum_e \iint \left[k_o^2 q_{2\omega}\{N\}\{N\}^T - p_{x2\omega}k_o^2\{N_x\}\{N_x\}^T - p_{y2\omega}k_o^2\{N_y\}\{N_y\}^T \right] dxdy$$

and

$$[B_{2\omega}] = \sum_e \iint \left[k_o^2 p_{z2\omega}\{N\}\{N\}^T \right] dxdy$$

These equations (7.4 and 7.5) may be solved using a split-step procedure; the propagation step in which the finite difference method is applied within a short interval and the non-linear step where the effect of the non-linear term is considered. Such a procedure will yield a matrix equation of the form (Hayata *et al.* 1991)

$$\{\phi_\omega\}_{i+1} = [L_\omega(\theta)]_i^{-1}[L_\omega(1-\theta)]_i\{\phi_\omega\}_i + j\frac{\Delta z}{2\beta p_{z\omega}}\{\psi_{NL}^\omega\} \qquad 7.6$$

$$\{\phi_{2\omega}\}_{i+1} = [L_{2\omega}(\theta)]^{-1}[L_{2\omega}(\theta-1)]\{\phi_{2\omega}\}_i + j\frac{\Delta z}{4\beta p_{z2\omega}}\{\psi_{NL}^{2\omega}\} \qquad 7.7$$

where

$$L_\omega(\theta) = -j2\beta_\omega[B_\omega]_i + \Delta z\theta([A_\omega]_i - \beta_\omega^2[B_\omega]_i)$$

$$L_\omega(1-\theta) = -j2\beta_\omega[B_\omega]_i + \Delta z(1-\theta)([A_\omega]_i - \beta_\omega^2[B_\omega]_i)$$

$$L_{2\omega}(\theta) = -j4\beta_{2\omega}[B_{2\omega}]_i + \Delta z\theta([A_{2\omega}]_i - \beta_{2\omega}^2[B_{2\omega}]_i)$$

and
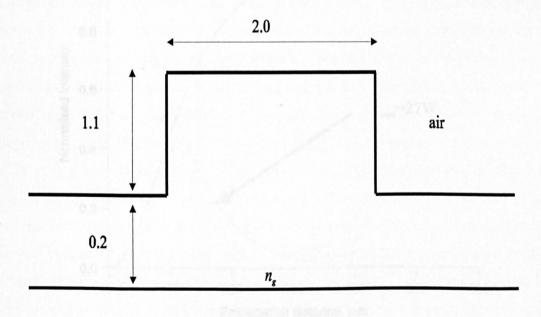
$$L_{2\omega}(1-\theta) = -j4\beta_{2\omega}[B_{2\omega}]_i + \Delta z(1-\theta)([A_{2\omega}]_i - \beta_{2\omega}^2[B_{2\omega}]_i)$$

7.3   Results of Numerical Simulations

7.3.1 Idealised waveguide

In the first instance, to test the accuracy of our method, the results obtained here will be compared to those obtained by Masoudi and Arnold (Masoudi and Arnold, 1995a). The waveguide to be considered is illustrated in Fig 7.1. The dimensions of the guide are as shown. The fundamental wavelength is given as $\lambda_\omega = 1.55 \mu m$ and the second harmonic wavelength is $\lambda_{2\omega} = 0.775 \mu m$. The refractive index parameters of the guide are chosen such that it is nearly perfectly phase matched. The index of refraction for the fundamental wavelength is $n_{g1} = 3.44$. Using the finite element method, the index of refraction at the second harmonic wavelength for which the two waves are nearly perfectly phase matched is obtained as $n_{g2} = 3.401473$.

Fig 7.1 Diagrammatic representation of rib waveguide used in the simulations, guide dimensions in μm.

The refractive index of the substrate for both wavelengths is given as $n_{sub} = 3.34$. The nonlinear tensor value is assumed to be 300 pm/V. Using the modal analysis method, the effective indices of both the fundamental and harmonic wavelength were found to be identical, $n_1^{eff} = n_2^{eff} = 3.385330$ as expected. In Fig. 7.2 the transfer of power from the fundamental to the generated second harmonic along the axial direction is shown. The power is normalised for both the fundamental and second harmonic fields. The results obtained here show excellent agreement with those obtained by Masoudi and Arnold (Masoudi and Arnold, 1995a). From the diagram, it can be seen that in an idealised devise with an input power of 27 W, the maximum power transfer from the fundamental to the second harmonic is achieved after a propagation distance of $400\mu m$.
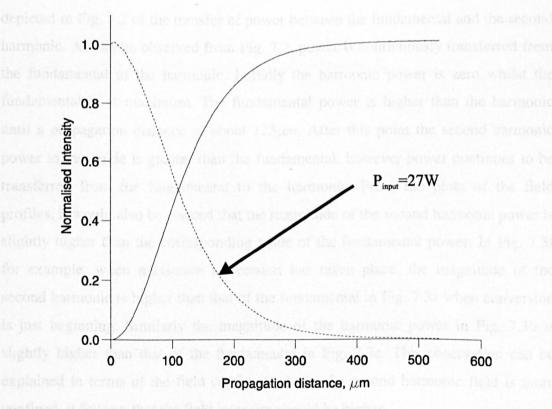

Fig. 7.2.   Showing the transfer of power from the fundamental to the generated second harmonic in an idealised phase matched waveguide.

Assuming no waveguide losses, Fig. 7.3 shows the field profiles of both the fundamental and second harmonic at different propagation distances. As the diagrams show the integrity of the field profile for both waves is maintained during the course of propagation. It can be clearly seen that as the second harmonic gains in intensity, the intensity of the fundamental decreases. It can be seen that the normalised fundamental power is initially high but then decreases with propagation distance. At a distance of 12μm the fundamental power has a value of about 105 a.u. (Fig. 7.3a). This value then decreases to 65 a.u. in Fig. 7.3c and decreases to a minimum value of 15 at a distance of 400μm or thereabouts. At the same time, the normalised second harmonic power increases from a minimum value (20 a.u. in Fig. 7.3b) at 12μm through (90 a.u. in Fig. 7.3d) to a maximum value (120 a.u. in Fig. 7.3f) at a propagation distance of 400μm. These results are in line with the situation depicted in Fig. 7.2 of the transfer of power between the fundamental and the second harmonic. As can be observed from Fig. 7.2, power is continuously transferred from the fundamental to the harmonic. Initially the harmonic power is zero whilst the fundamental is at maximum. The fundamental power is higher than the harmonic until a propagation distance of about $125\mu m$. After this point the second harmonic power in the guide is greater than the fundamental, however power continues to be transferred from the fundamental to the harmonic. From the plots of the field profiles, it would also be noticed that the magnitude of the second harmonic power is slightly higher than the corresponding value of the fundamental power. In Fig. 7.3f for example, when maximum conversion has taken place, the magnitude of the second harmonic is higher than that of the fundamental in Fig. 7.3a when conversion is just beginning. Similarly the magnitude of the harmonic power in Fig. 7.3b is slightly higher than that of the fundamental in Fig. 7.3e. This observation can be explained in terms of the field confinement. As the second harmonic field is more confined, it follows that the field intensity should be higher.
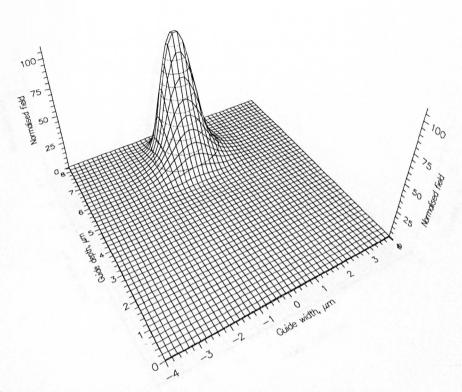
Fig. 7.3a. Fundamental field at a propagation distance of 12μm.
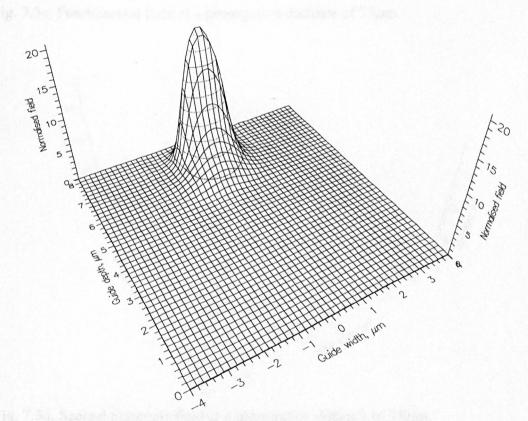

Fig. 7.3b. Second harmonic field at a propagation distance of 12μm.

Fig. 7.3c. Fundamental field at a propagation distance of 75μm.

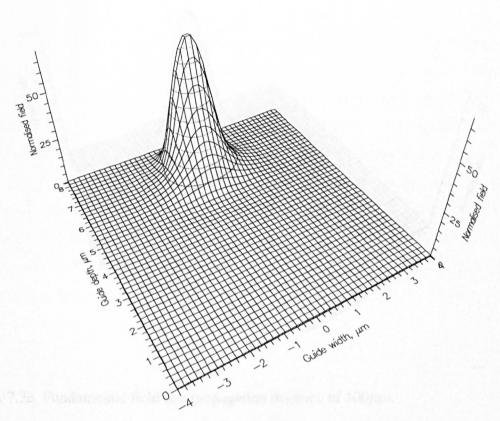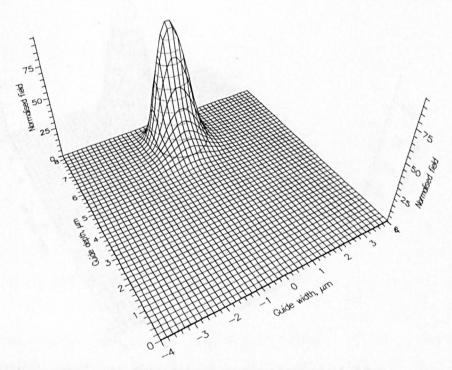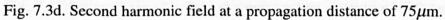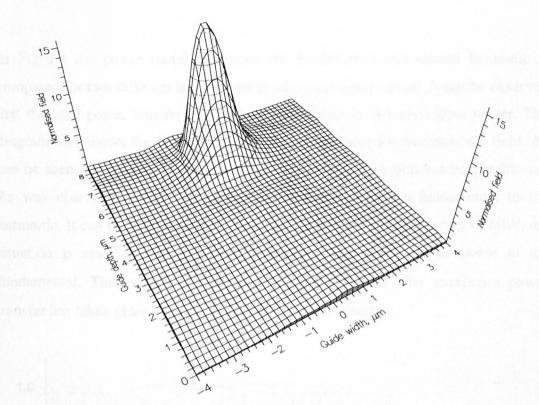Fig. 7.3d. Second harmonic field at a propagation distance of 75μm.

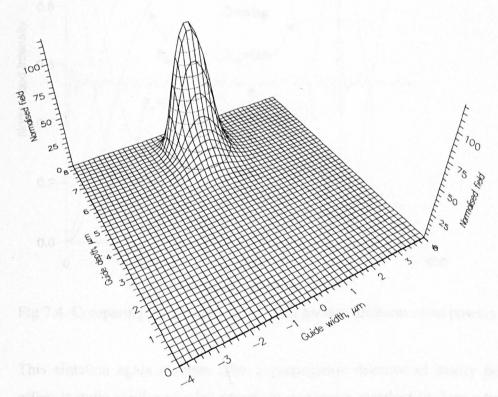Fig. 7.3e. Fundamental field at a propagation distance of 400μm.

Fig. 7.3f. Second harmonic field at a propagation distance of 400μm

In Fig 7.4 the power transfer between the fundamental and second harmonic is compared for two different input power levels of the fundamental. It can be observed that the total power transfer is achieved much faster for a higher input power. The diagram also shows the overlap integral and the spot size for the harmonic field. As can be seen, the overlap is minimal when maximum conversion has been achieved. As was observed in Fig. 7.2 power is transferred from the fundamental to the harmonic. It can be seen, however, from Fig. 7.4 that for an input power of 60W, the situation is reversed and power is now transferred from the harmonic to the fundamental. This occurs at a distance of about 295μm after maximum power transfer has taken place from the fundamental to the harmonic.
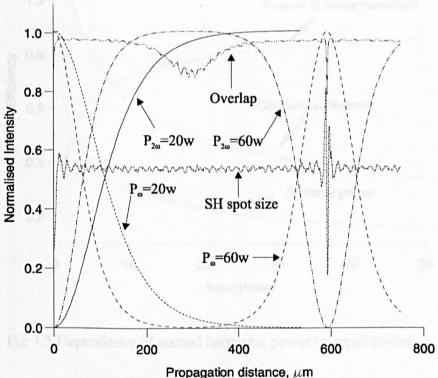
Fig 7.4. Comparing the efficiency of output for two different input powers.

This situation again reverses after a propagation distance of nearly 600μm. This effect is quite similar to what occurs in non-phase matched devices when power is continuously transferred between the fundamental and the harmonic. This result is

what would be expected as the waves are coupled and shows agreement with what has been previously reported (Masoudi and Arnold, 1995b).

Fig 7.5 shows the dependence of the conversion efficiency on a number of factors. From the diagram it can be deduced that the higher the input power, the more efficient the conversion rate. The conversion rate was calculated after a fixed propagation distance. The residual power is also minimal. The diagram also shows that at higher powers, a maximum conversion is obtained after a short propagation distance.
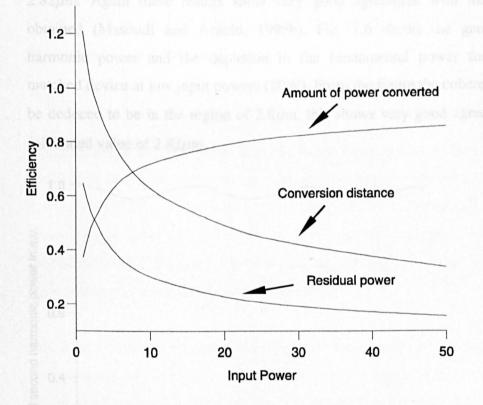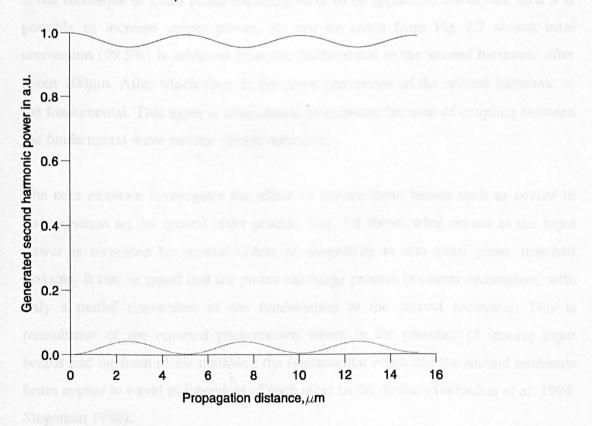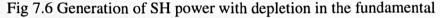

Fig 7.5 Dependence of second harmonic power on input power.

7.3.2 Second Harmonic generation in Practical waveguide

In the previous section, cascaded second harmonic generation in an idealised waveguide had been considered. In this, the guide parameters were carefully chosen such that the two waves were phased matched. In this section, results are presented

for cascaded second harmonic generation in a waveguide of practical importance. The guide parameters are as given in (Masoudi and Arnold 1995b), $n_{sub} = 3.34$, $n_g^\omega = 3.5$ and $n_g^{2\omega} = 3.6$. The fundamental wavelength again was taken as $\lambda_\omega = 1.55\mu m$, which corresponds to low loss optical communications wavelength. Applying the modal solution of the finite element method, the following effective indices were obtained for the first guide mode for both fields $n_{eff}^\omega = 3.446033$ and $n_{eff}^{2\omega} = 3.583327$. From these results the coherence length is calculated to be $l_c = 2.82\mu m$. Again these results show very good agreement with those previously obtained (Masoudi and Arnold, 1995b). Fig. 7.6 shows the generated second harmonic power and the depletion in the fundamental power for a non-phase matched device at low input powers (20W). From the figure the coherence length can be deduced to be in the region of $2.8\mu m$, this shows very good agreement with the calculated value of $2.82\mu m$.

Fig 7.6 Generation of SH power with depletion in the fundamental

The next example to be considered is the waveguide previously discussed in Chapter 6, shown in Fig 6.4. which has an air cladding, where the substrate is made of AlAs with a core of $Ga_xAl_{1-x}As$. The waveguide is assumed to have the following dimensions, $W=1.0\mu m$, $h=1.0\mu m$ and $t=0.2\mu m$. At the fundamental frequency, such a guide will support two quasi-TE modes. At a fractional aluminium concentration of $x=0.2$ and a fundamental wavelength of $1.064\mu m$, the substrate and core indexes are $n_{s1}=2.93$ and $n_{g1}=3.05$, respectively and the respective index values at second harmonic wavelength of $0.532\mu m$ are $n_{s2}=3.23$ and $n_{g2}=3.50$ (Whitbread and Robson, 1994). As was previously seen waveguide loss in such a waveguide is minimal and hence for the sake of simplicity loss will be neglected. The effective index for the fundamental and harmonic waves are found to be $n_{eff}^{\omega} = 2.982967$ and $n_{eff}^{2\omega} = 3.483319$ respectively.

If the technique of quasi phase matching were to be applied to the device then it is possible to increase output power. As can be noted from Fig 7.7 almost total conversion (99.5%) is achieved from the fundamental to the second harmonic after about 100μm. After which there is the down conversion of the second harmonic to the fundamental. This again is what should be expected because of coupling between the fundamental wave and the second harmonic.

The next example investigates the effect of intense input beams such as occurs in laser systems on the second order process. Fig. 7.8 shows what occurs as the input power is increased by several orders of magnitude in non-quasi phase matched systems. It can be noted that the power exchange process becomes incomplete, with only a partial conversion of the fundamental to the second harmonic. This is reminiscent of the reported phenomenon where in the presence of intense input beams and far from phase matching the fundamental beam and the second harmonic beam appear to travel independent of each other in the device (Torruellas *et al.* 1994, Stegeman 1996).

As the input power is further increased, this effect becomes even more pronounced. The two waves begin to travel within the medium affecting each other only minimally. This is more clearly shown in Fig 7.9 and Fig 7.10. It is interesting to note that the conversion level is at about 50%. In other words about half of the power travels as a fundamental wave and the other half travels as a harmonic wave.
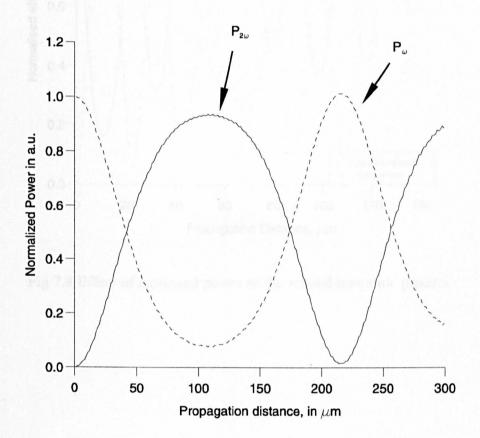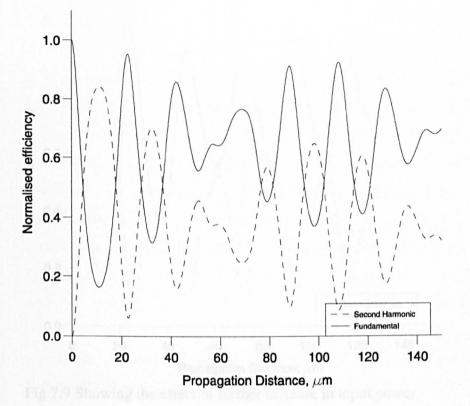

Fig 7.7 Showing the process of quasi phase matching with depletion in the fundamental.

Fig 7.8 Effect of increased power of the second harmonic process

Fig 7.9 Showing the effect of further increase in input power

Fig 7.10 Shows the independence of two waves within the waveguide

7.4   Summary

In this chapter the importance of taking into consideration the depletion of the fundamental beam is modelled. Maxwell's equation for the propagation of waves is written such that the fundamental wave is coupled to the harmonic wave through a source term. Results are compared with previously published data. For an idealised phase matched waveguide it is shown how the fundamental is converted into the second harmonic. It is seen that if allowed to propagate for sufficiently long distances all of the fundamental will be converted to the second harmonic. After maximum power has been transferred to the harmonic, it is observed that the harmonic power is then transferred to the fundamental. A practical waveguide in which the technique of quasi phase matching is applied is then considered. The conversion process is shown for different levels of input power. It is seen that at sufficiently high input powers, the generated second harmonic and the fundamental will travel independently of each other.

Chapter Eight

Conclusion and Suggestions for Future Work

8.1.1 General Conclusions

The primary objective of this work has been to develop a numerical method based on the finite element formulation and the beam propagation method for the characterisation of second harmonic generation in optical waveguides. The tasks outlined in the first chapter have been completed successfully with detailed analysis of the results obtained. The criteria for the validation of our results had been a comparison with experimentally available results and other published data. The validity of the method developed here was thus demonstrated.

Even though there are available a number of techniques for the study of optical waveguide problems, the finite element method has emerged as one of the most powerful offering a high degree of versatility and accuracy. In this work, the finite

element formulation with the use of vector **H** field and the penalty function to eliminate spurious solutions has been employed in the modal analysis section. In integrated optics there is the need to consider special boundary conditions at the dielectric interfaces. Since the **H** field is naturally continuous across dielectric interfaces and the associated natural boundary condition is that of an electric wall, then the most advantageous formulation in most practical cases is the magnetic vector **H** field formulation. To eliminate spurious modes a penalty function term is included which imposes the constraint $\nabla \cdot \mathbf{H} = 0$. Using this approach, problems involving arbitrary cross section, index profile, anisotropy and nonlinearity can easily be solved and this has been demonstrated through this work. Whilst most numerical approximate methods are applicable to guides with relatively regular geometries and material composition, the finite element method has been shown to be suitable for the treatment of arbitrary waveguide structures thus, enabling the development of efficient and flexible computer programs.

Chapter 2 was devoted to elucidating the mathematical background for the finite element method, which lies at the core of this work. The beam propagation method is also discussed in this chapter. These two then form the main algorithms used in this work. The distinguishing feature of this method being that the waveguide cross section is discretized in the transverse direction using the finite element method instead of the more familiar finite difference method. This enables the advantages of the finite element method to be incorporated into the beam propagation method.

In Chapter 3, we look at the theory underlying the phenomenon of second harmonic generation. Following established authors, the fundamental equations are derived from first principles. The physical origins are examined. This chapter also discusses phase matching a technique employed to increase the harmonic output. Also derived in this section is the finite element formulation to be used in later sections.

In Chapter 4, the finite element method is applied to the analysis of anisotropic waveguides. These guides are of practical importance, being used in the implementation of several devices including second harmonic generators, in particular for birefringence phase matching. Guides of arbitrary index distribution in both the transverse directions were investigated as well as waveguides with an arbitrary permittivity tensor. Various waveguide geometries were considered. Many research workers assume that in diffused waveguides, the guide dimensions are the same as the diffusion parameters. It was shown that near to cut off better results are obtained if the waveguide dimensions with graded index are assumed to be greater than the diffusion parameters themselves. Since computational resources can limit the accuracy of any numerical solution hence in the finite element method symmetry conditions are imposed in order to increase computational resources and hence accuracy. It was shown that in the analysis of anisotropic waveguides with off-diagonal refractive index tensor, it is not possible to exploit the physical symmetry of the guide.

Chapter 5 is devoted to the study of Cerenkov second harmonic generation in LiNbO$_3$ waveguides. Results were presented for optical waveguides with both 1-D and 2-D confinement. The evolution of the second harmonic for various cases and the generation of second harmonic power are also illustrated. In the simulation, the vector finite element method is used to find the modal solutions following which the FEM-based BPM program has been used to study the evolution of the second harmonic waves along the waveguide structure. The numerical approach developed here is accurate, computationally efficient and also very versatile. It allows practical and realistic waveguide structures with anisotropic material properties, diffused in both the transverse directions and with 2-D confinement to be considered. This approach can be used to optimise device designs for any particular operation.

The tendency in integrated optics has been towards the monolithic integration of devices. In semiconductor waveguides such a monolithic integration of fundamental

source with the second harmonic is possible. Chapter 6 describes the application of the accurate and efficient finite element method for the study of second harmonic generation in semiconductor waveguides. The effect of fabrication tolerance on the output power was demonstrated. It was shown that fabrication tolerances could lead to errors in domain length, which would result in substantial reduction in the generated power. The effect of loss in the waveguide was also considered. GaAs has a high nonlinear susceptibility compared to AlGaAs, however it also has a much higher loss factor. Chapter 6 also discusses the results obtained for second harmonic generation after taking into consideration the loss factor. These results demonstrate that for the reported values of non-linear susceptibility tensor and loss factor, $Ga_{0.2}Al_{0.8}As$ appears to be a better material for second harmonic generation. However it is also shown that if material loss can be reduced in GaAs then a better efficiency can be obtained.

In traditional second harmonic generation, the wave of interest has been the second harmonic wavelength and the maximisation of the efficiency of the process. The input beam has been assumed to be undepleted and not affected by the generated second harmonic. Whilst such an assumption may be valid at low intensities, it is not strictly valid in the presence of high intensity beams such as is provided by tightly focused laser source. The effect of the second harmonic on the fundamental can result in the mimicking of third order processes. In Chapter 7 this effect is modelled. It was shown that at sufficiently high input intensities, the two beams travel almost independently of each other.

8.2   Considerations for future Work

It has been shown through this work that the numerical method developed is computationally efficient and accurate. An important consideration for future work would be the implementation of a fully vectorial finite element-beam propagation

method. The development of such a numerical model will provide researchers with a powerful tool for the study and analysis of various waveguides.

Although there has been a substantial level of research work carried out to achieve optical switching using the third order nonlinearity, the unavailability of suitable materials with high non-linear coefficients has made it difficult to achieve low power optical switching. This has led to a shift of interest to the use of cascaded second order non-linear effects for all optical switching. In earlier work, the assumption had been that of an undepleted source field. This assumption is strictly not valid in the presence of intense laser beams. Chapter 6 of the present work does look at this effect in an idealised guide structure. The numerical approach presented here will help in the study and optimisation of such devices. It would be of practical interest to extend this work to realistic waveguides.

Although it has been reported that MQW region can have greater non-linear coefficient, thus far this parameter has not been adequately characterised. The method developed here can also be extended to model second harmonic generation in multiple quantum wells. As fabrication technology improves and material data become available, device parameters can be optimised and the model is, seen to be capable of incorporating important features such as material anisotropy, loss factor and diffused index profiles.

Appendix 1

Boundary Conditions

Given that **n** is the normal unit vector then the boundary conditions can be stated as follows:

1)   The tangential component of the electric field must be continuous

$$n \times (E_1 - E_2) = 0 \qquad\qquad \text{A1-1}$$

2)   The tangential component of the magnetic field must be continuous $n \times (H_1 - H_2) = 0$. The surface current density Js[A/m] may be discontinuous provided that surface current is flowing on the boundary surface

$$n \times (H_1 - H_2) = J_s . \qquad\qquad \text{A1-2}$$

3)   The normal component of the electric flux density must be continuous $n \cdot (D_1 - D_2) = 0$. The surface charge density $\rho_s [\text{C/m}^2]$ may however be discontinuous, provided a surface charge exists on the boundary surface,

$$n \cdot (D_1 - D_2) = \rho_s . \qquad\qquad \text{A1-3}$$

4)   The normal component of the electric flux density must be continuous

$$n \cdot (B_1 - B_2) = 0 \qquad\qquad \text{A1-4}$$

Appendix 2

Theory of the Minimum of a functional

Given the general differential equation

$$\nabla \times (p \nabla \times v) - \omega^2 qv = f \qquad\qquad\qquad \text{A2-1}$$

it can be shown that the vector function which satisfies the above curl curl equation also minimises the following functional

$$F = \langle \nabla \times (p \nabla \times v), v \rangle - \omega^2 \langle qv, v \rangle - \langle f, v \rangle - \langle v, f \rangle \qquad\qquad \text{A2-2}$$

The curl curl equation can be rewritten in the form

$$\left(\nabla \times (p \nabla \times) - \omega^2 q \right) v = f \qquad\qquad\qquad \text{A2-3}$$

Using equation (1.31) the above could be written as

$$Lv = f \qquad\qquad\qquad \text{A2-4}$$

The original curl-curl equation has now been cast in a more general form. An equation such as (A2-4) is a deterministic problem, the solution of which is uniquely determined by the source term f. The functional of the curl-curl equation, (A2-2) can now be written as

$$F = \langle Lv, v \rangle - 2\langle f, v \rangle \qquad\qquad\qquad \text{A2-5}$$

If it is assumed that v_o is a solution, then it follows that $f = Lv_o$. Making this substitution in the functional of equation (A2-5) the following is obtained

$$F = \langle Lv, v \rangle - \langle Lv_o, v \rangle - \langle Lv_o, v \rangle \qquad \text{A2-6}$$

It is obvious however that

$$F = \langle Lv, v \rangle - \langle Lv_o, v \rangle - \langle v, Lv_o \rangle \qquad \text{A2-7}$$

From the symmetry properties of the inner product and of the linear operator the above can be written as

$$F = \langle Lv, v \rangle - \langle Lv_o, v \rangle - \langle Lv, v_o \rangle \qquad \text{A2-8}$$

If the term $\langle Lv_o, v_o \rangle$ is now added and subtracted from the right hand side of equation (A2-8) the following is obtained

$$F = \langle Lv, v \rangle - \langle Lv_o, v \rangle - \langle Lv, v_o \rangle + \langle Lv_o, v_o \rangle - \langle Lv_o, v_o \rangle \qquad \text{A2-9}$$

This is actually equal to

$$F = \langle L\langle v - v_o \rangle, v - v_o \rangle - \langle Lv_o, v_o \rangle \qquad \text{A2-10}$$

The last term of equation (A2-10) $\langle Lv_o, v_o \rangle$, does not depend on the variable and hence is a constant. By definition

$$\langle L\langle v - v_o \rangle, v - v_o \rangle \geq 0 \qquad \text{A2-11}$$

with $\langle L\langle v - v_o \rangle, v - v_o \rangle = 0$ if and only if $v - v_o = 0$. It follows from the above considerations that the function assumes its minimal value precisely for $v = v_o$.

Appendix 3

Calculation of the Inverse of ε

It has been stated that ε is a 3x3 matrix. It should however be noted that some elements of this matrix are imaginary. Taking the above into consideration, the matrix can now be written as

$$\varepsilon = \begin{bmatrix} \varepsilon_{11} & \varepsilon_{12} & j\varepsilon_{13} \\ \varepsilon_{21} & \varepsilon_{22} & j\varepsilon_{23} \\ j\varepsilon_{31} & j\varepsilon_{32} & \varepsilon_{33} \end{bmatrix}$$

The inverse of this matrix is obtained by first finding the transpose of the co-factor matrix $\mathbf{C}^T$. The co-factor matrix is given by:

$$C = (-1)^{i+j} M_{ij}$$

where M_{ij} is a matrix the elements of which are as follows:

$$m_{11} = \varepsilon_{22}\varepsilon_{33} + \varepsilon_{23}\varepsilon_{32}$$

$$m_{12} = \varepsilon_{21}\varepsilon_{33} + \varepsilon_{23}\varepsilon_{31}$$

$$m_{13} = j\varepsilon_{21}\varepsilon_{32} - j\varepsilon_{22}\varepsilon_{31}$$

$$m_{21} = \varepsilon_{12}\varepsilon_{33} + \varepsilon_{13}\varepsilon_{32}$$

$$m_{22} = \varepsilon_{11}\varepsilon_{33} + \varepsilon_{13}\varepsilon_{31}$$

$$m_{23} = j\varepsilon_{11}\varepsilon_{32} - j\varepsilon_{12}\varepsilon_{31}$$

$$m_{31} = j\varepsilon_{12}\varepsilon_{23} - j\varepsilon_{13}\varepsilon_{22}$$

$$m_{32} = j\varepsilon_{11}\varepsilon_{23} - j\varepsilon_{21}\varepsilon_{13}$$

$$m_{33} = \varepsilon_{11}\varepsilon_{22} - \varepsilon_{12}\varepsilon_{21}$$

$$C = \begin{bmatrix} m_{11} & -m_{12} & m_{13} \\ -m_{21} & m_{22} & -m_{23} \\ m_{31} & -m_{32} & m_{33} \end{bmatrix}$$

$$C^T = \begin{bmatrix} m_{11} & -m_{21} & m_{31} \\ -m_{12} & m_{22} & -m_{32} \\ m_{13} & -m_{23} & m_{33} \end{bmatrix}$$

The determinant of the matrix ε is given by

$$det\, \varepsilon = \varepsilon_{11}(\varepsilon_{22}\varepsilon_{33} + \varepsilon_{23}\varepsilon_{32}) - \varepsilon_{12}(\varepsilon_{21}\varepsilon_{33} + \varepsilon_{23}\varepsilon_{31}) + j\varepsilon_{13}(j\varepsilon_{21}\varepsilon_{32} - j\varepsilon_{22}\varepsilon_{31})$$

The inverse of the matrix ε is given as

$$\varepsilon^{-1} = \frac{C^T}{det\,\varepsilon} = \begin{bmatrix} p_{11} & p_{12} & p_{13} \\ p_{21} & p_{22} & p_{23} \\ p_{31} & p_{32} & p_{33} \end{bmatrix}$$

where

$$p_{11} = \frac{\varepsilon_{22}\varepsilon_{33} + \varepsilon_{23}\varepsilon_{32}}{det\,\varepsilon}$$

$$p_{12} = -\frac{\varepsilon_{12}\varepsilon_{33} + \varepsilon_{13}\varepsilon_{32}}{det\,\varepsilon}$$

$$p_{13} = \frac{j\varepsilon_{12}\varepsilon_{23} - j\varepsilon_{13}\varepsilon_{22}}{det\,\varepsilon}$$

$$p_{21} = -\frac{\varepsilon_{21}\varepsilon_{33} + \varepsilon_{23}\varepsilon_{31}}{det\,\varepsilon}$$

$$p_{22} = \frac{\varepsilon_{11}\varepsilon_{33} + \varepsilon_{13}\varepsilon_{31}}{\det \varepsilon}$$

$$p_{23} = -\frac{j\varepsilon_{11}\varepsilon_{23} - j\varepsilon_{13}\varepsilon_{21}}{\boldsymbol{det}\,\varepsilon}$$

$$p_{31} = \frac{j\varepsilon_{21}\varepsilon_{32} - j\varepsilon_{22}\varepsilon_{31}}{\boldsymbol{det}\,\varepsilon}$$

$$p_{32} = -\frac{j\varepsilon_{11}\varepsilon_{32} - j\varepsilon_{12}\varepsilon_{31}}{\boldsymbol{det}\,\varepsilon}$$

$$p_{33} = \frac{\varepsilon_{11}\varepsilon_{22} - \varepsilon_{12}\varepsilon_{21}}{\boldsymbol{det}\,\varepsilon}$$

Appendix 4

The Element Matrices

From Maxwell's equation the following can be derived

$$p_x \frac{\partial^2 \phi}{\partial x^2} + p_y \frac{\partial^2 \phi}{\partial y^2} - p_z \beta^2 \phi + qk_o^2 \phi = 0$$

It can be shown that the functional which minimises the above equation is of the form

$$F = \int_\Delta \left(p_x \frac{\partial \phi^*}{\partial x} \frac{\partial \phi}{\partial x} + p_y \frac{\partial \phi^*}{\partial y} \frac{\partial \phi}{\partial y} + p_z \beta^2 \phi^* \phi - qk_o^2 \phi^* \phi \right) d\Omega = 0$$

Evaluating the terms individually the following is obtained

$$p_x \frac{\partial \phi^*}{\partial x} \frac{\partial \phi}{\partial x} = p_x \{\phi\}^T \frac{\partial N^T}{\partial x} \frac{\partial N}{\partial x} \{\phi\}$$

where

$$\frac{\partial N^T}{\partial x} \frac{\partial N}{\partial x} = \begin{vmatrix} a_2^2 & a_2 a_5 & a_2 a_8 \\ a_2 a_5 & a_5^2 & a_5 a_8 \\ a_2 a_8 & a_2 a_5 & a_8^2 \end{vmatrix}$$

$$p_y \frac{\partial \phi^*}{\partial y} \frac{\partial \phi}{\partial y} = p_y \{\phi\}^T \frac{\partial N^T}{\partial y} \frac{\partial N}{\partial y} \{\phi\}$$

where

$$\frac{\partial N^T}{\partial y} \frac{\partial N}{\partial y} = \begin{vmatrix} a_3^2 & a_3 a_6 & a_3 a_9 \\ a_3 a_6 & a_6^2 & a_6 a_9 \\ a_3 a_9 & a_6 a_9 & a_9^2 \end{vmatrix}$$

$$p_z \beta^2 \phi^* \phi = p_z \beta^2 \{\phi\}^T [N][N]\{\phi\}$$

where

$$[N][N] = \begin{vmatrix} N_1^2 & N_1 N_2 & N_1 N_3 \\ N_1 N_2 & N_2^2 & N_2 N_3 \\ N_1 N_3 & N_2 N_3 & N_3^2 \end{vmatrix}$$

$$qk_o^2 \phi^* \phi = qk_o^2 \{\phi\}^T [N][N]\{\phi\}$$

$$\frac{\partial F}{\partial \{\phi\}^T} = \int_\Delta \left(p_x \frac{\partial N^T}{\partial x} \frac{\partial N}{\partial x} \{\phi\} + p_y \frac{\partial N^T}{\partial y} \frac{\partial N}{\partial y} + p_z \beta^2 [N][N]\{\phi\} - qk_o^2 [N][N]\{\phi\} \right) d\Omega = 0$$

A simple rearrangement of the above will yield

$$\int_\Delta \left(qk_o^2 [N][N] - p_x \frac{\partial N^T}{\partial x} \frac{\partial N}{\partial x} - p_y \frac{\partial N^T}{\partial y} \frac{\partial N}{\partial y} \right) \{\phi\} d\Omega - \int_\Delta p_z \beta^2 [N][N]\{\phi\} d\Omega = 0$$

Making the following substitutions

$$[A] = \int_\Delta \left(qk_o^2 [N][N] - p_x \frac{\partial N^T}{\partial x} \frac{\partial N}{\partial x} - p_y \frac{\partial N^T}{\partial y} \frac{\partial N}{\partial y} \right) \{\phi\} d\Omega$$

and

$$[B] = \int_\Delta p_z \beta^2 [N][N]\{\phi\} d\Omega = 0$$

equation (a4.5) can be written as

$$[A]\{\phi\} - \beta^2 [B]\{\phi\} = 0$$

Using first order triangular elements, the matrix [A] and [B] are given as follows

$$A_{11} = qk_o^2 \frac{\text{area}}{6} - p_x \Delta a_2^2 - p_y \Delta a_3^2$$

$$A_{12} = qk_o^2 \frac{\text{area}}{12} - p_x \Delta a_2 a_5 - p_y \Delta a_3 a_6$$

$$A_{13} = qk_o^2 \frac{\text{area}}{12} - p_x \Delta a_2 a_8 - p_y \Delta a_3 a_9$$

$$A_{22} = qk_o^2 \frac{\text{area}}{6} - p_x \Delta a_5^2 - p_y \Delta a_6^2$$

$$A_{23} = qk_o^2 \frac{\text{area}}{12} - p_x \Delta a_5 a_8 - p_y \Delta a_6 a_9$$

$$A_{33} = qk_o^2 \frac{\text{area}}{6} - p_x \Delta a_8^2 - p_y \Delta a_9^2$$

$$B_{11} = p_z \beta^2 \frac{\text{area}}{6}$$

$$B_{12} = p_z \beta^2 \frac{\text{area}}{12}$$

$$B_{13} = p_z \beta^2 \frac{\text{area}}{12}$$

$$B_{22} = p_z \beta^2 \frac{\text{area}}{6}$$

$$B_{23} = p_z \beta^2 \frac{\text{area}}{12}$$

$$B_{33} = p_z \beta^2 \frac{\text{area}}{6}$$

APPENDIX 5

Publications by the Author Relevant to the Thesis

Katsriku, F.A., Rahman, B.M.A. & Grattan, K.T.V.: "Finite Element Analysis of Second Harmonic Generation in GaAs and AlGaAs Waveguides". IEEE Journal of Quantum Electronics, March 2000, pp 282-289.

Katsriku, F.A., Rahman, B.M.A. & Grattan, K.T.V.: "Modelling the Effects of Loss and Fabrication Error for Second Harmonic Generation in Semiconductor Waveguides". Nonlinear Guided Waves and their Applications. Topical Meeting, 1-3 September 1999, pp 348-350. Dijon France.

Rahman, B.M.A., Obayya, S.S.A., Buah P.A., **Katsriku, F.A.** & Grattan, K.T.V.: "Modelling of axially non-uniform photonics devices using finite element based vectorial BPM." 3rd International Conference on Photonics, pp 497-502, Prague 21-23 June 1999.

Rahman, B.M.A., Rajarajan M., Wongcharoen T., **Katsriku, F.A.,** Buah P.A., Meyer M. & Grattan, K.T.V.: "Rigorous Characterisation of Photonic Devices Using The Finite element Method". In Photonics '98 IIT Delhi India, Dec. 14 – 18 1998.

Katsriku, F.A., Rahman, B.M.A. & Grattan, K.T.V.: "Numerical Study of Second Harmonic Generation in Semiconductor Waveguides". OSA Non-linear Optics: Topical Meeting on Devices and their Applications, Hawaii, Aug. 1998.

Rahman, B.M.A., **Katsriku, F.A**. & Grattan, K.T.V.: "Accurate Modelling of Second Harmonic Generation in Optical Waveguides". SPIE Conference on "Physics & Simulation of Optoelectronic Devices", San Jose, California, January 1998. SPIE Vol. 3283, pp.748 - 758.

Katsriku F.A., Rahman B.M.A. and Grattan K.T.V. (1997). Numerical modeling of second harmonic generation in optical waveguides using the finite element method <u>IEEE Journal of Quantum Electronics 33</u> (10): 1727-1733.

Katsriku F.A., Rahman B.M.A. and Grattan K.T.V. (1996). Finite element analysis of diffused anisotropic optical waveguides. <u>Journal of Lightwave Technology LT-14</u> (5): 780-786

References

Abid Z.E., Johnson K.L. and Gopinath A. (1993). Analysis of dielectric guides, by vector transverse magnetic fields finite element. Journal of Lightwave Technology 11 (10):1545-1549.

Adachi S. (1985). GaAs, AlAs, and $Al_xGa_{1-x}As$ - material parameters for use in research and device applications. Journal of Applied Physics 58 (3): R1-R29.

Adachi S. (1988). Optical properties of $Al_xGa_{1-x}As$ alloys. Physical Review B-Condensed Matter 38 (17):12345-12352.

Adachi S. (1989). Optical dispersion relations for GaP, GaAs, GaSb, InP, InAs, InSb, $Al_xGa_{1-x}As$ and $In_{1-x}Ga_xAs_yP_{1-y}$. Journal of Applied Physics 66 (12): 6030 – 6040.

Adams M.J. (1981). An introduction to optical waveguides. (New York: John Wiley & Sons).

Aitchison J.S., Villeneuve A. and Stegeman G.I. (1995). All-optical switching in two cascaded nonlinear directional couplers. Optics Letters 20 (7): 698-700.

Aitchison J.S., Hutchings D.C., Kang J.U., Stegeman G.I. and Villeneuve A (1997). The nonlinear optical properties of AlGaAs at the half band gap. IEEE Journal of Quantum Electronics 3: 341-348.

Aitchison J.S., Street M.W., Whitbread N.D., Hutchings D.C., Marsh J.H., Kennedy G.T. and Sibbett W. (1998). IEEE Journal of Selected Topics in Quantum Electronics 4: 695-700.

Alferov Zh.I., Andreev V.M., Portnoi E.L. and Trukkan M.K. (1970). AlAs-GaAs heterojunction injection lasers with a low-room temperature threshold. Soviet Physics Semiconductors 3: 1107-1110.

Anwar N., Themistos C., Rahman B.M.A. and Grattan K.T.V. (1999). Design considerations for an electrooptic directional coupler modulator. Journal of Lightwave Technology LT-17 (4): 598-605.

Armstrong J.A., Bloembergen N., Ducuing J. and Persham P.S. (1962). Interactions between light waves in a nonlnear dielectric. Physics Review 127 : 1918-1939.

Ashkin A., Boyd G.D. and Dziedzic J.M. (1966). Resonant optical second harmonic generation and mixing. IEEE Journal of Quantum Electronics 2: 109-124.

Austin M.W. (1984). Theoretical and experimental investgation of GaAs/GaAlAs and n/n* GaAs rib waveguides. Journal of Lightwave Technology 2 (5): 688-694.

Bava G.P., Montrosset I., Sohler W. and Suche H. (1987). Numerical modelling of Ti:LiNbO3 integrated optical parametric oscillators. IEEE Journal of Quantum Electronics 23: 42-51.

Berk A.D. (1956). Variational principles for electromagnetic resonators and waveguides. IRE Transactions on Antennas Propagation AP-4: 104-111.

Bersiner L. Hempelmann U. and Strake E. (1991). Numerical analysis of passive integrated-optical polarization splitters: comparison of the finite-element method and beam-propagation method results. Journal of Optical Society of America-B 8 (2): 422-433.

Bloembergen N. (1965). Nonlinear Optics. (New York: W.A. Benjamin).

Bossavit A. and Mayergoyz I. (1989). Edge elements for scattering problems. IEEE Transactions on Magnetics 25 (4): 2816-2821.

Burke S.V. (1990). Spectral index method applied to two nonidentical closely separated rib waveguides. IEE Proceedings-J 137 (10):

Butcher P.N. and Cotter D. (1990). The Elements of Nonlinear Optics. (Newcastle upon Tyne: Cambridge University Press).

Chiang K.S. (1985). Construction of refractive-index profiles of planar dielectric waveguides from the distribution of effective indexes. Journal of Lightwave Technology LT-3 (2): 385-391.

Chiang K.S. (1986). Dual effective-index method for the analysis of rectangular dielectric waveguides. Applied Optics 25: 2169-2174.

Chiang K.S. (1994). Review of numerical and approximate methods for the modal analysis of general optical dielectric waveguides. Bell Systems Technical Journal 26 S133-S134.

Chiang K.S. (1996). Analysis of the effective-index method for the vector modes of rectangular-core dielectric waveguides. IEEE Transactions on Microwave Theory Techniques MTT-44 (5): 692-700.

Chinn R.S. (1976). Intracavity second harmonic generation in a Nd pentaphosphate laser. Applied Physics Letters 29: 176-179.

Dagli N. and Fonstad C.G. (1987). A new method of analyzing and modelling integrated optoelectronic components. In IEEE Microwave and Millimeter-wave monolithic Circuits Symposium: 39-41.

Csendes Z.J. and Silvester P. (1970). Numerical solution of dielectric loaded waveguides: I-finite element analysis. IEEE Transactions on Microwave Theory Techniques MTT-18: 1124-1131.

Daly P. (1984). Finite element approach to propagation in elliptical and parabolic waveguides. International Journal of Numerical Methods 20 (4): 681-688.

Davies J.B. (1989). The finite element method. In: Numerical techniques for microwave and millimeter-wave passive structures. Ed. by Itoh T. (New York: Wiley) pp. 33-132.

Davies J.B. (1972). Review of numerical solution of the hollow-waveguide problem. IEE Proceedings 119 (1): 33-37.

Delacourt D., Armani F., and Papuchon M. (1994). Second-harmonic generation efficiency in periodically poled LiNbO$_3$ waveguides. IEEE Journal of Quantum Electronics 30 (4): 1090-1099.

Dixon G.J. (1993). Compact Blue-Green lasers get down to business. Circuits and Devices (11): 18-22.

Dixon G.J. (1997). Periodically poled lithium niobate shines in the IR. Laser Focus World (5): 105-111.

English W.J. and Young F.J. (1971). An E vector variational formulation of Maxwell's equation for cylindrical waveguide problems. IEEE Transactions on Microwave Theory Techniques MTT-19: 40-46.

Erteza I.A. and Goodman J.W. (1995). A scalar variational analysis of rectangular dielectric waveguides using Hermite-Gaussian modal approximations. Journal of Lightwave Technology LT-13 (3): 493-506.

Feit M.D. and Fleck J.A. Jr. (1980). Computation of mode properties in optical fiber waveguides by a propagating beam method. <u>Applied Optics 19</u> (7): 1154-1164.

Fejer M.M., Magel G.A., Jundt D.H. and Byer R.L. (1992). Quasiphase-matched second harmonic generation: Tuning and tolerances. <u>IEEE Journal of Quantum Electronics 28</u> (): 2631-2654.

Fejer M.M. (1994). Quasi-phasematched nonlinear optical frequency conversion. <u>IEEE LEOS Newsletter</u> (12): 19-22.

Fleck J.A. Jr. and Feit M.D. (1978). Beam propagation in uniaxial anisotropic media. <u>Journal of. Optical Society of America 73</u>: 920-926.

Fernandez F.A. and Lu Y. (1990). Variational finite element analysis of dielectric waveguides with no spurious solutions. <u>Electronic Letters **26** (12)</u> : 2125-2126.

Fluck D., Pliska T., Gunter P., Beckers L. and Buchal C. (1996). Cerenkov-type second-harmonic generation in $KNbO_3$ channel waveguides", <u>IEEE Journal of Quantum Electronics 32</u> (6): 905-916.

Franken P.A., Hill A.E., Peters C.W. and Weinreich G. (1961). Generation of optical harmonics. <u>Physics Review Letters 7</u>: 118-119.

Franken P.A. and Ward J.F. (1963). Optical harmonics and nonlinear phenomena. <u>Review of Modern Physics 35</u> : 23-39.

Fujimura M., Kintaka K., Suhara T. and Nishihara H. (1993). $LiNbO_3$ waveguide quasi-phase-matching second harmonic generation devices with ferroelectric-domain-inverted gratings formed by electron-beam scanning. <u>Journal of Lightwave Technology LT-11</u> (8): 1360-1368.

Garrett C.G.B. and Robinson F.N.H. (1966). Miller's Phenomenological rule for computing nonlinear susceptibilities. IEEE Journal of Quantum Electronics 2: 328.

Giordmaine J.A. (1962). Mixing of light beams in crystals. Physics Review Letters 8. pp. 19.

Goell J.E. (1969). A circular-harmonic computer analysis of rectangular dielectric waveguides. Bell Systems Technical Journal 48 (9): 2133-2160.

Goyal I.C., Gallawa R.L. and Ghatak A.K. (1993). Improved variational analysis of inhomogeneous optical waveguides. Journal of Lightwave Technology LT-11 (10): 1575-1578.

Gwneuch H. (1995). Personal communication.

Hall R.N., Fenner G.E, Kingsley J.D., Soltys T.J. and Carison R.O. (1962). Coherent light emission from GaAs junctions. Physical Review Letters 9 (9): 366-368.

Harrington R.F. (1967). Matrix methods for field problems. Proceedings IEEE 55 (2): 136-149.

Harvey A.F. (1970). Coherent Light. (London: Wiley).

Hashizume N., Kondo T., Onda T., Ogasawara N., Umegaki S. and Ito R. (1992). Theoretical analysis of Cerenkov-type optical SHG in slab waveguides. IEEE Journal of Quantum Electronics 28 (8): 1798-1815.

Hayashi I., Panish M.B., Foy P.W. and Sumski S. (1970). Junction lasers which operate continuously at room temperature. Applied Physics Letters 17 (3): 109-111.

Hayata K. and Koshiba M. (1991). Numerical study of guided-wave sum-frequency generation through second-order nonlinear parametric processes. Journal of Optical Society of America-B 8 (2): 449-458.

Hayata K., Koshiba M. Eguchi M. and Suzuki M. (1986). Vectorial finite element method without any spurious solutions for dielectric waveguiding problems using transverse magnetic-field component. IEEE Transactions on Microwave Theory Techniques MTT-34 (11): 1120-1124.

Hayata K., Miura K. and Koshiba M. (1988). Finite element formulation for lossy waveguides. IEEE Transactions on Microwave Theory Techniques MTT-36 (2): 268-276.

Helmfrid S., Laurell F. and Arvidsson G. (1993). Optical parametric amplification of a 1.54-μm single-mode DFB laser in a Ti:NbO$_3$ waveguide. Journal of Lightwave Technology LT-11 (9): 1459-1469.

Hempelmann U. (1999). All-optical modulation in second order nonlinear directional couplers by second-harmonic generation. Nonlinear Guided waves and their Applications. Technical Digest: 345-347.

Hocker G.B. and Burns W.K. (1977). Mode dispersion in diffused channel waveguides by the effective index method. Applied Optics 16 (1): 113-118.

Hotta M., Geshiro M, Arashiba T. and Sawa S. (1994). A design consideration for optical power dividers composed of three coupled waveguides. IEEE Transactions on Microwave Theory and Techniques MTT-42(7): 1167-1171.

Hunsperger R.G. (1984). Integrated Optics: Theory and Technology. 2nd ed. (Berlin: Springer-Verlag).

Ikeuchi M., Sawami H. and Niki H. (1981). Analysis of open-type dielectric wave-guides by the finite-element iterative method. IEEE Transactions on Microwave Theory and Techniques MTT-29(3) : 234-239.

Ironside C.N. Aitchison J.S. and Arnold J.M. (1993). An all-optical switch employing the cascaded second-order nonlinear effect. IEEE Journal of Quantum Electronics 29 (10): 2650-2654.

Jenkins D.W. (1990). Optical-Constants of $Al_xGa_{1-x}As$. Journal of Applied Physics Vol.68 (4): 1848-1853.

Jenkins R.M., Heaton J.M., Wight D.R., Parker J.T., Birbeck J.C.H., Smith G.W. and Hilton K.P. (1994). Novel 1xN and NxN integrated optical switches using self-imaging multimode GaAs/AlGaAs waveguides. Applied Physics Letter 64 (6): 684-686.

Jones-Bey H. (1998). Researchers find high-power blue light. Laser Focus World. Vol.34, (11) : 15-16.

Kao K.C. and Hockham G.A. (1966). Dielectric-fibre surface waveguides for optical frequencies. Proceedings IEE 113: 1151-1158.

Kapany N.S. (1967). Fibre Optics: Principles and applications. (New York: Academic Press).

Kapron F.P., Keck D.B. and Maurer R.D. (1970). Applied Physics Letter 17 : 423-425.

Katz C. and Werner H. (1982). Implementation of non-linear boundary-conditions in finite-element analysis. Journal of Computers and structures 15 (3): 299-304

Kendall P.C., McIlroy P.W.A. and Stern M.S. (1989). Spectral index method for rib waveguide analysis. Electronic Letters 25 (2): 107-108.

Kelaidis C., Hutchings D.C. and Arnold J.M. (1994). Asymmetric two-step GaAlAs quantum well for cascaded second-order processes. IEEE Journal of Quantum Electronics 30 (12): 2998-3005.

Kinkata K., Fujimura M. and Suhara T. (1996). High-efficiency LiNbO$_3$ waveguide second harmonic generation with ferroelectric domain inverted gratings fabricated by applying voltage. Journal of Lightwave Technology LT-14 (3): 462-468.

Knox R.M. and Toulios P.P. (1970). Integrated Circuits for the millimeter through optical frequency range. In Proceedings of MRI Symposium on Submillimeter Waves, ed. by Fox J. (Brooklyn: Polytechnic Press), pp. 497-516.

Kobelansky A.J. and Webb J.P. (1986). Eliminating spurious modes in finite element waveguide problems by using divergence-free fields. Electronic Letters 22 (11): 569-570.

Koshiba M., Hayata K. and Suzuki M. (1986). Finite-element solution of anisotropic wave-guides with arbitrary tensor permittivity. Journal of Lightwave Technology 4 (2): 121-126.

Koshiba M. (1990). The finite-element method. In: Analysis methods for electromagnetic wave problems. Ed. by Yamashita E. (London: Artech House) pp 1-31.

Koshiba M. (1992). Optical waveguide analysis. (Tokyo: McGraw-Hill).

Koshiba M. Hayata K. and Suzuki M. (1984). Approximate scalar finite-element analysis of anisotropic optical waveguides with off-diagonal elements in a permittivity tensor. IEEE Transactions on Microwave Theory Techniques MTT-32 (6): 587-593.

Koshiba M., Ishii H. and Suzuki M. (1982). Simple equivalent network for a rectangular dielectric image guide. Electronic Letters 18 (11): 473-474.

Koshiba M.and Suzuki M. (1985). Vectorial wave analysis of optical waveguides with rectangular cross-section using equivalent network approach. Electronic Letters 21 (22): 1026-1027.

Krijnen G.J.M., Torruellas W., Stegeman G.I., Hoekstra H.J.W.M. and Lambeck P.V. (1996). Optimization of second harmonic generation and nonlinear phase shift in the Cerenkov regime. IEEE Journal of Quantum Electronics 32 (4): 729-737.

Kumar A., Thyangarajan K. and Ghatak A.K. (1983). Analysis of rectangular-core waveguides: An accurate perturbation approach. Optics Letters 8 (1): 63-65.

Lagu R.K. and Ramaswamy R.V. (1986). A variational finite-difference method for analyzing channel waveguides with arbitrary index profiles IEEE Journal of Quantum Electronics 22 (6): 968-976.

Leo G., Dreten R.R. and Jongerius M.J. (1992). Cherenkov second harmonic generation in multilayer waveguide structures. IEEE Journal of Quantum Electronics 28 (2): 534-546 1992.

Li M.J., De Micheli M., He Q. and Ostrowsky D.B. (1990). Cerenkov configuration SHG in proton-exchanged lithium niobate guides. IEEE Journal of Quantum Electronics 26 (8): 1384-1393.

Mabaya N., Lagasse P.E. and Vandenbulcke P. (1981). Finite element analysis of optical waveguides. IEEE Transactions on Microwave Theory Techniques MTT-29 (6): 600-605.

Mahalakshmi V., Shenoy M.R. and Thyagarajan K. (1996). Evolution of the intensity profile of Cerenkov second-harmonic radiation with propagation distance in planar waveguides. IEEE Journal of Quantum Electronics 32 (1): 137-144.

Maker P.D., Terhune R.W., Nisenoff M. and Savage C.M. (1962). Effects of dispersion and focusing on the production of optical harmonics. Physics Review Letters 8: 21.

Marcatili E.A.J. (1969). Dielectric rectangular waveguides and directional couplers for integrated optics. . Bell Systems Technical Journal 48 (9): 2071-2101.

Marcuse D. (1980). Principles of Quantum Electronics. (New York: Academic Press).

Masoudi H.M. and Arnold J.M. (1995)a. Parallel beam propagation method for the analysis of second harmonic generation. IEEE Photonic Technology Letters 7 (4): 400-402.

Masoudi H.M. and Arnold J.M. (1995)b. Modeling second-order nonlinear effects in optical waveguides using a parallel-processing beam propagation method. IEEE Journal of Quantum Electronics 32 (12): 2107-2113.

Miller R.C. (1964). Optical second harmonic generation in piezoelectric crystals. Applied Physics Letters 5: 17

Mizuuchi K., Yamamoto K., Kato M., and Sato H. (1994). Broadening of the phase-matching bandwidth in QPM second harmonic generation. IEEE Journal of Quantum Electronics 30 (7): 1596-1604.

Nakamura S. (1994). Zn-doped InGaN growth and InGaN/AlGaN double-heterostructure blue-emitting diodes. Journal of Crystal Growth (145): 911-917.

Nathan M.I., Dumke W.P., Burns G., Dill F.H. Jr. and Lasher G. (1962). Stimulated emission of radiation from GaAs p-n junctions. Applied Physics letters 1 (3): 62-64.

Ng F.L. (1974). Tabulation of methods for the numerical solution of the hollow waveguide problem. IEEE Transactions on Microwave Theory Techniques MTT-22 (1): 322-329.

Peng S.T. and Oliner A.A. (1981). Guidance and leakage properties of a class of open dielectric waveguides: Part I-Mathematical formulations. IEEE Transactions on Microwave Theory Techniques MTT-29 (9): 843-855.

Pichot Ch. (1982). Exact numerical solution for the diffused channel waveguide. Optical Communications 41 (4): 169-173.

Pola J.R.P., Biehlig W. and Lederer F. (1996). A generalisation of the spectral index method toward multiple rib waveguides. Journal of Lightwave Technology 14 (3): 454-461

Quist T.M., Rediker R.H., Keyes R.J., Krag W.E., Lax B., McWhorter A.L. and Zeigler H.J. (1962). Semiconductor maser of GaAs. Applied Physics letters 1 (4): 91-92.

Rahman B.M.A. and Davies J.B. (1984). Finite-element analysis of optical and microwave problems IEEE Transactions on Microwave Theory Techniques MTT-32 (1): 20-28.

Rahman B.M.A. and Davies J.B. (1984). Finite-element solution of integrated optical waveguides. Journal of Lightwave Technology LT-2 (10): 682-688.

Rahman B.M.A. and Davies J.B. (1984). Penalty function improvement of waveguide solution by finite element. IEEE Transactions on Microwave Theory Techniques MTT-32 (8): 922-928.

Rahman B.M.A. and Davies J.B. (1985). Vector-H finite element solution of GaAs/GaAIAs rib waveguides. IEE Proceedings-J Optoelectronics 132 (6): 349-353.

Rajarajan M., Rahman B.M.A. and Grattan K.T.V. (1998). Numerical study of spot-size expanders for efficient OEIC to SMF coupling. IEEE Photonic Technology Letters (10): 1082-1084.

Rajarajan M., Rahman B.M.A. and Grattan K.T.V. (1999). A rigorous comparison of the performance of directional couplers with multimode interference devices. Journal of Lightwave Technology LT-17 (2): 243-248.

Ramo S., Whinnery J.R. and Van Duzer T. (1994). Fields and waves in communication electronics. (New York: John Wiley & Sons).

Reddy J.N. (1993). An Introduction to the Finite Element Method. (Singapore: McGraw-Hill, Inc.).

Rektorys K. (1980). Variational Methods in Mathematics Science and Engineering. (Dordrecht-Holland: D. Reidel Publishing Company).

Reneger R. and Sohler W. (1988). Efficient second harmonic generation in Ti:LiNbO$_3$ channel waveguide resonators. Journal of Optical Society of America-B 5 (2): 267-277 1988.

Sanford N.A. and Connors J.M. (1989). Optimization of the Cerenkov sum-frequency generation in proton exchange Mg:LiNbO3 channel waveguides. Journal of Applied Physics 65(4):1429-1437

Schulz N., Bierwith K., Arndt F. and Koster U. (1990). Finite-difference method without spurious solutions for the hybrid mode analysis of diffused channel waveguides. IEEE Transactions on Microwave Theory Techniques MTT-38 (6): 722-729.

Schweig E and Bridges W.B. (1984). Computer analysis of dielectric waveguides: A finite difference method. IEEE Transactions on Microwave Theory Techniques MTT-32: 531-541.

Sharma A. and Bindal P. (1992). An accurate variational analysis of single mode diffused channel waveguides. Optical and Quantum Electronics 24: 1359-1371.

Sharma A. and Bindal P. (1993). Analysis of diffused planar and channel waveguides IEEE Journal of Quantum Electronics 29 (1): 150-153.

Silvester P. (1969). A general high-order finite-element wavegude analysis program. IEEE Transactions on Microwave Theory Techniques MTT-17 (4): 204-210.

Smith D.S, Riccius H.D. and Edwin R.P. (1976). Refractive indices of lithium niobate. Optical Communication 17 (6): 332-335.

Stegeman G.I. (1996). Cascading second order processes for nonlinear optics. LEOS Newsletter. (8): 3-5.

Stern M.S., Kendall P.C. and McIlroy P.W.A. (1990). Analysis of the spectral index method for vector modes of rib waveguides. IEE Proceedings-J 137 (1): 21-26.

Strake E., Bava G.P. and Montrosset I. (1988). Guided modes of Ti:LiNbO3 channel waveguides: A novel quasi-analytical technique in comparison with the scalar finite-element method. Journal of Lightwave Technology LT-6 (6): 1126-1135.

Sudbo A.S. (1992). Why are accurate computations of mode fields in rectangular dielectric waveguides difficult. Journal of Lightwave Technology LT-10 (4): 418-419.

Suhara T. and Nishihara H. (1990). Theoretical analysis of waveguide second-harmonic phase matched with uniform and chirped gratings IEEE Journal of Quantum Electronics 26 (7): 265-1276.

Tamir T. (1979). Integrated Optics. 2nd Ed. (New York: Springler-Verlag).

Tamir T. (1990). Guided wave optoelectronics. 2nd Ed. (Berlin: Springer-Verlag).

Themistos C., Rahman B.M.A., Hadjicharalambous A. and Grattan K.T.V. (1995). Loss/Gain characterization of optical waveguides. Journal of Lightwave Technology LT-13 (8): 1760-1765.

Torruellas W.E., Krijnen G., Kim D.Y., Schiek R., Stegeman G.I., Vidakovic P. and Zyss J. (1994). Cascading nonlinearities in an organic single crystal core fiber: the Cerenkov regime. Optics Communication 112(11):122-130.

Tzolov V.P. and Fontaine M. (1996). A passive polarization converter free of longitudinally-periodic structure. Optics Communication 127(6):7-13.

Tzuang C.K and Itoh T. (1986). Finite-element analysis of slow-wave schottky contact printed lines. IEEE Transactions on Microwave Theory Techniques MTT- 34 (12): 1483-1489.

Webjörn J., Siala S., Nam D.W. Waarts R.G. and Lang R.J. (1997). Visible laser sources based on frequency doubling in Nonlinear waveguides. IEEE Journal of Quantum Electronics 33 (10): 1673-1686.

Weitzman P.S. and Osterberg U. (1993). A modified beam propagation method to model second harmonic generation in optical fibers. IEEE Journal of Quantum Electronics 29 (5): 1437-1443.

Whitbread N.D. and Robson P.N. (1994). Theoretical analysis of passive visible surface-emitting second harmonic generators. IEEE Journal of Quantum Electronics 30 (1): pp. 139-382.

Wongchareon T., Rahman B.M.A. and Grattan K.T.V. (1997). Electro-optic directional coupler switch characterization. Journal of Lightwave Technology LT-15 (2): 377-1765.

Worm S.B. and Pregla R. (1984). Hybrid-mode analysis of arbitrarily shaped planar microwave structures by the method of lines. IEEE Transactions on Microwave Theory Techniques MTT- 32 (2): 191-196.

Wu R.B. and Chen C.H. (1986). A scalar variational conformal mapping technique for weakly guiding dielectric waveguides. IEEE Journal of Quantum Electronics 22 (5): 603-609.

Yamanouchi K., Kamiya T. and Shibayama K. (1978). New leaky surface waves in anisotropic metal-diffused optical waveguides. IEEE Transactions on Microwave Theory Techniques MTT- 26 (4): 298-305.

Yariv A. (1971). Introduction to Optical Electronics. (New York: Holt, Rinehart and Winston Inc.).

Yariv A. (1989). Quantum Electronics. (New York: Wiley).

Yeh C., Ha K. Dong S.B. and Brown W.P. (1975). Arbitrarily shaped inhomogeneous optical fiber or integrated optical waveguides. Journal of Applied Physics 46 (5): 2125-2129.

Yeh C., Ha K. Dong S.B. and Brown W.P. (1979). Single mode optical waveguides. Applied Optics 18 (10): 1490-1504.

Yevick D. (1994). A guide to electric field propagation techniques for guided wave optics. Optical Quantum Electronics 26 : 185-197.

Yoo S.J.B., Bhat R., Caneau C. and Koza M.A. (1995). Quasi-phase-matched second-harmonic generation in AlGaAs waveguide with periodic domain inversion achieved by wafer-bonding. Applied Physics Letters 66 (6): 3410-3412.

Zernike F. and Midwinter J.E. (1973). Applied Nonlinear Optics. (New York : Wiley & Sons).